

# Design of Microwave Components using Direct Metal Laser Sintering

by

Deepak Shamvedi

A Thesis submitted in fulfilment of the degree of  
DOCTOR OF PHILOSOPHY



School of Engineering Technology

Supervisors:

Dr. Ramesh Raghavendra  
Dr. Paul O'Leary

Submitted to the Waterford Institute of Technology

September 2018

## Declaration

I hereby declare that this document is entirely my own work and does not contain material previously published by any other author, except where due reference or acknowledgment has been made. Furthermore, I declare that this document has not been previously been submitted to any other institution for any other academic award.

Deepak Shamvedi  
W20061369

# ABSTRACT

## Design of Microwave Components using Direct Metal Laser Sintering

by

Deepak Shamvedi

Additive Manufacturing holds significant promise for microwave component design, enabling the production of previously un-manufacturable, complex designs through 3D printing.

The research here reports the modelling, simulation, fabrication and testing of several microwave components, including the world's first ever 3D metal printed Sierpinski gasket antenna, with multiple resonance characteristics. One concern of 3D metal printing relates to surface finish. The impact of inherent surface roughness on the performance of the printed antenna has also been evaluated. Further, two different surface treatment techniques have been used and the RF improvement has been assessed. Considering the fact that these treatments may not be available to the wider RF community, two other possible ways to limit the surface roughness have also been highlighted and tested.

3D printing, being a layer-by-layer process, enables the designing of self-supportive structures through topological design optimization. This property has been utilized to design self-supportive, non-solid interior microwave components, to reduce their weight. The results showed the weight of the metal printed inner lattice antenna to be even lighter than a similar metal-coated (solid) polymer antenna, fabricated with comparatively similar RF performance.

In another exploitation, an alternative approach to mounting an antenna to its feeding circuitry has been developed, by printing an intricate, N-type female feed together with the microwave component, as a single monolithic component.

A final development related to enhancing the performance of existing antennas, including the fabrication of a novel horn antenna, with in-built periodic structures positioned at bespoke positions for side-lobe reduction and the first ever attempt at 3D printing an artificial dielectric lens, for possible 5G and power applicator applications.

# ACRONYMS

ABS:	Acrylonitrile-Butadiene Styrene
AM:	Additive Manufacturing
BJ:	Binder Jetting
CAD:	Computer Aided Design
CD:	Compact Disk
CST:	Computer Simulation Technology
DED:	Directed Energy Deposition
DLP:	Digital Light Processing
DMLF:	Direct Metal Laser Fabrication
DMLS:	Direct Metal Laser-Sintering
DP:	Direct Printing
EBFFF:	Electron Beam Free Form Fabrication
EBG:	Electronic Band Gap
EBM:	Electron Beam Melting
EDM:	Electrical Discharge Machining
EM:	Electromagnetic
FDM:	Fused Deposition Melting
LENS:	Laser Engineered Net Shaping
LOM:	Laminated Object Manufacturing
MJ:	Material Jetting
OM:	Optical Microscope
PBF:	Powder Bed Fusion
PLA:	Polylactic Acid
PSD:	Particle Size Distribution

RF:	Radio Frequency
RP:	Rapid Prototyping
SEBM:	Selective Electron Beam Melting
SLA:	Stereolithography
SLM:	Selective Laser Melting
SLS:	Selective Laser Sintering
VNA:	Vector Network Analyser
VSWR:	Voltage Standing Wave Ratio
WLI:	White Light Interferometer

*To my wonderful family*

# ACKNOWLEDGEMENT

I was fortunate to be given a chance to work with amazing peers throughout my PhD research work at Waterford Institute of Technology.

My supervisors, Dr. Ramesh Raghavendra and Dr. Paul O’Leary are the most amazing supervisors one can have. Their guidance and motivation have always encouraged me to do more and come up with creative solutions to the problem in hand. Both of them have been patient enough to correct me and advise me with all my small mistakes in my research work.

Furthermore, it was my pleasure to work with amazing colleagues such as Eoghan O’Donoghue, Dr. Sara Karam and all the members of SEAM who made these years an amazing experience. I would especially like to thank Dr. Oliver McCarthy and Cyril Danilenkoff, who despite my constant pestering, have always kept their doors open to guide me throughout my research work.

I would also like to thank, Michael McCarthy, Keelan Murphy and Philip Creevy for being there whenever I needed them.

Last but not the least, my family and my best friends, who have been amazing these years by constantly motivating, supporting and believing in me, at times when it was tough for me to even believe in myself.

# TABLE OF CONTENTS

ABSTRACT.....	II
ACRONYMS.....	III
ACKNOWLEDGEMENT.....	VI
TABLE OF CONTENTS.....	VII
LIST OF FIGURES.....	XI
LIST OF TABLES.....	XV
1 CHAPTER 1.....	1
1.1 Motivation.....	1
1.2 Research Objectives and Achievements.....	5
1.3 Thesis Outline.....	7
1.4 Publications Associated with this Research.....	8
1.5 Summary.....	10
1.6 References.....	11
2 CHAPTER 2.....	12
2.1 Introduction to Additive Manufacturing.....	12
2.1.1 All-Metal Additive Manufacturing.....	13
2.2 Progress in 3D Printed Microwave Components.....	15
2.2.1 3D Metal-Coated Polymer Printed Microwave Components.....	16
2.2.2 3D Metal Printed Microwave Components.....	21
2.3 Summary.....	25
2.4 References.....	26
3 CHAPTER 3.....	31

3.1	Introduction.....	31
3.2	Sierpinski Gasket Antenna.....	33
3.3	Antenna Description .....	34
3.4	Mechanical Considerations.....	36
3.4.1	“Ring width” effect.....	36
3.4.2	Structural ambiguity.....	37
3.4.3	Build orientation .....	38
3.4.4	Support structures .....	39
3.4.5	Feed point challenges.....	42
3.5	Post-Processing.....	45
3.5.1	Heat treatment.....	45
3.5.2	Wet blasting.....	49
3.5.3	Polishing .....	52
3.6	Surface Morphology .....	55
3.6.1	Surface analysis parameters.....	58
3.7	RF Results and analysis.....	60
3.7.1	Measurements after heat treatment.....	62
3.7.2	Measurement after wet blasting.....	65
3.7.3	Measurement after polishing.....	68
3.8	Summary.....	71
3.9	References.....	73
4	CHAPTER 4 .....	77
4.1	Introduction.....	77
4.2	Monocone Antenna.....	79
4.3	Antenna Design and Manufacturing .....	80
4.4	Surface Roughness Analysis.....	84
4.5	RF Results.....	86
4.6	Summary.....	89
4.7	References.....	90

5	CHAPTER 5 .....	91
5.1	Introduction.....	91
5.2	Antenna Fabrication.....	92
5.2.1	Solid metal printed antenna.....	94
5.2.2	Hollow metal printed antenna.....	96
5.2.3	Inner lattice metal printed antenna.....	99
5.2.4	Metal-coated polymer printed antenna.....	101
5.3	Mechanical Testing.....	106
5.4	RF Results.....	107
5.5	Summary.....	109
5.6	References.....	111
6	CHAPTER 6 .....	113
6.1	Introduction.....	113
6.2	Antenna Fabrication.....	115
6.3	Build Orientation and its Effect on Surface Roughness.....	115
6.4	Results.....	119
6.5	Summary.....	121
6.6	References.....	123
7	CHAPTER 7 .....	124
7.1	Introduction.....	124
7.2	Horn Antenna & Periodic Structure Configuration .....	125
7.2.1	Horn antenna.....	125
7.2.2	Periodic structures.....	126
7.3	Antenna Fabrication.....	128
7.4	RF Results.....	129
7.5	Summary.....	133
7.6	References.....	135
8	CHAPTER 8 .....	136

8.1	Introduction.....	136
8.2	Artificial Dielectric Lenses .....	138
8.3	Lenses Design and Fabrication .....	139
8.4	RF Simulation Results .....	143
8.4.1	Bi-concave lens .....	144
8.4.2	Plano-concave lens.....	146
8.5	Summary.....	148
8.6	References.....	149
9	CHAPTER 9 .....	152
9.1	Conclusion .....	152
9.1.1	Significance of this work .....	153
9.1.2	Limitations of this work.....	153
9.2	Future work.....	154
9.2.1	Future work associated as an extension to the thesis .....	154
9.2.2	Future work in the medium to long term .....	156
	APPENDIX.....	XVII

# LIST OF FIGURES

Figure 1: Application of 3D printing in various industrial fields: a) architectural models [3] b) organ printing in medical fields [5] c) KalamSat - world's lightest satellite [6] d) lightweight metal printed bike frame [8] e) mm wave Tera-hertz waveguide [9] .....	4
Figure 2: 3D Printed 10 GHz patch antennas with a) conductive paint, b) copper tape with solder, c) copper tape with conductive epoxy [28] .....	17
Figure 3: 3D printed and copper-plated a) WR-90 rectangular waveguide, b) WR-10 split block waveguide [31].....	18
Figure 4: Photograph of a) fabricated Luneburg lens, b) Luneburg lens fed by a mounted waveguide [36].....	19
Figure 5: Photos of the fabricated THz EMXT horn antenna [38] .....	20
Figure 6: Photo of the 3D printed horn antenna [39] .....	21
Figure 7: Prototype of the 3D printed antenna array [40].....	22
Figure 8: 3D Conformal slotted waveguide antenna array [41].....	23
Figure 9: 3D metal-printed horn antenna, (a) perforated prototype (b) horn antenna under test [43] .....	24
Figure 10: Sierpinski gasket antenna fabricated using DMLS technology on Ti-6Al-4V .....	35
Figure 11: Simulated variation in frequency bands due to ring width effect (all dimensions in mm) .....	37
Figure 12: Illustration of overlapping tetrahedrons during the build .....	38
Figure 13: Possible orientation angles for the construction of 3D printed structure using DMLS technique a) 0°, b) 45°, c) 90° [20] .....	39
Figure 14: 3D metal printed Sierpinski gasket antenna with build support structure .....	41
Figure 15: Sierpinski gasket antenna fabricated with support structures, a) post Wire-EDM, b) removal of support structures using long nose pliers, c) process of removal of supports .....	42
Figure 16: Mounting an antenna onto the feed setup.....	43
Figure 17: Configurations of monopole antenna [23].....	44
Figure 18: Conductive trace between antenna and ground due to epoxy.....	44
Figure 19: 5x WLI scan of 3D metal printed Sierpinski gasket antenna along Z-direction (top surface of the antenna) after heat treatment .....	47
Figure 20: 5x WLI scan of 3D metal printed Sierpinski gasket antenna along XY-direction (lateral surfaces of the antenna) after heat treatment. ....	47

Figure 21: Visualization of surface current density of a Sierpinski gasket antenna using CST at 8.4 GHz.....	48
Figure 22: Process of wet blasting using abrasive media and compressed air to reduce the surface finish of the printed surface [27].....	49
Figure 23: 500x OM scans of 3D metal printed Sierpinski gasket antenna a) along Z-direction (top surface of the antenna) and b) along XY- plane (lateral surfaces of the antenna) after wet blasting.....	50
Figure 24: 5x WLI scan of 3D metal printed Sierpinski gasket antenna along Z- direction (top surface of the antenna) after wet blasting .....	51
Figure 25: 5x WLI scan of 3D metal printed Sierpinski gasket antenna along XY- direction (lateral surface of the antenna) after wet blasting .....	51
Figure 26: 500x OM scans of 3D metal printed Sierpinski gasket antenna along a) Z-direction (top surface of the antenna) and b) along the XY- plane (lateral surface of the antenna) after polishing.....	53
Figure 27: 5x WLI scan of 3D metal printed Sierpinski gasket antenna along Z direction (top surface of the antenna) after polishing.....	54
Figure 28: 5x WLI scan of the 3D metal printed Sierpinski gasket antenna along the XY-plane (lateral surface of the antenna) after polishing.....	54
Figure 29: 500x OM scans of the 3D metal printed Sierpinski gasket antenna post heat treatment a) along the Z direction (top surface of the antenna), b) along the XY plane (lateral surface of the antenna) after heat treatment c) along the edge section of the lateral surface, showing both the flat top and side. ....	57
Figure 30: Surface roughness parameters .....	58
Figure 31: Antenna radiation measurement setup for E-plane gain measurement .....	61
Figure 32: 3D metal printed Sierpinski gasket antenna, after heat treatment .....	62
Figure 33: Simulated and measured return loss after heat treatment .....	63
Figure 34: Simulated and measured gain radiation pattern a) 4.2 GHz b) 8.4 GHz .....	64
Figure 35: Sierpinski gasket antenna fabricated after wet blasting.....	66
Figure 36: Comparison of simulated return loss with anticipated base radius of 0.6mm and the measured results obtained after antenna was wet blasted (all the dimension are in mm).....	67
Figure 37: Simulated and measured E- plane realised gain radiation pattern a) 4.2 GHz b) 8.4 GHz .....	68
Figure 38: Sierpinski gasket antenna after polishing.....	69
Figure 39: Comparison of simulated return loss with anticipated base radius of 0.10 mm and the measured results obtained after antenna was polished (all the dimensions are in mm).....	70
Figure 40: Simulated and measured gain radiation pattern a) 4.2 GHz b) 8.4 GHz .....	71
Figure 41: 3D monocone antenna with an integrated feed .....	81

Figure 42: 3D model illustration of the (a) monocone antennas with an integrated feed, (b) N-type female feed.....	82
Figure 43: Experimental prototype and monocone antenna with an integrated feed.....	83
Figure 44: Photographs of 3D monocone antenna with an integrated feed, (a) elevated view (b) perspective view.....	84
Figure 45: 5x WLI scan for surface roughness measurement of the lateral side of 3D metal printed monocone antenna fabricated using two different materials (a) Titanium alloy (Sierpinski gasket antenna), (b) Maraging Steel.....	86
Figure 46: Simulated and measured return loss of 3D monocone antenna with an integrated feed .....	87
Figure 47: Simulated and measured VSWR .....	87
Figure 48: Simulated and measured gain radiation pattern a) 4.75 GHz b) 5.2 GHz c) 5.8 GHz.....	88
Figure 49: 3D metal printed lattice structures heat sinks, fabricated with varying unit cell length dimensions along the fins a) 5mm, b) 7.5 mm, and c) 12 mm.....	93
Figure 50: 3D metal printed first iteration solid Sierpinski gasket antenna with build support..	95
Figure 51: 3D metal printed solid antenna with CD as ground plane.....	96
Figure 52: CST simulation of surface current distribution along the surface of antenna .....	98
Figure 53: Illustration of hollow antenna with internal support.....	98
Figure 54: 3D metal printed hollow antenna with CD as ground plane.....	99
Figure 55: 3D metal printed inner lattice antenna with CD as ground plane.....	100
Figure 56: 3D Polymer printed antenna a) post printing b) post metal-coating.....	102
Figure 57: 3D metal-coated polymer printed antenna with CD as ground plane.....	104
Figure 58: 3D model illustration of the antennas fabricated with their interior structure.....	105
Figure 59: 3D printed cubes for mechanical testing, arranged according to their weight, left to right: solid, hollow, polymer and lattice .....	106
Figure 60: Simulated and measured return loss comparison graph of antennas .....	108
Figure 61: Simulated and measured realized E-plane gain of 3D printed antennas a) Solid b) Hollow c) Lattice d) Polymer.....	109
Figure 62: 3D metal printed horn antenna with support structures, constructed using different possible build orientations a) 45°, b) 90°, c) 180° .....	115
Figure 63: CST simulation of total electric field of a horn antenna.....	116
Figure 64: Horn antennas printed using DMLS sectioned in half for the surface measurement. The antennas were printed with three different orientations a) 45°, b) 90°, c) 180°.....	117
Figure 65: WLI (5x) and OM (400x) scans of the inner cavity of the horn antennas, built with three different orientations a) 45°, b) 90°, c) 180°.....	118
Figure 66: Effect on the surface finish of the 3D printed component due to build orientation and the staircase effect.....	119

Figure 67: Return loss comparison graph .....	120
Figure 68: 2D realized gain comparison graph .....	121
Figure 69: A standard gain horn antenna in (a) Perspective view and (b) Side view .....	126
Figure 70: Row formation of pyramidal periodic structure .....	128
Figure 71: Proposed horn antenna with periodic structures .....	129
Figure 72: Simulated and measured return loss .....	130
Figure 73: 2D realised comparison simulation gain, for different frequencies in X-band.....	131
Figure 74: 2D realised gain comparison simulation gain of horn antenna, with varying periodic structure height to the one with constant height along the rows .....	132
Figure 75: 2D realised gain, simulation and measurement comparison graph .....	133
Figure 76: Simulated comparison of 3D radiation pattern.....	133
Figure 77: The geometry of the proposed artificial dielectric lenses a) bi-concave b) plano-concave .....	142
Figure 78: Schematic diagram of a bi-concave artificial dielectric lens [11] .....	143
Figure 79: Focusing action of a beam energized with a horn antenna using a bi-concave artificial dielectric lens at 77 GHz, simulated using CST .....	145
Figure 80: Carpet representation of the focusing action of the Bi-concave artificial dielectric lens at 77 GHz, simulated using CST.....	146
Figure 81: Focusing action of a beam energized with a horn antenna using a plano-concave artificial dielectric lens at 60 GHz, simulated using CST.....	147

## LIST OF TABLES

Table 1: Simulated and measured gain of Sierpinski gasket antenna after heat treatment, as a function of surface roughness .....	64
Table 2: Simulated and measured gain of Sierpinski gasket antenna as a function of reducing surface roughness, post wet-blasting .....	68
Table 3: Simulated and measured gain of Sierpinski gasket antenna as a function of surface roughness, post polishing.....	71
Table 4: Dimensions of antenna and integrated feed .....	82
Table 5: Mechanical comparison of 3D printed components .....	105
Table 6: Mechanical properties comparison of 3D printed cubes.....	107
Table 7: Surface roughness measurements of the inner cavity of the horn antennas, built with three different orientations.....	119
Table 8: Variation of height of periodic structures on the basis of rows .....	128
Table 9: Dimensions of artificial dielectric lenses.....	141

# 1 CHAPTER 1

## INTRODUCTION

### ABSTRACT

**This chapter briefly introduces the motivation behind the research conducted and also explains some basic principles and ideas. The research questions, objectives and the achievements are also presented. Finally, this chapter ends with the thesis layout.**

### 1.1 MOTIVATION

3D printing is an Additive Manufacturing (AM) technique, which allows a component to be built in a layer-by-layer fashion to form a 3D object using digital blueprints. One of the major advantages of 3D printing lies in the production of components, where conventional manufacturing techniques have reached their limits. The technology allows one to build virtually any geometry imaginable, within some printing constraints which will be described later in this work, allowing designers to explore previously unexplored possibilities. When 3D printing was first developed, three decades ago, as rapid prototyping, the sole purpose of it was to prototype an object in order to test functionality [1][2]. However, while prototyping is still an important use, now 3D printing has also been adopted in a plethora of fields, such as, architecture, medical, automotive etc. to innovate and improve end products.

Continuous development in the field of AM is one of the reasons for the significant growth of 3D printing applications in all areas of manufacturing. For example, due to the bespoke nature of AM, one application of 3D printing is in prototyping products for later upscaling in the architectural industry. The technology allows architects to retain all of the freedom of intrinsic artistic design expected of architects, without sacrificing

structural rigidity, which helps the civil engineers to subsequently build quickly and to plan stages better [3].

Another high impact example is in the medical field. Biomedical engineers can now design custom made body parts and even organs, with perfect functionality. Porous structures are now possible to replace bones in the human body, facilitating enhanced bone in-growth [4]. One of the materials of choice for 3D biomedical printing, is Titanium, to serve as a long-time replacement of bone, as it is a biocompatible material, is accepted by the human body and exhibits a high specific strength. 3D printing of organs has a great potential to revolutionize the medical sector by improving the quality and extending the average life expectancy of millions of people [3]-[5].

In mechanical engineering there are also positive developments. For example, recently, Renishaw collaborated with a British bicycle design and manufacturing company and came up with the world's first 3D metal printed bike frame [6]. This was achieved by topological optimisation and fabricating the bike's frame out of titanium, allowing the structure to be both strong and light-weight. As the frame of the bike was 3D printed, it gave the engineers an opportunity to further alter the weight, by designing both hollow and lattice structures, removing any material which is not essential, without sacrificing the strength of the overall structure.

AM advances are only on earth but the applications are not occur not only on Earth, but there are also plans to take this exciting technology to outer space, as NASA is planning to station a 3D printer inside the International Space Station. This offers the flexibility to not only avoid stockpiling spare parts, in anticipation of a failure, but to design new parts, redesign existing parts or possibly to even print parts that cannot be transported. Their proposed printer could then be used to repair existing satellites, which can then be assembled by robotic arms, or even eventually lead to the creation of new satellites. As the commonly used metals and polymers in 3D printing cannot be used in Outer Space, researchers are working on a new type of plastic, polyetherimide/polycarbonate, which is stronger than the traditional plastic and possesses and meets the outgassing in vacuum requirements [7]. Adding to the many applications of 3D printing for space-borne applications, last year the world's lightest 3D printed satellite was reported and was launched by NASA. The satellite was fabricated using carbon fibre and weighed only 64 grams [8].

Of the many promising applications of AM, one area that attracted early interest is in the design of microwave components, which is the focus of this research work. The idea of designing microwave components through the application of AM is interesting for several reasons. As in other areas of AM, designs, which were un-manufacturable earlier, can now be realised within a short lead time and with the fine detail often needed for microwave components. Initially, the main area of research interest was in utilizing AM to manufacture microwave components using Stereolithography (SLA), a 3D printing technique, which uses a plastic polymer as a fabricating material. In the process, the physical structure is fabricated using non-conducting thermoplastics and is then usually metallized or painted in order to make the printed electromagnetic component functional [9]. Fabricating microwave components in this way, on the one hand has the advantage of being lightweight (compared to the same component being fabricated using conventional manufacturing techniques and from metal) but on the other hand does not offer significant mechanical structural strength. In addition to that, the electromagnetic behaviour of the component is also distorted if contact with other objects causes any abrasion on its coated surface. Another disadvantage in comparison to metal printing can be the need to take the dielectric properties of the polymer into account when designing microwave components.

**Figure 1** depicts the application of 3D printed components in various fields a) architectural modelling [3] b) organ printing in the medical field [5] c) KalamSat – the world’s lightest satellite [6] d) a lightweight metal printed bike frame [8] and e) a mm wave Tera-hertz waveguide [9].

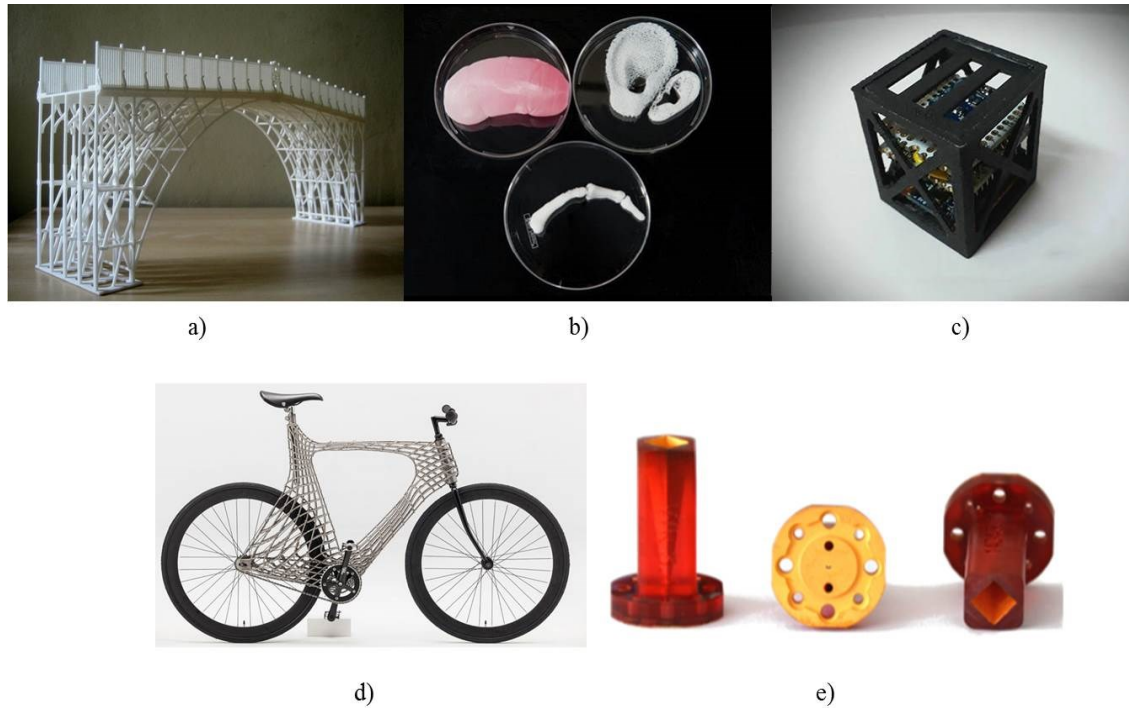


Figure 1: Application of 3D printing in various industrial fields: a) architectural models [3] b) organ printing in medical fields [5] c) KalamSat - world's lightest satellite [6] d) lightweight metal printed bike frame [8] e) mm wave Tera-hertz waveguide [9]

All of the components investigated in this thesis were fabricated using only metal alloys (with the exception of one metal-coated polymer antenna, for comparison purposes, as will be explained later), which would possess all the benefits of 3D polymer printing, such as realizable conformal shapes, while also offering the possibility of still being lightweight, through careful design.

There are different 3D printing techniques available. Although all 3D objects are created by adding layer-upon-layer of a material; the material itself varies from technology-to-technology. Industry already uses different raw materials, using techniques such as FDM (Fused Deposition Melting), Digital Light Processing (DLP), SLM (Selective Laser Melting), SLS (Selective Laser Sintering), LOM (Laminated Object Manufacturing), SLA (Stereolithography), and EBM (Electron Beam Melting). All these techniques print 3D structures with high precision and accuracy, but with different component characteristics.

The AM parts in this research were produced using a DMLS technology, which is a form of SLS technique, and is an all-metal 3D printer as explained in detail in **Chapter 2**. The

DMLS machine resident at the SEAM (South Eastern Applied Materials) Research Centre in Waterford Institute of Technology was used for this thesis work.

## **1.2 RESEARCH OBJECTIVES AND ACHIEVEMENTS**

Recent research, presented in the next chapter, has shown early demonstrations of the potential of metal AM in printing 3D microwave components. However, the research work has, to date, been mainly limited to the fabrication of horn antennas and waveguide arrays only. The research work presented here takes the next step towards untapping the potential of AM, by addressing the challenges faced in the fabrication of more complex microwave components.

For this research work, the following key research topics have been identified to clarify the main objectives of the thesis. These questions have been identified and addressed accordingly along with the answers in the corresponding chapters.

- The feasibility of designing complex shape geometry for a microwave component is where it all started. However, to realize the complex geometries using an all-metal 3D printer, the possible mechanical constraints must also be identified and overcome.
- There is also a concern associated with 3D printing, regarding the inherent surface roughness of the printed product. A clear and in-depth understanding is required to know the impact of surface roughness on the electromagnetic behavior of the microwave components.
- Once the microwave component has been fabricated, it has to go through a series of post-processing steps, where some of the steps may be regarded as essential and some as optional. This study includes gaining an in-depth understanding of the influence of post-processing operations on the surface morphology of the overall structure and their subsequent impact on the performance of the microwave component, in order to understand the relative importance of each step in terms of impact on microwave performance.
- The research work also aims to use 3D metal printing to improve the performance of a state-of-art horn antenna by looking at new possibilities to fabricate antennas with a reduced level of side-lobes and improved focussing capabilities. This is a

concept which has been limited up to now to simulations, due to the manufacturing constraints posed by conventional techniques.

- 3D printing is also well known for producing lattice and non-solid interior structures, in order to reduce the weight of the component, while maintaining a significant structural strength. This research work explores the properties of 3D printing, to fabricate lightweight microwave components for potential wireless communication applications, where strength need not be compromised or may be only partly compromised.
- To further exploit the potential of fabrication of lattice structures through 3D printing, a brief attempt has also been made during this research work, even though not part of this thesis, to fabricate complex 3D printed fractal heat sink antenna using the DMLS technique. The study was done to fabricate the heat sinks for eventual microwave antenna deployment, with increased surface area, which could reduce the thermal resistance in comparison to a typical finned heat sink, further improving the radiation efficiency and gain of the microwave component.

The investigation of these research topics has led to some achievements:

- The importance of factors such as build orientation and external support structures, while designing the world's first ever 3D metal printed 2<sup>nd</sup> iteration Sierpinski gasket antenna, has been highlighted;
- Post-processing steps does indeed have an effect on the microstructural, as well as the electromagnetic performance, of the microwave component. The effect of reducing surface roughness, in a step-by-step manner, has been reported in terms of antenna gain and return loss measurements;
- The research also reports manufacturing a metal antenna, which is lighter than the equivalent metal-coated, polymer antenna;
- The research presents the first working prototype of a horn antenna with reduced side-lobes by selectively printing periodic structures inside the horn;
- The thesis also reports on work done towards enhancing the directivity of a horn antenna for spot-focusing applications with the potential fabrication of 3D metal printed artificial dielectric lenses, for the millimetre wave frequency range.

### 1.3 THESIS OUTLINE

The document is laid out as a series of published and yet to be published papers, which complies with WIT rules for PhD thesis, where the PhD thesis may be presented in conventional form (chapter-based) or as a series of published works. Each of the conceptual papers is presented in a single chapter. However, some papers overlap naturally into more than one chapter, and so warrant a brief mention in more than their core chapter.

The first chapter in this work, **Chapter 2** is an overview of the progress in the fabrication of 3D printed microwave components. It also describes the availability of different AM technologies, in the industry which use both polymer and metal as the raw material.

**Chapter 3** summarizes the design restrictions, fabrication and post-processing requirements, especially the removal of surface roughness, from the world's first ever 3D metal printed 2<sup>nd</sup> iteration Sierpinski gasket antenna. Other challenges faced, such as the 'ring width' effect, constraints in manufacturing challenges, such as structural ambiguity between the 3D printed parts from their original geometry and mounting of complex shaped antenna to the excitation feed, are discussed in detail.

The findings of **Chapter 3** give a new insight into the problem faced when mounting an antenna onto the feeding circuitry. This give rise to an additional research question, which is the subject of **Chapter 4**. In this chapter, an alternative approach is taken, integrating a signal feed to a 3D metal printed monocone antenna, instead of using solder or epoxy glue.

**Chapter 5** is based on the design of a lightweight antenna, utilizing the potential of 3D printing in designing non-solid structures. Several mechanical, and design constraints, required to print hollow as well as inner lattice structured antennas, have also been detailed in-depth. Other requirements such as the minimum wall thickness, as well as the requirement for escape holes, used to remove the 'trapped', unsintered metal powder from the printed antenna, are also reported. The research also reports, for the first time, the weight of a metal antenna to be comparatively lighter than its equivalent metal coated polymer printed antenna, with higher strength-to-weight ratio.

**Chapter 6** presents an investigative study of the influence of the build orientation on the surface roughness of the 3D metal printed horn antenna. The work should help the future antenna designers, who wish to utilize 3D printing technology for the fabrication of the RF/ microwave components with limited surface roughness.

Demonstrating the applications where 3D metal printed antennas may be most useful, **Chapter 7** and **Chapter 8** are focussed towards improving the performance of state-of-the-art antennas, using 3D metal printing technologies. With the knowledge gained in both the respective areas of antenna design and AM, the chapters report first-of-their-kind, fabricated horn antennas, with reduced side lobes. **Chapter 8** refines the concept of fabrication of artificial dielectric lenses, which mimics the properties of naturally occurring dielectric media, having an index of refraction less than one, utilized in the thesis to spot focus the incoming electromagnetic waves at a desired location, at mm wavelengths.

Finally, **Chapter 9** concludes the work of this thesis and lays down a brief outline of potential future work that can be carried out in the area of designing 3D printed microwave components.

## **1.4 PUBLICATIONS ASSOCIATED WITH THIS RESEARCH**

A list of peer-reviewed conference and journal papers arising from the research work conducted are featured below. I was responsible for most of the work carried out, which includes novel ideas for the design of the 3D microwave component, their modelling, simulations, measurements, analysis of the results and writing.

### **Published**

1. Deepak Shamvedi, Oliver McCarthy, Eoghan O'Donoghue, Paul O'Leary, Ramesh Raghavendra - "Surface Treatment of 3D Metal Printed Microwave Components", *18th Research Colloquium on Radio Science and Communications for a Smarter World, Dublin, Ireland; p.p. 8-10, March/2017.*
2. Deepak Shamvedi, Oliver McCarthy, Eoghan O'Donoghue, Paul O'Leary, Ramesh Raghavendra - "3D Metal Printed Sierpinski Gasket Antenna", *2017*

*International Conference on Electromagnetics in Advanced Applications (ICEAA), Verona, Italy; p.p. 633-636, September/2017.*

*DOI: 10.1109/ICEAA.2017.8065326*

3. Deepak Shamvedi, Oliver McCarthy, Eoghan O'Donoghue, Paul O'Leary, Ramesh Raghavendra - "Improved Performance of 3D Metal Printed Antenna through Gradual Reduction in Surface Roughness", *2017 International Conference on Electromagnetics in Advanced Applications (ICEAA), Verona, Italy; p.p. 669-672, September/2017.*

*DOI: 10.1109/ICEAA.2017.8065335*

4. Deepak Shamvedi, Oliver McCarthy, Eoghan O'Donoghue, Paul O'Leary, Ramesh Raghavendra - "3D Metal Printed Monocone Antenna with an Integrated Feed", *Proceedings of 47<sup>th</sup> European Microwave Conference (EuMW), Nuremberg, Germany, p.p. 168-171, October/2017.*

*DOI: 10.23919/EuMC.2017.8230826*

5. Deepak Shamvedi, Cyril Danilenkoff, Sara Karam, Paul O'Leary, Ramesh Raghavendra - "3D Printed Periodic Structures in a Horn Antenna for Side-lobe Reduction using Direct Metal Laser Sintering", *2017 IET Loughborough Antennas & Propagation Conference (LAPC), Loughborough, UK, p.p. 1-4, November/2017.*

*DOI: 10.1049/cp.2017.0244*

6. Deepak Shamvedi, Oliver McCarthy, Eoghan O'Donoghue, Paul O'Leary, Ramesh Raghavendra - "Progress in 3D Metal Printed Microwave Components – An Overview", *12<sup>th</sup> European Antenna & Propagation Conference (EuCAP), London, UK, p.p. 1-4, April/2018.*

7. Deepak Shamvedi, Cyril Danilenkoff, Paul O'Leary, Ramesh Raghavendra - "Investigation of the Influence of Build Orientation on the Surface Roughness of the 3D Metal Printed Horn Antenna", *12<sup>th</sup> European Antenna & Propagation Conference (EuCAP), London, UK, p.p. 1-4, April/2018.*

8. Deepak Shamvedi, Oliver McCarthy, Cyril Danilenkoff, Eoghan O'Donoghue, Paul O'Leary, Ramesh Raghavendra - "3D Metal Printed Heat Sinks with Longitudinally Varying Lattice Structure Sizes using Direct Metal Laser Sintering", *Journals of Virtual and Physical Prototyping*, vol. 13, no. 4, pp. 301-310, May/2018.  
DOI: 10.1080/17452759.2018.1479528
9. Deepak Shamvedi, Paul O'Leary, Ramesh Raghavendra - "Design Approach for Successful Fabrication of 3D Printed Microwave Components", *21<sup>st</sup> International Conference on Advances in Materials & Processing Technologies, (AMPT 2018) Dublin, Ireland, September/2018.*
10. Deepak Shamvedi, Oliver McCarthy, Eoghan O'Donoghue, Paul O'Leary, Ramesh Raghavendra - "Improving the Strength-to-Weight Ratio of 3D Printed Antennas: Metal versus Polymer", *IEEE Antennas and Wireless Propagation Letters*.  
DOI: 10.1109/LAWP.2018.2870944

## 1.5 SUMMARY

The motivation for pursuing this research work is presented in this chapter. The key problems associated with the 3D printing microwave components have been identified in this chapter and addressed in subsequent chapters of this thesis. The key research questions are considered and presented along with pointers to the chapters, where they are discussed in detail. The contributions made by the research in this thesis are listed in a consolidated form along with an overview of the progress in the fabrication of 3D printed microwave components. The chapter describes the achievements made in the respective field in the form of publications arising from the work done towards this thesis, and are listed at the end.

## 1.6 REFERENCES

1. H. Kodama, “Automatic method for fabricating a three- dimensional plastic model with photo- hardening polymer”, *Review of Scientific Instruments*, vol. 52, no. 11, pp. 1770-1773, 1981.
2. C. Hull, “Stereolithography: Plastic prototype from CAD Data without tooling”, *Modern Casting*, vol. 8, pp. 38, August/1988.
3. A. Gebhardt and M. Fateri, “3D printing and its applications”, *RTEjournal - Forum für Rapid Technologie*, vol. 10, no. 1, January/2013.
4. C. Bergmann, M. Lindner, W. Zhang and K. Koczur, “3D printing of bone substitute implants using calcium phosphate and bioactive glasses”, *Journal of the European Ceramic Society*, vol. 30, no. 12, pp. 2563-2567, September/2010.
5. Y. Brazier, (Online) “3D-printed kidney technique enables transplant for 2-year-old”, *Medical News Today*, January/2016.
6. Renishaw, (Online) “First metal 3D printed bicycle frame manufactured by Renishaw for Empire cycles”, (<http://www.renishaw.com/en/first-metal-3d-printed-bicycle-frame-manufactured-by-renishaw-for-empire-cycles--24154>), [Accessed: 9<sup>th</sup> January 2018].
7. Sculpteo, (Online) “3D printing in space: The next revolution?” (<https://www.sculpteo.com/blog/2017/11/29/3d-printing-in-space-the-new-revolution/>), [Accessed: 15<sup>th</sup> December 2017].
8. 3ders, (Online) “3D printed carbon fiber helps 18-year-old Indian student make lightest satellite ever”, (<https://www.3ders.org/articles/20170515-3d-printed-carbon-fiber-helps-18-year-old-indian-student-make-lightest-satellite-ever>), [Accessed: 8<sup>th</sup> June 2017].
9. A. von Bieren, E. De Rijk, J.-P. Ansermet and A. Macor, “Monolithic metal-coated plastic components for mm-wave applications”, *39<sup>th</sup> International Conference on Infrared, Millimeter, and Terahertz waves (IRMMW-THz)*, Tucson, USA, September/2014.

# 2 CHAPTER 2

## LITERATURE REVIEW

### ABSTRACT

**An overview of different AM technologies available in industry and its progress in the fabrication of 3D microwave components is presented in this chapter. The work highlights the promising future of 3D printing for the fabrication of microwave components.**

### 2.1 INTRODUCTION TO ADDITIVE MANUFACTURING

AM has been around for almost three decades. In the early 1980's the 3D printing concept was heard for the first time and at the time, it was known as Rapid Prototyping (RP) technology. The idea was originally conceived to have a quick prototyping of the product, sometimes with ease, so that it could be manufactured more reliably, at a low cost or for customer visualisation etc. The first work in this area was reported by Dr. Kodama of Nagoya Municipal Industrial Research Institutes, Japan [1]. He published a paper in this regard, but unfortunately failed to file a patent on the same within the deadline. He modelled 3D objects by exposing liquid photo-hardening polymer to UV rays for curing and then stacking them into solidified layers. Soon after that, the first patent in RP was filed by Charles Hull [2], who created full 3D objects using the process of polymerization, with the help of a computer. That process is nowadays well-known as Stereolithography. Shortly afterwards, in 1986, Carl Deckard filed a patent [3], on an alternative 3D printing process, called Selective Laser Sintering. The concept behind this was to use the laser to fuse material into each other, layer-over-layer, in order to form a 3D object. Later, in 1994, the first generation of DMLS was developed by Rapid Product Innovations and EOS GmbH for RP of all-metal parts, as one single monolithic component [4].

Since then, progress in the field of RP has been enormous, as it became a fast-growing technology. Now there are several different techniques to form 3D objects, which can be fabricated directly from Computer Aided Design (CAD) data. Moreover, 3D printing has no longer been limited to RP alone, but is now creating objects that can be used as end products as well. There are different AM techniques available for 3D development. Although, all 3D objects are created by adding layer-upon-layer, there is a common misconception that AM and 3D printing are both synonyms, which is certainly not true, as there are many other processes that differ in their layer manufacturing. In fact, even the term “3D printing” itself is a misnomer, as it’s not actually 3D printing, but repeated 2D printing, which allows the component to be built from the bottom to the top, from a digital blueprint. In 2010, the American Society for Testing and Materials (ASTM) group broadly classified the AM techniques into 7 categories, differing in their method of layer manufacturing. The categories include Vat Polymerisation, Material Jetting (MJ), Binder Jetting (BJ), Powder Based Fusion (PBF), Material Extrusion, Direct Energy Deposition (DED) and Sheet Lamination [5].

Depending on the application, designers can select a different technology and raw material to address a particular application. These different materials include ceramic, plastic, wax, paper, living cells, sand and last, but not least, metals. As the main focus of this research is on all-metal printing, any discussion of technologies, which use other materials as the raw material, won’t be considered beyond this point.

### **2.1.1 ALL-METAL ADDITIVE MANUFACTURING**

All-metal AM can be classified into two broad groups based on the thermal energy source used:

- **Direct Metal Laser Fabrication (DMLF):** In this technique, thermal energy from a focused laser is used to melt the metallic powder using a high-powered laser [6]. The technology can be classified further, depending on the powder application methods. Some techniques need the metallic powder to be spread in the chamber beforehand, on which the laser is later applied [7]. These techniques are Selective Laser Sintering (SLS) [8], Selective Laser Melting (SLM) [9], and Direct Laser Metal Sintering (DMLS) [10]. One of the major difference between the DMLS process used in this work and the SLM process is that in the latter one achieves a

full melt, which means the technique can be used for individual metals such as Aluminium, while with DMLS, as the laser sinters the metallic powder, it can only work on metallic alloys such as Titanium Alloy, Aluminium Alloy, etc.

On the other hand, there are techniques which consist of powder deposition, coupled with melting the powder in-situ. Such technologies are Laser Engineered Net Shaping (LENS) technology [11], Direct Metal Deposition (DMD) [12] and Direct Light Forming (DLF) [13].

- Selective Electron Beam Melting (SEBM): Unlike DMLF, SEBM uses a focused electron beam as the thermal energy source, in a vacuum environment, to create a molten pool on a metallic substrate. Technologies that use an electron beam as the thermal source are Electron Beam Free Form Fabrication (EBFFF) [14] and Electron Beam Melting (EBM) [15].

The two preferred all-metal 3D printing technologies are Electron Beam Melting (EBM) and Direct Metal Laser Sintering (DMLS). Both EBM and DMLS are used to produce 3D metal parts, by selective fusion and consolidation of metal powder, with most of the unused metal powder being recycled in the machine after sieving. What differentiates EBM from DMLS is that in the EBM process the powder is melted by a powerful electron beam (typically around 3,500 watts). On the other hand, the DMLS technique (which is used in this research) uses a precise, high-power laser (200-500 watts) to melt a thin layer of metal powder. Thanks to the accuracy and precision of the laser, it is possible to form a 3D component with a high level of detail. This is the reason that DMLS typically produces a smoother surface finish compared to components printed using EBM [16]. From the printing metal selection point of view, DMLS also offers more options than EBM for the designer, ranging from alloys of Inconel, Aluminium, Copper, Chromium, Stainless Steel, Maraging Steel, and Titanium. However, not all versions of EBM, in particular, and DMLS printers, to a lesser extent, can work with all metal alloys listed above.

## 2.2 PROGRESS IN 3D PRINTED MICROWAVE COMPONENTS

The idea of designing microwave components through the application of AM is interesting for several reasons. Some designs, which were un-manufacturable earlier, can now be realized. Early research work focused mainly on manufacturing microwave components using Stereolithography, one of the AM techniques, which uses a plastic polymer as a fabricating material, for example Acrylonitrile-Butadiene Styrene (ABS) or Polylactic Acid (PLA) [17]-[21]. In that process, the physical structure is fabricated using non-conducting thermoplastics and depending on the application is then usually metallized or painted in order to enable it to function electromagnetically [22]. Although the most widely used 3D printing materials are ABS and PLA, recent research has used novel materials, which can nonetheless be printed with the available 3D printing technologies.

Two of the materials, which have gain ample of amount of research attention, towards fabrication of microwave components, are NinjaFlex and the graphene-based Polybutylene Terephthalate (PBT). NinjaFlex, which is composed of thermoplastic and rubber, offers flexibility, elasticity and high strength properties compared with other 3D printing materials, which makes it a good candidate for the fabrication of wearable electronic applications [23]. Fabricating microwave components in this way has the advantage of being inherently lightweight, flexible and less expensive. Similarly, graphene-based Polybutylene Terephthalate (PBT) is a 3D printable conductive filament, with an electrical resistivity of  $<0.01 \Omega \text{ m}$ . The measured resistivity of the polymer is enough to fabricate low-cost sensors, circuits and possibly wearable electronics [24].

On the one hand, the above-mentioned advantages makes 3D polymer printing an excellent choice for the fabrication of microwave components. On the other hand, the electromagnetic behaviour of the component can be distorted, if contact with other objects causes any abrasion on its coated surface. Also, metal-coated polymer components are also not a good choice for harsh environments, as well as for high-power applications.

In that scenario, fabricating microwave components out of metal alone possess all the previously-mentioned benefits of polymer printing. Although, from a monetary point of

view, metal printing technology has been expensive for the mass production of components; however, it does offer some benefits, such as the realisation of complex shapes, lighter weights, through hollow or lattice structures, with enhanced structural strength over the polymer printing or even traditional manufacturing techniques. Fabricating a microwave component using only metal not only eliminates the necessary extra processing step of metal coating over standard polymer printing but also a good choice for applications where polymer printed components reach certain performance limits. Nonetheless, even with the distinct advantages of the metal printed microwave component over the polymer one, the research done in the respective field has been very much limited, primarily due to the limited access to the technology.

In this chapter, a literature review on the progress of both metal-coated, 3D polymer printed microwave components and all-metal, 3D printed microwave components, has been demonstrated, in the form of case studies. In this review, challenges faced by the different authors for 3D printing microwave components have also been highlighted.

### **2.2.1 3D METAL-COATED POLYMER PRINTED MICROWAVE COMPONENTS**

**Patch antenna:** 3D printing technology has been widely utilized towards the fabrication of customized substrate structure, in terms of the fabrication of the dielectric substrate with varied thickness, filling and shape (conformal). The technology also allows the designer the freedom to choose substrate materials with different mechanical and electrical properties (permittivity) [25]-[28]. In one piece of research, the author has 3D printed and tested several substrate structures towards the fabrication of patch antennas for space-borne-applications [28]. As in space, where the environment can be harsh, numerous factors affect the performance of the antenna, such as high temperature, vacuum, magnetic fields, electromagnetic radiation, etc. The author printed patch antennas using FDM technology, with ABS being the dielectric material, and conducted measurements to understand the behaviour of 3D printed, ABS material under space conditions. To make the antenna EM functional, conductive paint and copper tape were used for the metallic portions of the antennas. In normal conditions, the antennas performed with some inaccuracies. Moreover, the author faced a major problem in mounting the connector, to feed the antenna circuitry. With the application of solder, there was a huge risk of causing damage to the polymer printed antenna. As an alternative, in

this research a conductive epoxy has also been used for the antenna connection to the feeding circuitry. **Figure 2** shows three different 3D printed antennas, with a working frequency of 10 GHz, fabricated on ABS as the dielectric material, with different techniques being used to metallize the patch of the antenna.

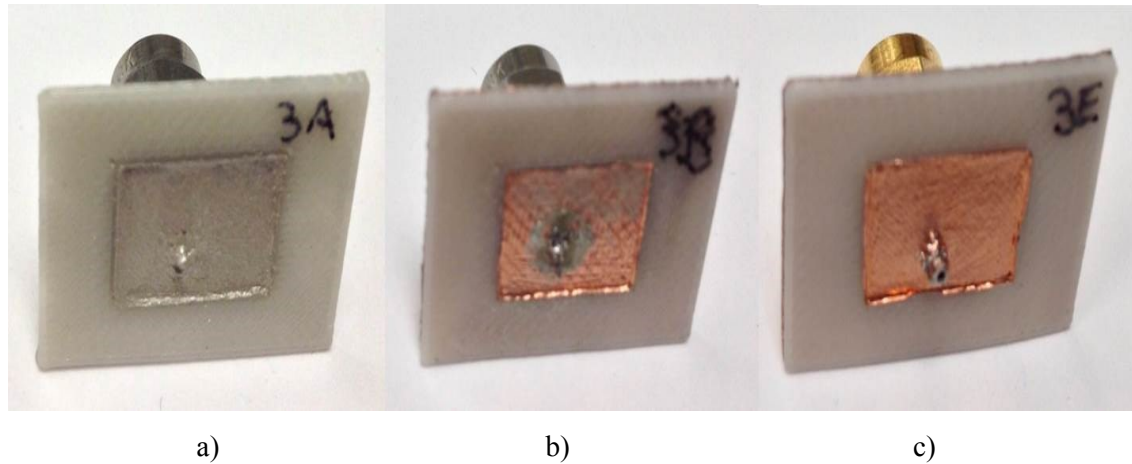


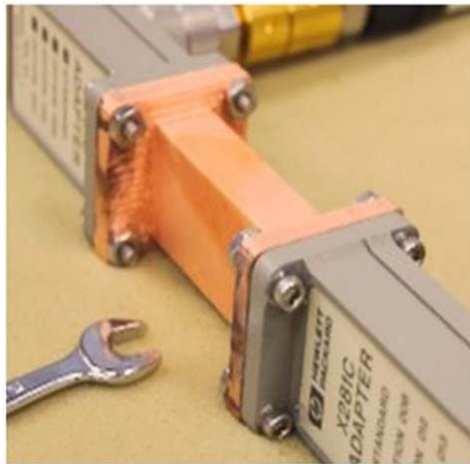
Figure 2: 3D Printed 10 GHz patch antennas with a) conductive paint, b) copper tape with solder, c) copper tape with conductive epoxy [28]

In addition, for realistic space measurements, the antenna parameters were measured under a Sr-90 source, for radiation testing and also in a vacuum chamber. The results concluded with extensive antenna surface damage, likely to further worsen if the measurements are performed for prolonged periods.

**Waveguide:** Design of waveguides has also been one of the microwave components which has received a lot of recent attention towards its fabrication for the applications ranging to even THz range [29]-[31]. The successful performance of 3D printed metal-pipe rectangular waveguides (MPRWGs) in X-Band, as one detailed below, has given researchers the confidence to move up to the W-band and even beyond, where manufacturing tolerance is a key issue due to the small size requirements [31].

To benchmark the performance of the 3D printed MPRWGs, in this research [31], two different 3D printing technologies have been used to fabricate two different waveguides. A low cost FDM technology printer has been used for the fabrication of the X-band MPRWS, whereas a more sophisticated, high resolution SLA technology printer has been used for the fabrication of a W-band split-block waveguide. As the internal dimensions

of a single-piece millimetre structure were too small to have acceptable metal plating, a split-block approach was adopted. For this reason, the waveguide was fabricated in two halves and then later assembled into one waveguide. Once printed by distinct printers, the printed components were then metallized using electroless plating. Both of the copper-plated 3D printed waveguides are shown in **Figure 3**.



a)



b)

Figure 3: 3D printed and copper-plated a) WR-90 rectangular waveguide, b) WR-10 split block waveguide [31]

It was also found that the component fabricated with the high-resolution SLA printer had a lower surface roughness value, almost 4 times lower, compared to the component fabricated with the FDM printer. In terms of RF performance, the performances of both the 3D printed MPRWGs were in good agreement when compared to the corresponding off-the-shelf commercial waveguides.

**Luneburg lens antenna:** The lenses for microwave applications are usually designed with varying reflective indices to manipulate the EM waves for the desired application. Towards the fabrication of the lenses it is extremely challenging to vary the dielectric properties with location within the lens. In that respect, 3D printing serves as a platform for rapidly fabricating dielectric materials with different relative permittivities. The variation in the permittivity of the material can be introduced by varying the size of the air voids into the host materials, thus the effective permittivity of the lens [32]-[36]. One such research is detailed here, where the author has designed and fabricated a Luneburg lens antenna, for the X-band [36]. The selection of the lens for 3D printing has been done

due to its complex, and time-consuming fabrication process, if done using conventional methods. In order to vary the relative permittivity of the spherically symmetric lens, to achieve the desired gradient index, the sizes of the unit cell cubes were varied gradually towards the centre of the lens, in discrete steps, with the maximum cube size being in the center of the lens, as shown in **Figure 4a**. This was done in order to vary the permittivity distribution, by changing the filling ratio of the unit cells, to achieve the desired antenna radiation characteristics. The Luneburg lens antenna was energised using a WR-90 waveguide as shown in **Figure 4b**.

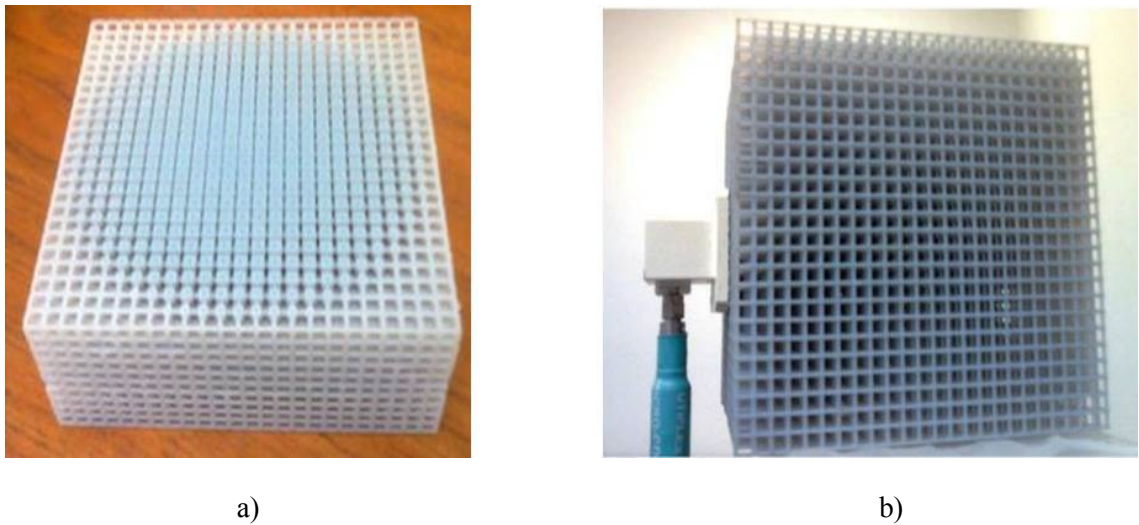


Figure 4: Photograph of a) fabricated Luneburg lens, b) Luneburg lens fed by a mounted waveguide [36]

Both the gain and directivity of the antenna were found to be increased over the frequency band. With side lobes 25 dB below the level due to the increased effective aperture, the measurement result shows a highly directional beam for all the measured frequency bands. This kind of lens antenna possesses wide angle radiation scanning and the ability to form multiple beams, while simultaneously achieving high gain, factors which are important for applications such as radar remote sensing.

**Terahertz horn antenna:** Due to the structural dimension of horn antennas, it is considered to be one of the easiest choices of antenna in terms of fabrication, not only for conventional manufacturing, but especially, when being 3D printed. An ample amount of research work has been conducted, in which the laser-based layer-by-layer SLA/FDM process has been used directly from three-dimensional CAD files in the successful

printing of the antenna [37] [38]. However, the structure of the antenna becomes more challenging for fabrication when it is designed for millimetre wave or the Terahertz frequency range. The prototypes of devices at such high frequencies can be fabricated by micromachining. However, the method requires expensive infrastructure and is time-consuming as well.

To prove the feasibility of a 3D printer to create arbitrary shaped horn antennas, as well as waveguide structures at the Terahertz range, a lot of research has recently been conducted. In one piece of research [38], the authors designed a Terahertz horn antenna based on a hollow-core electromagnetic crystal structure, which was fabricated using an all-dielectric FDM printer, as shown in **Figure 5**.

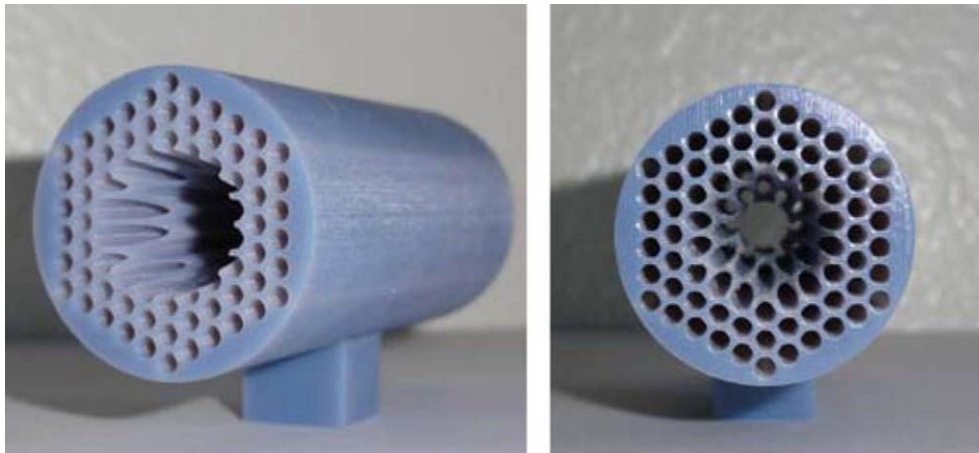


Figure 5: Photos of the fabricated THz EMXT horn antenna [38]

The placement of the periodic structures around the cavity of the horn antenna has been used in this research to act as a frequency band gap, at which electromagnetic wave propagation is forbidden in the crystal. This results in a highly directional beam, of a particular frequency, passing through, as the periodic crystal structure around the hollow core of the horn confines the EM waves within and guides the wave propagation along the channel. This clever structure has proved to greatly reduce the radiation loss along the propagation path. The simulation and the measurement results confirm the highly directional radiation pattern in the designed passbands.

### 2.2.2 3D METAL PRINTED MICROWAVE COMPONENTS

**Horn antenna:** Horn antennas are considered to be easy to fabricate, either polymer printed or 3D metal printed. The structure itself is self-supportive and requires minimum supports to be generated (if printed in its natural orientation). In this research, two identical Ku-Band (12-15 GHz) horn antennas were printed in [39], with slightly different directivity and gain. The antennas were manufactured using EBM technology with aluminium alloy (AlSi10Mg), used as the fabricating material. To the best of author's knowledge, the research was the first to evaluate the effect of extreme surface roughness on the 3D printed antennas. The photograph of the printed antennas is shown in **Figure 6**.



Figure 6: Photo of the 3D printed horn antenna [39]

Once printed, the average surface roughness of the antenna was measured to be of the order of 20-40 $\mu\text{m}$ , with no post-processing steps taken, to polish or otherwise improve the surface finish of the printed components. For RF/microwave components, it is well known that if the surface roughness of an electromagnetic component is of the order of the skin depth, performance will be significantly degraded, and that additional surface roughness further increases the losses, increasing as a function of frequency. In this work, it was concluded that of the two printed antennas, the antenna with the higher measured surface roughness had an extra 1 dB loss in the transmission coefficient of the antenna, compared with the standard off-the-shelf horn antenna. However, the losses regarding surface roughness would be more severe for higher frequency bands.

**Waveguide fed antenna array:** The antenna presented in this research is a relatively large 8x8 wideband waveguide array, with an integrated corporate-fed network, fabricated using DMLS technology as a single piece of metal, using the aluminium alloy, AlSi10Mg, as shown in the **Figure 7** [40]. One of the advantages of using 3D printing technique over the conventional fabrication technique is to eliminate the layers' gap and alignment problems, if made using milling, due to the accuracy of DMLS. The antenna fabricated consists of four layers: a corporate-feed waveguide network at the lowest layer, an aperture plate, a cavity plate and a radiation slot plate at the top-most layer.

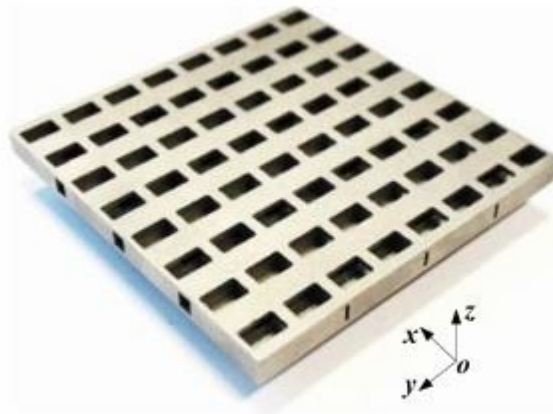


Figure 7: Prototype of the 3D printed antenna array [40]

The array was fed with a standard sub-miniature version A (SMA) connector and achieved an antenna efficiency of more than 80% over a wide bandwidth of 1.9 GHz, in the 15.0 GHz band, with a VSWR value below 2 over the bandwidth of interest. The obtained results verified that 3D metal printing is an easy and efficient way for realizing complex and multilayer waveguide antenna arrays.

**3D conformal slotted waveguide antenna array:** To address a real world complex antenna design, the authors of the publication [41], designed and fabricated a slotted waveguide antenna, with a conformal shape as shown in **Figure 8**. The antenna was fabricated in AlSi10Mg alloy using DMLS. The antenna has been fed through a perpendicularly conformal waveguide array composed of centrally inclined slots. With the average surface roughness at 17  $\mu\text{m}$ , no post-processing has been performed on the printed antenna. The geometrical inaccuracies, including surface roughness as well as deviations of the printed component from the design, were cited as the main reason for discrepancies between the measured and the simulated antenna results.



Figure 8: 3D Conformal slotted waveguide antenna array [41]

The antenna was printed with an orientation of  $45^\circ$  with respect to the build platform, which could be another reason for the differences between the simulated and measured results. This assumption is based on the findings of [42], where the author has stressed the importance of build orientation on the mechanical properties, such as tensile strength, surface roughness and fatigue limit of the DMLS printed components. According to those findings, the samples deviate in dimension from the design mainly in the  $90^\circ$  and  $45^\circ$  build orientation (with respect to the build platform), partly due to layer orientation, but also due to surface roughness, which is found to be higher for the  $90^\circ$  and  $45^\circ$  build orientations. As for electromagnetism, whenever the amplitude of the surface roughness is higher than the skin depth of the microwave components, scattering of the waves occurs and the performance of the component deteriorates. In that case, to avoid such geometrical inaccuracies, the printed microwave component should be orientated at an angle to minimize surface roughness, without compromising the tensile strength of the overall structure.

Furthermore, to detach the loosely attached material particles from the printed component, and to minimize the surface roughness of the printed microwave component, surface treatment techniques should have been used, to avoid discrepancies in the results.

**Lightweight perforated waveguide horn antenna:** Utilizing the strength of 3D printing, which is not only in designing of complex structures but also in fabricating lightweight structures, in [43], the perforation technique has been used for fabricating a lightweight horn antenna. In the work, an X-band pyramidal horn antenna that employs this technique

has been manufactured using DMLS as shown in **Figure 9**, for the applications where weight is at a premium.

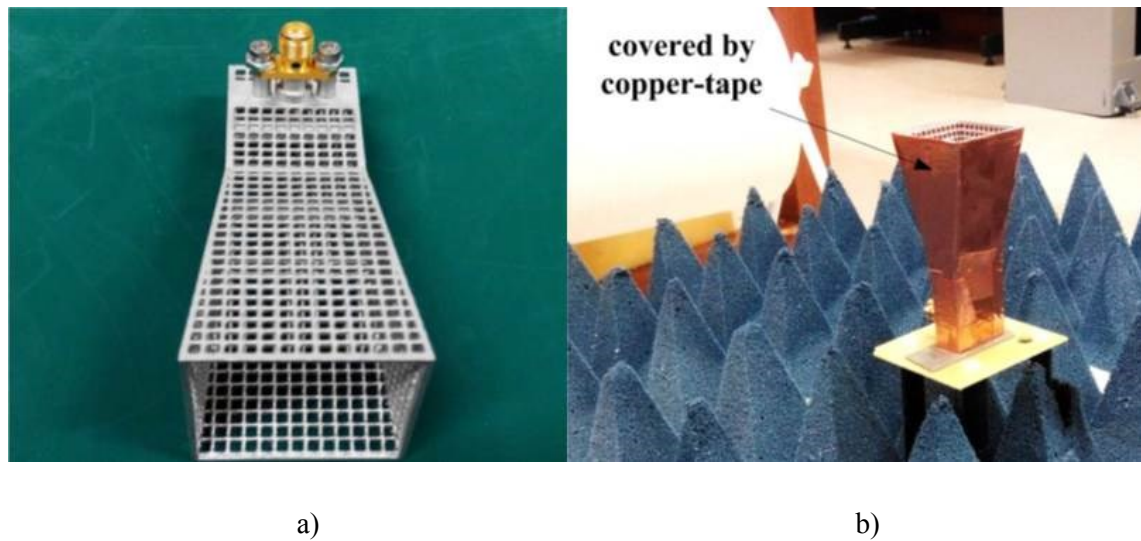


Figure 9: 3D metal-printed horn antenna, (a) perforated prototype (b) horn antenna under test [43]

This research in [43], exploits the ability of DMLS in printing thin-walled structures, which has recently received considerable attention; for fabricating lightweight structures. The results show the reduction in the weight of the antenna structure to be around two-thirds of the total weight of the equivalent complete antenna structure. In this research, the numerical analysis software Ansys HFSS (High Frequency Structure Simulator) has been used to analyse the E-field distribution. The simulations were performed on the effect of energy stored within the horn antenna versus the increasing perforation density in the grid walls of the antenna. Results prove that most of the energy was stored within the perforated walls of the horn antenna, showing it to be a promising approach for achieving lightweight based RF components and antennas.

The results prove that both the design and the manufacturing approach are simple and promising for achieving lightweight waveguide-based RF components and antennas. However, the perforation performed on the outer surface of the antenna can make the antenna structure prone to damage, resulting in inconsistent results, if employed in real life applications. In that regard, mechanical testing of lightweight 3D metal printed antenna is highly recommended, to complement the RF results and to safeguard its usage for real world applications in the near future.

## 2.3 SUMMARY

3D printing technology, in particular, metal printing, has started to show great potential in providing an efficient solution towards the fabrication of complex shaped microwave components in near future. However, there have been some concerns regarding geometric inaccuracies, as well as the surface finish of the printed component, which could potentially degrade the performance of the electromagnetic components. In this chapter a brief overview of available AM technologies in industry and its foremost application in fabrication of microwave components, have been highlighted.

*\*\* Publication arises from this chapter has been presented in:*

*12<sup>th</sup> European Antenna & Propagation Conference (EuCAP), London, UK, April/2018*

## 2.4 REFERENCES

1. H. Kodama, "Automatic method for fabricating a three-dimensional plastic model with photo-hardening polymer", *Review of Scientific Instruments*, vol. 52, no. 11, pp. 1770-1773, 1981.
2. C. Hull, "Method and apparatus for production of three-dimensional objects by stereolithography", *US Patent no. 4,575,330*, 1984.
3. C. R. Deckard, "Method and apparatus for producing parts by selective sintering", *US Patent no. 4863538*, 1986.
4. M. Shellabear, O. Nyrhilä, "DMLS – Development history and state of the art", *2004 LANE conference, Erlangen, Germany, September/ 2004*.
5. ISO/ASTM 52900:2015, (Online) "Additive manufacturing - General principles - terminology", (<https://www.iso.org/obp/ui/#iso:std:iso-astm:52900:ed-1:v1:en>), [Accessed: 9<sup>th</sup> January 2016].
6. E.C. Santos, M. Shiomi, K. Osakada, T. Laoui, "Rapid manufacturing of metal components by laser forming", *International Journal of Machine Tools and Manufacture*, vol. 46, no. 12-13, pp. 1459-1468, 2006.
7. Loughborough University, (Online) "Additive Manufacturing Research Group – About Additive Manufacturing", (<http://www.lboro.ac.uk/research/amrg/about/>), [Accessed: 17<sup>th</sup> November 2017].
8. H. Miura, T. Osada, H. Ishibashi, K. Okawachi, M. Uemura, M. Fujita, N. Arimoto, "Development of selective laser sintering for titanium alloy powder— 3rd report", *Funtai Oyobi Fumatsu Yakin/Journal of the Japan Society of Powder and Powder Metallurgy*. vol. 55, no. 10, pp. 738–742, 2008.
9. E. Chlebus, B. Ku'znicka, T. Kurzynowski, B. Dybała, "Microstructure and mechanical behaviour of Ti-6Al-7Nb alloy produced by selective laser melting", *Journals of Materials Characterization*, vol. 62, no. 5, pp. 488–495, 2011.
10. J. Lind, J. Hanninen, J. Kotila, O. Nyrhila, T. Syvanen, "Rapid manufacturing with direct metal laser sintering". *Proceedings of Material Research Society*, vol. 758, pp. 17-22, 2003.
11. B.V Krishna, S. Bose, A. Bandyopadhyay, "Low stiffness porous Ti structures for load-bearing implants", *Acta Biomaterialia*, vol. 3, no. 6, pp. 997–1006, 2007.

12. J. Mazumder, J. Choi, K. Nagarathnam, J. Koch, D. Hetzner, "The direct metal deposition of H13 tool steel for 3-D components", *The Journal of The Minerals, Metals & Materials Society*, vol.49, no. 5, pp 55–60, 1997.
13. J.O. Milewski, G. K Lewis, D.J. Thoma, G.I Keel, R.B Nemec, R. A Reinert, "Directed light fabrication of a solid metal hemisphere using 5-axis powder deposition", *Journal of Materials Processing Technology*, vol. 75, no. 1-3, pp. 165–172, 1998.
14. K. M. B. Tamingier, R. A. Hafley, "Electron beam freeform fabrication: a rapid metal deposition process", *Proceedings of the 3<sup>rd</sup> Annual Automotive Composites Conference, Troy, MI., September/2003*.
15. O.L.A Harrysson, O. Cansizoglu, D.J. Marcellin-Little, D.R Cormier, H.A West, "Direct metal fabrication of titanium implants with tailored materials and mechanical properties using electron beam melting technology", *Materials Science and Engineering: C*, vol. 28, no. 3, pp. 366–373, 2008.
16. B. Wysocki, P. Maj, R. Sitek, J. Buhagiar, K. J. Kurzydłowski, W. Świąszkowski, "Laser and electron beam additive manufacturing methods of fabricating Titanium bone implants", *Journals of Applied Sciences*, vol. 7, 2017.
17. S. Zhang, C. C. Njoku, W. G. Whittow, J. C. Vardaxoglou, "Novel 3D printed synthetic dielectric substrates", *Microwave and Optical Technology Letters*, vol. 57, no. 10, pp. 2344-2346, Oct/ 2015.
18. E. Kohler, S. Rahiminejad and P. Enoksson, "Evaluation of 3D printed materials used to print WR10 horn antennas", *27<sup>th</sup> Micromechanics and Microsystems Europe Workshop IOP Publishing Journal of Physics: Conference Series*, pp. 1-5, 2016.
19. M. Mirzaee, S.Noghanian, L. Wiest, and I. Chang, "Developing flexible 3D Printed antenna using conductive ABS materials", *IEEE International Symposium on Antennas and Propagation & USNC/URSI National Radio Science Meeting*, pp. 1305-1309, Vancouver, BC, Canada, July/2015.
20. J.A. Andriambeloson, P.G. Wiid, "A 3D-Printed PLA Plastic Conical Antenna with Conductive-Paint Coating for RFI Measurements on MeerKAT site", *2015 International Conference on Electromagnetics in Advanced Applications (ICEAA), Turin, Italy, September/2015*.

21. M. Vorst, J. Gumpinger, “Applicability of 3D printing techniques for compact Ku-band medium/high-gain antennas”, *10<sup>th</sup> European Conference on Antennas and Propagation (EuCAP), Davos, Switzerland, 2016*.
22. A. von Bieren, E. De Rijk, J.-P. Ansermet and A. Macor, “Monolithic metal-coated plastic components for mm-wave applications”, *39<sup>th</sup> International Conference on Infrared, Millimeter, and Terahertz waves (IRMMW-THz), Tucson, USA, September/2014*.
23. S. Moscato., R. Bahr, T. Le, M. Pasian, M. Bozzi, L. Perregrini, M. M. Tentzeris, “Infill dependent 3D-Printed material based on NinjaFlex filament for antenna applications”, *IEEE Antennas and Wireless Propagation Letters, vol. 15, pp. 1506-1509, 2016*.
24. K. Gnanasekaran, T. Heijmans, S. van Bennekom, H. Woldhuis, S. Wijnia, G. de With, H. Friedrich, “3D printing of CNT- and graphene-based conductive polymer nanocomposites by fused deposition modeling” *Applied Materials Today vol. 9, pp. 21-28, 2017*.
25. M. I. M. Ghazali, E. Gutierrez, J. C. Myers, A. Kaur, B. Wright, P. Chahal, “Affordable 3D Printed Microwave Antennas”, *IEEE 65<sup>th</sup> Electronic Components and Technology Conference (ECTC), pp. 240-246, San Diego, CA, USA, 2015*.
26. J.M. Floch, B. E. Jaafari, A. E. S. Ahmed, “New compact broadband GSM/UMTS/LTE antenna realised by 3D Printing”, *2015 European Conference on Antennas and Propagation (EuCAP), Lisbon, Portugal, May/2015*.
27. S. Jun, B. Sanz-Izquierdo and M. Summerfield, "UWB antenna on 3D printed flexible substrate and foot phantom", *2015 Loughborough Antennas & Propagation Conference (LAPC), Loughborough, UK, 2015*.
28. K. Belvin, “(Master's Thesis) Examining 3D Printed antennas for spaced based applications”, *University of New Mexico, May/ 2015*.
29. W. J. Otter, N. M. Ridler, H. Yasukochi, K. Soeda, K. Konishi, J. Yumoto, M. Kuwata-Gonokami, S. Lucyszyn “3D printed 1.1 THz waveguides”, *IET Electronic Letters vol. 53, no. 7, pp. 471–473, 2017*.
30. J. Yang, J. Zhao, C. Gong, H. Tian, L. Sun, P. Chen, L. Lin, W. Liu, “3D printed low-loss THz waveguide based on Kagome photonic crystal structure”, *Optics Express, vol. 24, no. 20, pp. 22454-22460, 2016*.
31. M. D’Auria, W. J. Otter, J. Hazell, B. T. W. Gillatt, C. Long-Collins, N. M. Ridler, S. Lucyszyn, “3-D printed metal-pipe rectangular waveguides,” *IEEE*

- Transactions on Components, Packaging and Manufacturing Technology*, vol. 5, no. 9, pp. 1339–1349, 2015.
32. M. Liang, X. Yu, R. Sabory-García, W.-R. Ng, M. E. Gehm, H. Xin, "Broadband electronically beam scanning structure using Luneburg lens", *IEEE International Microwave Symposium, Seattle, WA, USA, June/2013*.
  33. G. Du, M. Liang, R. Austrebert, S.-Garcia, C. Liu, H. Xin, "3-D Printing implementation of an X-band Eaton lens for beam deflection", *IEEE Antennas and Wireless Propagation Letters*, vol. 15, pp. 1487-1490, 2016.
  34. F. Pivit, E. Doumanis, D. Kozlov, M. Gueye, M. Gimersky- "Compact 60-GHz Lens Antenna with Self-Alignment Feature for Small Cell Backhaul", *2017 IEEE-APS Topical Conference on Antennas and Propagation in Wireless Communications (APWC), Verona, Italy, p.p. 280-283, September/2017*.
  35. S. Zhang, "Design and fabrication of 3D-printed planar Fresnel zone plate lens", *IET Electronics Letters*, vol. 52, no. 10, pp. 833-835, May 2016.
  36. M. Liang, W.-R. Ng, K. Chang, K. Gbele, M. E. Gehm, H. Xin, "A 3-D Luneburg lens antenna fabricated by polymer jetting rapid prototyping", *IEEE Transactions on Antennas and Propagations*, vol. 62, no. 4, pp. 1799-1807, 2014.
  37. A. Macor, E. de Rijk, S. Alberti, T. Goodman, J.-P. Ansermet, "Three-dimensional stereolithography for millimeter wave and terahertz applications", *Review of scientific instruments*, vol. 83, no. 4, pp. 046103, 2012.
  38. Z. Wu, M. Liang, W.-R. Ng, M. Gehm, H. Xin, "Terahertz horn antenna based on hollow-core electromagnetic crystal (EMXT) structure," *IEEE Transactions on Antennas and Propagation*, vol. 60, no. 12, pp. 5557–5563, 2012.
  39. C. Garcia, R. Rumpf, H. Tsang and J. Barton, "Effects of extreme surface roughness on 3D printed horn antenna," *IET Electronic Letters*, vol. 49, no. 12, pp. 734 - 736, 2013.
  40. G.-L. Huang, S.-G. Zhou, T.-H. Chio, T.-S. Yeo, "3-D metal-direct-printed wideband and high-efficiency waveguide-fed antenna array", *IEEE MTT-S International Microwave Symposium*, pp. 1-4, Phoenix, AZ, USA, May/ 2015.
  41. A. G.-Martin, Y. Quere, E. Rius, L. Fourtignon, C. Person, G. Lesueur, T. Merlet, "Design and manufacturing of a 3-D conformal slotted waveguide antenna array in Ku-band based on Direct Metal Laser Sintering" *2016 IEEE Conference on Antenna Measurements & Applications (CAMA), NY, USA, Oct/2016*.

42. W. D. Vree, “(Master’s Thesis) On the influence of build orientation on the mechanical properties of direct metal laser sintered (DMLS) Ti-6Al-4V flexures”, *Technical University of Delft, April/ 2016*.
43. G-L Huang, S.-G Zhou, C.-Y.-D. Sim, T-H. Chio, T. Yuan, “Lightweight perforated waveguide structure realized by 3-D Printing for RF applications” *IEEE Transactions on Antennas & Propagation, vol. 65, pp. 3897 – 3904*.

# 3 CHAPTER 3

## 3D METAL PRINTED SIERPINSKI GASKET ANTENNA: DESIGN, CHALLENGES AND SOLUTION

### ABSTRACT

The design, simulation, and fabrication of the first ever 3D metal printed 2<sup>nd</sup> iteration Sierpinski gasket antenna, with multiple resonance characteristics is reported in this research. The antenna is fabricated with the Titanium alloy Ti-6Al-4V, using the DMLS technique on an EOS M280 system. RF considerations, such as the Hohlfeld-Cohen-Rumsey principle (“Ring width effect”), as well as mechanical considerations, such as antenna mounting issues and support structures required for overhanging parts of a design in 3D printing, are also thoroughly studied and discussed. The research also presents the performance evaluation of a 3D metal printed antenna, as the surface roughness is gradually reduced using different surface treatment techniques. Following an initial assessment, the surface roughness has been reduced gradually, in stages, using surface treatment techniques, initially wet blasting and later, polishing. To monitor the surface morphological changes on the surface antenna, an Optical Microscope (OM) and a White Light Interferometer (WLI) have been used. Finally, both the realised gain and the return loss ( $S_{11}$ ) are measured, to track the RF performance changes for the 3D metal printed antenna, as a function of reducing surface roughness.

### 3.1 INTRODUCTION

With the advent of 3D printing, complex parts, which were extremely difficult or in some cases impossible to manufacture at all using conventional tooling methods, can now be built with a short lead time, with good reliability and the high level of precision [1]. In a very short span of time, application for AM have been found in almost all leading engineering areas, such as aerospace, automotive, medical fields, consumer products and military, as described in **Chapter 1**. 3D parts can now be fabricated directly from CAD data, sliced into stacks or in a layer-by-layer fashion, without the need to plan the transformation from 2D into 3D, which would otherwise be required, if starting with a

planar design. On the other hand, 3D printing has its own process requirements, which will be outlined later.

Recently, there has been a significant growth in the research field of 3D printing for RF/Microwave components, as detailed in **Chapter 2**. These 3D components can be fabricated either by using laser-based, layer-by-layer SLA polymer or by using DP (Direct Printing), where digital (discrete) patterns are impressed upon a substrate. When the physical structure is fabricated using non-conducting thermoplastics, such as Acrylonitrile Butadiene Styrene (ABS), it is then usually metallized or painted in order to make the printed electromagnetic component functional. Uniform coating or selective coating, also known as printing, adds an extra processing step over standard polymer printing and also has to be done very precisely, to achieve acceptable electromagnetic performance from the component.

This research presents the fabrication of the first ever 2<sup>nd</sup> iteration, 3D metal printed, Sierpinski gasket antenna for wireless applications, using DMLS, on an EOSINT M280 [2]. In earlier published research works, DMLS has already been used to manufacture microwave components, to name a few, a waveguide fed antenna array, as well as a perforated lightweight horn antenna, while EBM has been used to manufacture a 3D printed metallic horn antenna. Both the DMLS and EBM manufactured microwave components have been produced as early demonstrations of the power of AM, using metallic materials. The selection of the Sierpinski gasket antenna has been done as another early example of 3D printing, where the geometry is more complex than the other, previously manufactured components. The aim is to push the limits of 3D metal printing in complex antenna manufacturing. To help realize this goal, Computer Simulation Technology (CST) [3], the microwave simulation software, was used to provide simulation results.

The CST simulation played an important role in the design and development of the final solution. The final design CST files were directly exported in .STI format, which is compatible with, and can be used directly by, the 3D metal printing software. However, 3D metal printing manufacturing also imposes some unexpected restrictions on the antenna design, which will be outlined later in the thesis. These restrictions meant that several iterations were required to create the initial antenna design and to produce the

final prototype, each stage of which required careful analysis through CST simulation. The final role of CST was in both confirming and benchmarking the measured results. The variation between the measured and simulation results required further investigation of the measurement process and a detailed examination of the antenna construction.

### **3.2 SIERPINSKI GASKET ANTENNA**

The Sierpinski gasket is named after the Polish mathematician Sierpinski, who described some of the main properties of a fractal shape in 1916 [4]. In this case, the discontinuities (or fractals), increase the perimeter of the material, due to which the antenna achieves multiple electrical lengths, to receive and transmit electromagnetic radiation within a specified area or surface, which lead to multiband behavior [5]. Historically, this feature was exploited a lot in 2D antenna designs, but in this research, a 3D extension is presented. Instead of triangles, tetrahedrons are arranged in a self-symmetric fashion, with the ability to receive (or transmit) multiband RF signals, as different parts of the antenna are self-symmetric at multiple scales. Self-similar and other related fractal-shaped antennas have attracted much research, thanks to their geometrical properties, to produce small, multiband antennas, high-directivity antennas, low side-lobe antennas and under-sampled array antennas [6]-[10].

There are two different methods to generate the Sierpinski gasket geometry: 1) the Multiple Copy Method and 2) the Decomposition Method. In the Multiple Copy Method, an equilateral triangle is generated and then two more copies of the first triangle are attached to the corners of the original triangle. This step is repeated until the size of the monopole/fractal equals the length of the design wavelength. In the Decomposition Method, one designs an equilateral triangle encompassing the entire geometry, with the height of the antenna equal to the wavelength of the monopole. Midpoints of the sides of the triangle are then joined together in the design, now creating four internal triangles, the center one of which will be hollow, and the outer three triangles will be solid. Each new triangle side length is half the side length of the original triangle. Each iteration of the Decomposition Method yields this same scaling by a factor of two. With each scale realized, a new resonant frequency is obtained, defined by the wavelength related to the scale factor of a new triangle.

Considerable research work has been done with respect to a 2D version of the Sierpinski gasket antenna. In those publications, the antennas are shown to have self-symmetries that help to achieve multiband characteristics, while also possessing miniaturized characteristics. However, to the best of the authors' knowledge, a 3D Sierpinski antenna has only been built twice [11]-[12]. Anguera J, et al, presented a very light-weight, fractal-shaped, Sierpinski-carpet, cylindrical hole, monopole antenna, fabricated with metallized foam, where the antenna possessed multiband characteristics [11]. In [12], the first 3D full-metal version of a Sierpinski gasket antenna was manually fabricated using brass as the fabricating material. The antenna possessed multiband characteristics; however, differences between computational and measured results could be easily seen, which author cited to have occurred due to geometrical inaccuracies during the manual fabrication of this complex shaped antenna. The manual fabrication challenges mean that the differences between the measured and simulation results will increase, if the radiating monopole structure were designed for a higher frequency, because of the challenges posed by the more compact structure.

### 3.3 ANTENNA DESCRIPTION

The antenna was fabricated using the DMLS machine, EOSINT M280, with the Titanium alloy Ti-6Al-4V as the conducting material, a material commonly used in medical and flexure based applications, due to its strength and biocompatibility [13] [14]. Even though the electrical conductivity of this alloy is  $5.61 \times 10^5$  S/m, lower than Copper  $5.87 \times 10^7$  S/m or Aluminium  $3.56 \times 10^7$  S/m, but the differences in the CST simulation results between the alloy and even a perfect electrical conductor (PEC), was negligible for both antenna gain and the reflection loss. Even though the material selection does have an impact on the efficiency of the microwave component, this is beyond the scope of this research.

The choice of the material for the fabrication of antenna is awkward, as will be seen later; however, the alloy type does offer properties of toughness and high strength, which leads to joints between each tetrahedron, which are twice as strong as similar aluminum joints. The alloy used also possesses properties like corrosion resistance and a high strength-to-weight ratio, as it is 45% lighter than the steel [15].

The antenna designed is a 2<sup>nd</sup> iteration Sierpinski gasket antenna having a large side length of 46.7 mm corresponding to the frequency of 7.5 GHz. The selection of operating frequency was done keeping in mind the 3D manufacturing height constraints and the available Vector Network Analyser (VNA) measurement range (up to 20 GHz). Moreover, the work presented will serve as a proof of concept for the successful fabrication of this and other complex-shape antennas and, for this antenna, can also be replicated for different wavelengths, for future multiband applications. Following the rules of 3D printing, one should acknowledge that even though the Sierpinski fractal design may look simple, but it is complex at the same time. It consists of an arrangement of stacked pyramids one-upon-another, to form a 3D geometry. A rectangular copper clad PCB ground plane, of 160 mm x 100 mm, with 1 mm thickness, has been used to serve as a finite ground plane to the printed antenna as shown in **Figure 10**.



Figure 10: Sierpinski gasket antenna fabricated using DMLS technology on Ti-6Al-4V

To energise the antenna, a straight panel mount N-type connector has been glued with the help of conductive silver epoxy adhesive, having volume resistivity  $< .001\Omega\text{-cm}$  [16].

## 3.4 MECHANICAL CONSIDERATIONS

3D metal printing does not lend itself to the easy fabrication of the microwave components. There are a few key mechanical considerations, which should always be taken into account prior to the print. A few of them are listed in the following section.

### 3.4.1 “RING WIDTH” EFFECT

Unlike a 2D realization, the 3D Sierpinski gasket antenna cannot be realized with infinitely small joints. For this reason, to print an antenna in an upside-down orientation, a minimum of 1.90 mm base diameter (0.95 mm base radius) was required for the successful fabrication of the antenna. This value for the base diameter was chosen based on prior experience in this area, to achieve the 3D design without any metal drooping occurring, which in this case was utilized to successfully build the antenna. Furthermore, to connect the antenna with a feeding circuitry, the base diameter should be big enough to facilitate soldering, if required. The base diameter of the Sierpinski gasket antenna forms a ring-like shape, due to which the effect on the RF performance of the antenna, from increasing or decreasing the width of the ring, has been named the “ring width effect” in this research.

The ring width of the Sierpinski gasket antenna possesses a significant importance from the perspective of multiband or frequency invariant features. V. H. Rumsey, in the early sixties, established what is now known as Rumsey’s Principle and the current notion of broadband antennas. According to Rumsey’s Principle, if the geometry of an antenna is solely the function of an angle, then the antenna parameters will be independent of the frequency [17]. Therefore, as was done in this research, increasing the height to the repetitive structure would cause no change to the antenna parameters. However, in 1999 Hohlfeld and Cohen proposed an extension to Rumsey’s Principle, known as the HCR (Hohlfeld-Cohen-Rumsey) condition, stating that self-symmetry is one of the underlying requirements [18]. For an antenna to be frequency independent, it needs to be symmetric along the origin as well, where the origin is the antenna feeding point. However, the HCR condition will not be considered further in this work, as the flare angle will remain fixed at approximately  $60^\circ$ , with the slight variation caused by the ring width having little impact in simulations.

All the research work mentioned earlier stressed the importance of the parametric value towards the feeding point of the monopole antenna, as it dictates the impedance bandwidth of the antenna, especially in a case when the geometry of an antenna is a function of an angle. In that regard, CST simulations were carried out on varying the ring width parameter of the antenna as shown in **Figure 11**. Through the simulation, it was observed that even a minor increase in the parametric value of ring width radius ( $r$ ) causes an antenna to possess a wider bandwidth and leads the antenna resonance frequency dip to be shifted towards the higher frequency bands. With the shift being significant towards the higher frequencies, which in this case is at fundamental frequency of 8.4 GHz.

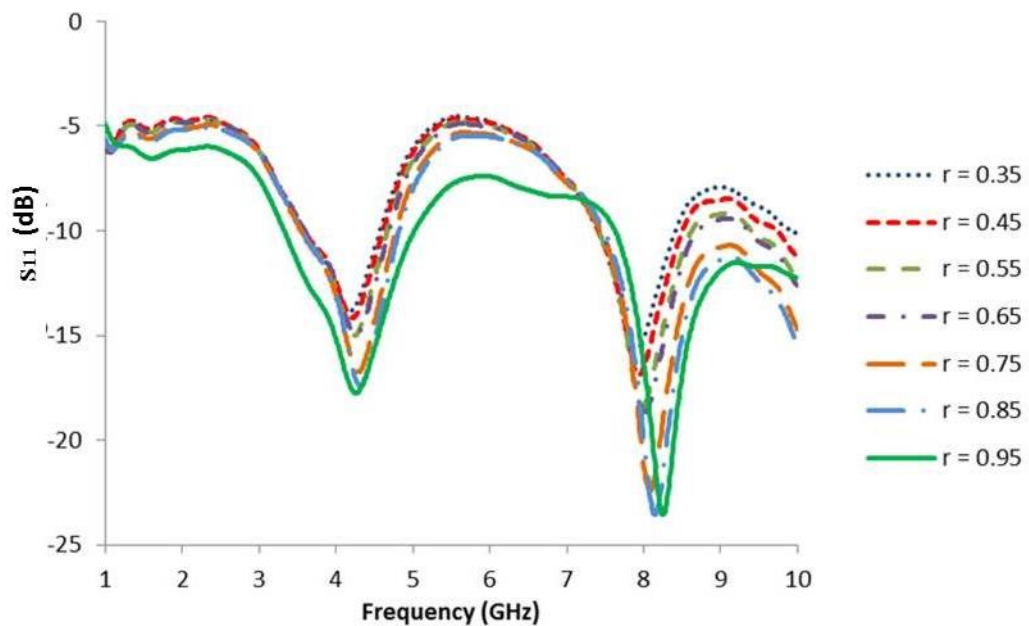


Figure 11: Simulated variation in frequency bands due to ring width effect (all dimensions in mm)

Note also that the ring width may be further increased when soldering or conductive epoxy is applied to the feed point used to mount the antenna onto the feed. This was observed while analysing the measured results, as it further adds to discrepancies in the results. In order to deal with this, should it be a problem, the antenna geometry can be tuned accordingly and can be also designed for other wavelengths.

### 3.4.2 STRUCTURAL AMBIGUITY

A three-dimensional Sierpinski gasket antenna is an arrangement of tetrahedrons in a self-symmetric fashion stacked one upon another, which gives the antenna multiband characteristics. However, in practice, a 3D Sierpinski gasket antenna cannot be realized

with infinitely small joints (unlike a 2D realization) to be mechanically rigid, for example when connecting tetrahedrons in the same layer. In practice, one tetrahedron should overlap the adjacent one, as shown in **Figure 12**. This was confirmed during the visual inspection of the printed antenna, as it was observed that the triangular sides were not perfectly equilateral. This means that the surface area is no longer in the shape of an equilateral triangle, but is now simply an isosceles triangle, as only the two vertical straight edges of a single tetrahedron remain the same, albeit shorter than their design.

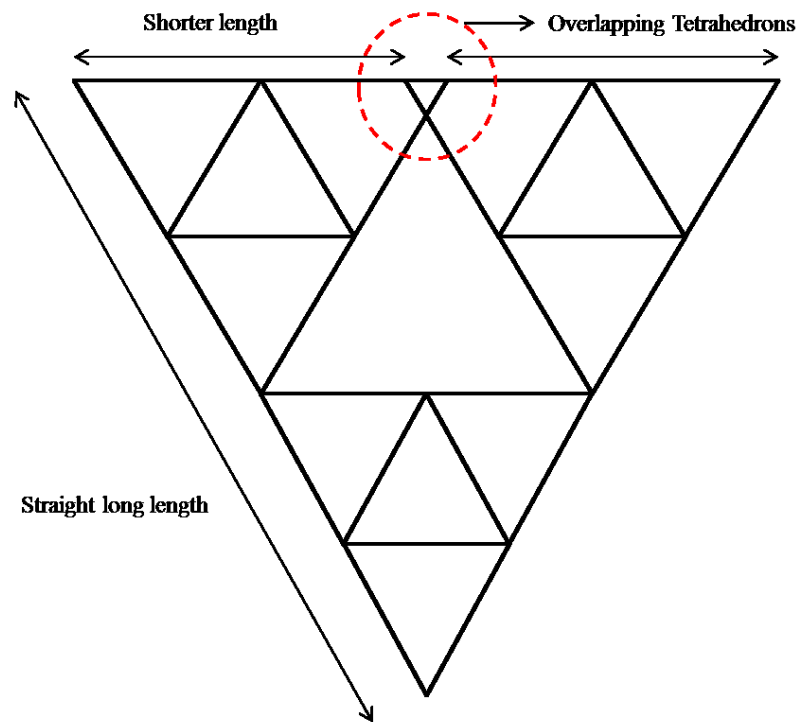


Figure 12: Illustration of overlapping tetrahedrons during the build

This length change affects the resonant frequency, but only in a small manner, as the variation in length is a small fraction of the total length in this case. However, it does not affect the multiband behavior of the antenna, as the structure is still self-symmetric.

### 3.4.3 BUILD ORIENTATION

Recent research has shown that build orientation plays an important role in influencing the construction time as well as the mechanical properties of the printed structure, such as tensile strength, residual stress, fatigue, as well as surface roughness, which can be important to RF performance. In [19] [20], the authors have emphasized the importance

of considering the build orientation of the test samples during the design process. It was concluded that construction (build) time and mechanical properties, such as tensile strength, surface roughness, and fatigue are highly dependent on the orientation of the build. In [20], mechanical properties of the printed structure, at three common build orientations of  $0^\circ$ ,  $45^\circ$ , and  $90^\circ$ , were assessed. The orientations are shown in **Figure 13**, where  $90^\circ$  is vertical and perpendicular to that of the build plate, whereas  $0^\circ$  is horizontal and parallel and,  $45^\circ$  means it is at an angle of  $45^\circ$  orientation with respect to the building platform. From that research, the author concluded that when printing a structure at an angle of  $90^\circ$ , the structure will possess lower tensile strength as well as fatigue compared to when the build orientation is either  $0^\circ$  or  $45^\circ$ . However, the build orientations of  $45^\circ$  and  $90^\circ$  also resulted in higher surface roughness compared to the other  $0^\circ$  orientation, which indicates a trade-off between surface roughness and other mechanical properties. Notwithstanding this, due to the complex geometry of the Sierpinski antenna, it was decided to choose a build orientation of  $90^\circ$ , with respect to the building platform, for the successful fabrication of the antenna.

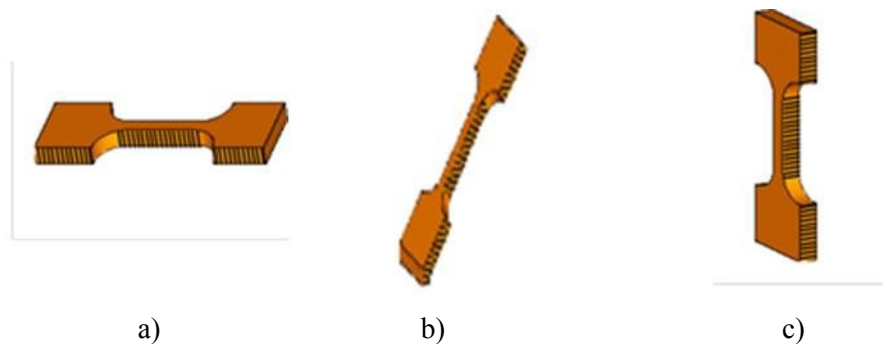


Figure 13: Possible orientation angles for the construction of 3D printed structure using DMLS technique a)  $0^\circ$ , b)  $45^\circ$ , c)  $90^\circ$  [20]

A detailed investigation of the influence of build orientation on the surface roughness and its subsequent impact on the performance of a 3D metal printed horn antenna has been covered in **Chapter 6**.

### 3.4.4 SUPPORT STRUCTURES

In the process of 3D printing, where models are built layer-by-layer, each layer is supported by previously printed layers underneath. In such a case, in order to print structures with shallow angles (with reference to the horizontal plane building plate) and

cantilever sections/ unsupported areas, extra support structures are needed to ensure the printed objects' integrity and print quality. This helps avoid droop deformation, caused by the combination of angles that are too shallow and the high temperatures required for DMLS. An industry rule-of-thumb with DMLS, is that support structures are needed if the structure has an overhanging angle ( $\theta$ ) less than a material-specific value. For example, with the Ti-6Al-4V alloy used here, the angle  $\theta=45^\circ$ , where the angle is again measured with respect to the building plate [21]. Ignoring the maximum overhanging support angle can lead to both overall object droop and also even a more localized, small-scale droop, the latter of which can appear as increased surface roughness. The overhanging angle varies from material-to-material, as well as from technique-to-technique, and also depends on other factors, such as manufacturing layer thickness (height), the width of the printed line, and the melt temperature, to ensure a high print quality. While the proposed Sierpinski gasket antenna fulfil the condition of the maximum overhanging angle for the alloy Ti-6Al-4V using DMLS, i.e.  $\theta=60^\circ$ , a conservative approach was taken and support structures were added, as shown in **Figure 14**.

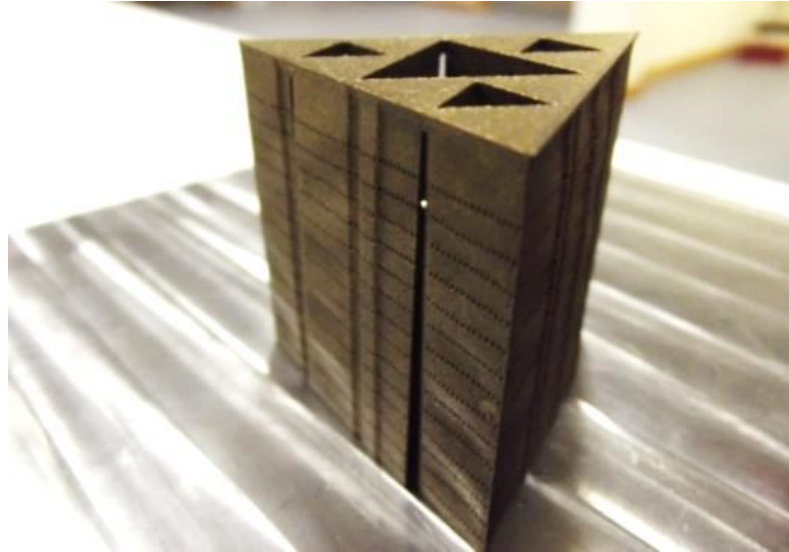


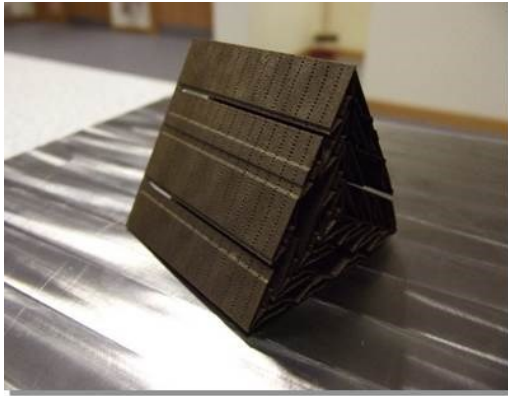
Figure 14: 3D metal printed Sierpinski gasket antenna with build support structure

The supports appear as individual pillars, constructed as a network of interconnected pieces, deliberately brittle for easy subsequent removal from the model. All 3D printed structures, which require supports, also require this extra post-processing removal step. These sacrificial structures are not a part of the original modeling file and hence are added later, according to the needs of the modelled design. Although the support structures can be regarded as a necessary evil, they also serve another useful purpose in heat dissipation during the printing process, which further greatly aids the build accuracy during post-processing, as discussed in detail in in this chapter later.

As the supports are sacrificial, the laser scan pattern during their build is not dense, compared to the rest of the build. Due to the intentionally scanned sparse hatching pattern, the support structure's build lacks structural strength and is easy to remove during the post-processing steps. Unlike metal printing, in the case of a polymer printed structure, there is an option to use support structures which are soluble in an aqueous solution. These kinds of supports not only help towards the successful fabrication of the structure, but also have minimum effect on the built surface roughness. In [22], the author has created a 3D polymer printed Hilbert cube, and built support structures, with the help of Polyvinyl alcohol (PVA), which is a low-temperature thermoplastic that is soluble in water to speed up the removal process. However, this is certainly not the case in metal printing. It should be added, however, that there are different types of support structures, which can

be built, depending on the requirement of the original design file, but discussion on them is beyond the scope of this research.

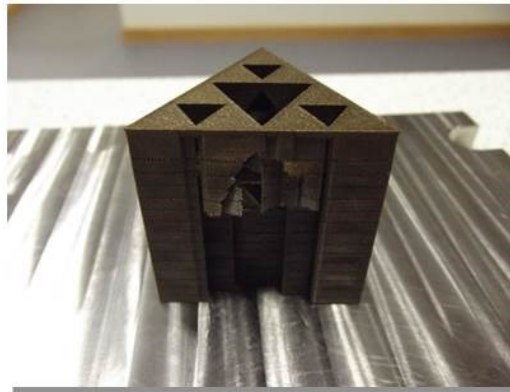
In order to further facilitate this process of removal, small holes were added in the CAD design of the support structures, prior to the print, which made it easier to remove during post-processing. As shown in **Figure 15**, the support structures were removed using needle nose pliers and metal spatulas.



a)



b)



c)

Figure 15: Sierpinski gasket antenna fabricated with support structures, a) post Wire-EDM, b) removal of support structures using long nose pliers, c) process of removal of supports

### 3.4.5 FEED POINT CHALLENGES

After the antenna fabrication, the next task was to connect the antenna circuitry to an N-type connector. One of the major challenges faced, as the antenna was fabricated from Titanium, was to establish an RF antenna connection with a feeding circuitry. The chosen

Titanium alloy (Ti-6Al-4V) is very difficult to solder, as the metal oxidizes readily as its temperature elevates during soldering, making it extremely difficult to solder an antenna onto a connector. For this reason, the antenna was glued onto the connector with the help of a conductive silver epoxy adhesive.

The challenge with the gluing process of achieving a consistent, perpendicular orientation was not easy. As can be seen in **Figure 16**, a laboratory clamp was employed to mount the antenna onto the feed, with varying success, exacerbated by the long curing times (over 24 hours in some cases).



Figure 16: Mounting an antenna onto the feed setup

Mounting an antenna in this way may lead to variation in the input impedance from one mounting to another, and hence, a better stable setup has been proposed in **Chapter 4**. That setup will reduce the variation in the input impedance, and potentially can eliminate the mounting process, especially if the designed geometry for 3D metal printing is a fractal-shaped or helical. This also minimizes losses, which may occur due to discontinuities in the joints from the mounting process. The variation in the inclination of the antenna due to the mounting set up in this case is quite small and shouldn't affect the performance of the antenna. As in [23], the author performed experiments on the variation of the input impedance due to changes in the tilt angle of a planar monopole antenna. The VSWR results in the research showed that the impedance bandwidth was the same for deviations from normal incidence ( $\theta$ ) of between  $0^\circ$  and  $22.5^\circ$ , while further increasing

the slant angle resulted in a significant reduction of bandwidth as illustrated in **Figure 17**. In practice, deviations in the tests to date were always only a few degrees from the normal.

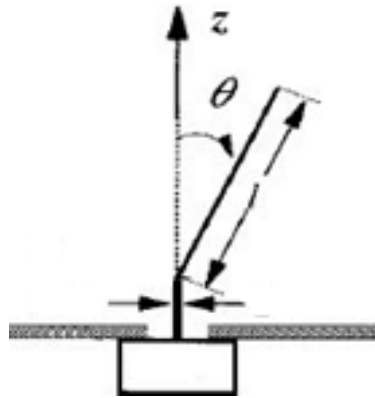


Figure 17: Configurations of monopole antenna [23]

Interestingly, the application of the conductive epoxy to mount the antenna onto the feeding circuitry was a difficult task also in terms of trying to control the location of the epoxy applied. Even a small trace of conductive glue between the antenna feed and the ground plane forms an electrical connection and can short the antenna as shown in **Figure 18**.

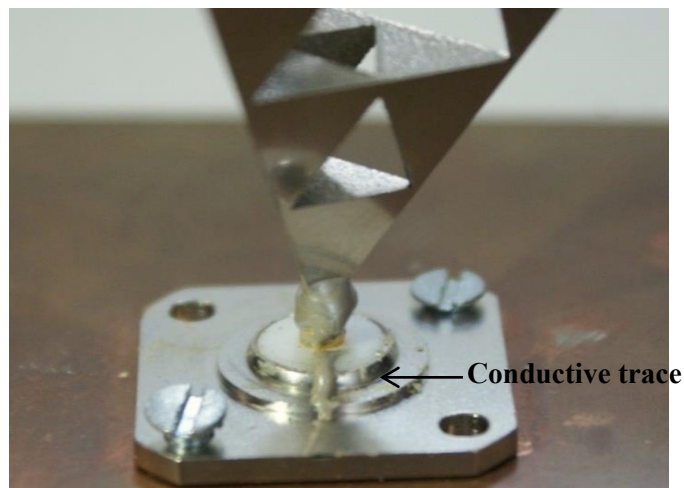


Figure 18: Conductive trace between antenna and ground due to epoxy

Moreover, the connection is not strong and can easily be removed without damaging the feed connection, with the help of a soldering iron's heat, if the glue has already dried.

## 3.5 POST-PROCESSING

Once the 3D metal Sierpinski antenna is printed using the EOSINT M280, it has to go through a series of post-processing steps in order to make the antenna more robust, to separate it from the build plate and support structures, both for aesthetics and for RF functionality.

The series of post-processing operations to carry this out include respectively: Heat treatment in a thermal vacuum chamber, guillotining with a wire EDM (Electrical Discharge Machining), long nosed pliers' removal of support structures (as detailed earlier), wet blasting using Aquablast 1515 followed by polishing using EcoMet™ Grinder Polisher [24][25]. In this research, the impact of the inherently present surface roughness on the 3D metal printed antenna will also be evaluated. One of the aims of this research is to see if roughness adds any significant losses to the performance of an antenna and if post-processing steps such as wet blasting and polishing bring an improvement in performance or if they are optional from an RF perspective.

### 3.5.1 HEAT TREATMENT

In the case of DMLS, which is a heat-based process, once the sintering process begins, the laser does not heat up the whole of the chamber homogeneously, due to which temperature gradients are formed at localized spots all over the printed structure. The high temperature gradient further leads to high thermal gradients and hence, residual stresses across the structure. Without support structures in place, heat can dissipate through the powder and break off the part or otherwise lead to warping. To reduce the residual stress and also the separate thermal stress from the printed component, heat treatment is performed. This brings physical stability to the 3D metal printed parts by reducing the internal stresses, which can otherwise cause brittleness, particularly at the isolated locations in the structures, and often leads to the sudden breakage or bending of the 3D metal printed parts [26].

The necessity of doing heat treatment and stress relief cycles vary from material to material (alloy to alloy). However, in this research heat treatment was performed on the

Ti-6Al-4V alloy antenna, in a controlled temperature environment at 635°C for 3.5 hours followed by uncontrolled cooling of the structure in a vacuum.

### 3.5.1.1 EDM (ELECTRICAL DISCHARGE MACHINING)

Prior to heat treatment, the antenna is too fragile to be separated from the build plate or its own support structures. Post heat treatment, once the thermal and residual stresses are reduced, the printed structure is then sufficiently robust so that the EDM technique could be used, in order to gradually separate the printed structure from the building platform. The EDM technique used here is Wire EDM, where the electrical discharge, via a dielectric medium in the breakdown, from one electrode (the wire) to another electrode (the part of the antenna to be cut) is a subtractive process used on metals that are too hard to machine using other techniques. EDM is used where the subtraction is too difficult and/or as can be the case with printed targets that are brittle to not be damaged by the cutting forces.

During the fabrication of a 3D printed structure, a common practice is to print a thin layer of the support structure on the top of building platform on which the 3D printed part should be printed. The support structure will avoid any kind of damage to the actual part, while the Wire-EDM is being performed.

### 3.5.1.2 POST HEAT TREATMENT SURFACE ANALYSIS

**Figure 19** and **Figure 20** show WLI images of the 3D metal printed Sierpinski gasket antenna top, horizontal surface (here the surface containing the Z-axis) and one of the inclined lateral faces (here a surface in the plane defined only by the X- and Y-axis) after heat treatment. As can be easily seen from the images in **Figure 19**, there are streamline grooves on the antenna top, horizontal surface profile. This profile is predominantly caused due to the hatching process whereas dense spherical-shaping roughness is visible along the lateral side of the antenna as shown in **Figure 20**. This could be due to the sticking of airborne sintering source powder to the newly welded lateral surface of the antenna, and also due to the partial sintering of particles to the surface of the part, as discussed in detail in **Section 3.6**. Adding to this, one more profound reason for the higher value of surface roughness on the lateral side of the antenna was due to the removal of support structures.

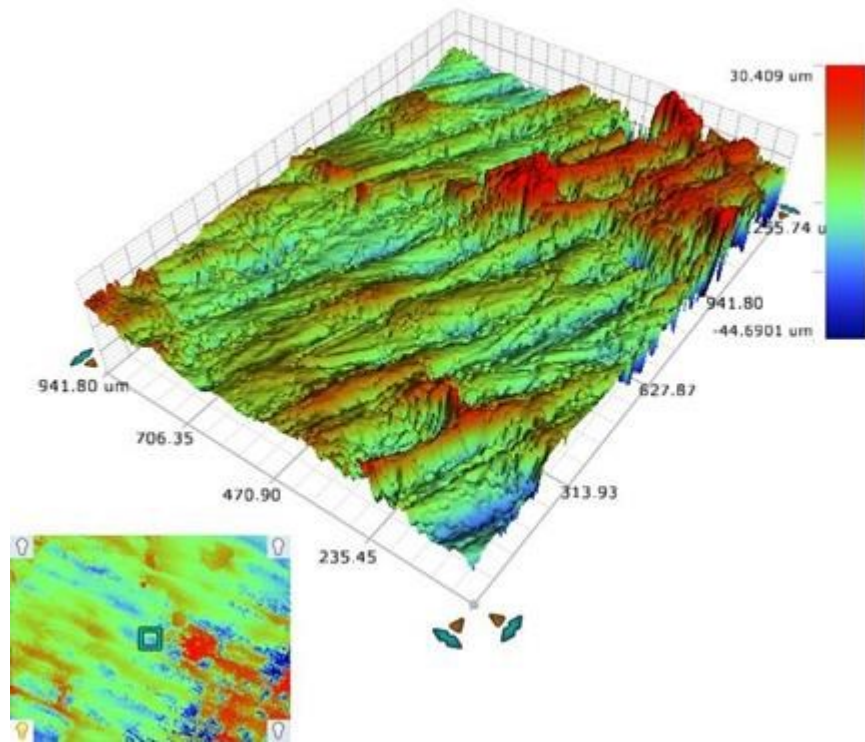


Figure 19: 5x WLI scan of 3D metal printed Sierpinski gasket antenna along Z-direction (top surface of the antenna) after heat treatment

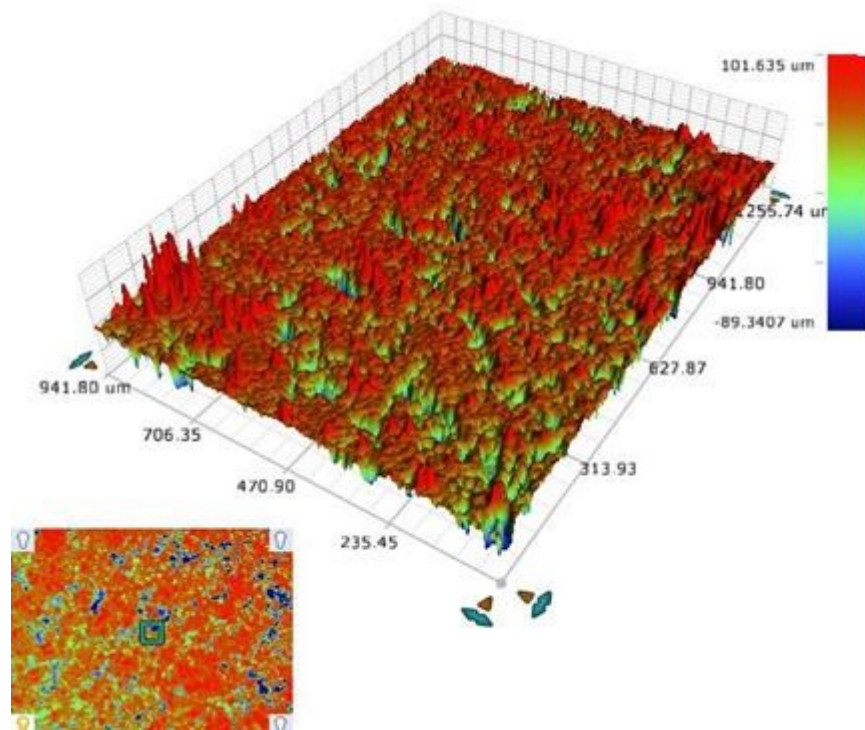


Figure 20: 5x WLI scan of 3D metal printed Sierpinski gasket antenna along XY-direction (lateral surfaces of the antenna) after heat treatment.

In order to analyze the impact on RF performance due to each post-processing stage, OM as well as WLI measurement and analysis, were done in tandem with RF measurements. The RMS value  $R_q$  of surface roughness on the top, flat surface was found to be  $7.7 \mu\text{m}$ , and that of the lateral surface to be  $14.47 \mu\text{m}$ . As the surface roughness increases the random scattering of electromagnetic waves, it is important to know that the geometry of the Sierpinski gasket antenna is such that most of the surface current flows through the lateral side of the antenna (triangular surface areas connected to the apex), which was also confirmed through the CST simulations as shown in the **Figure 21**.

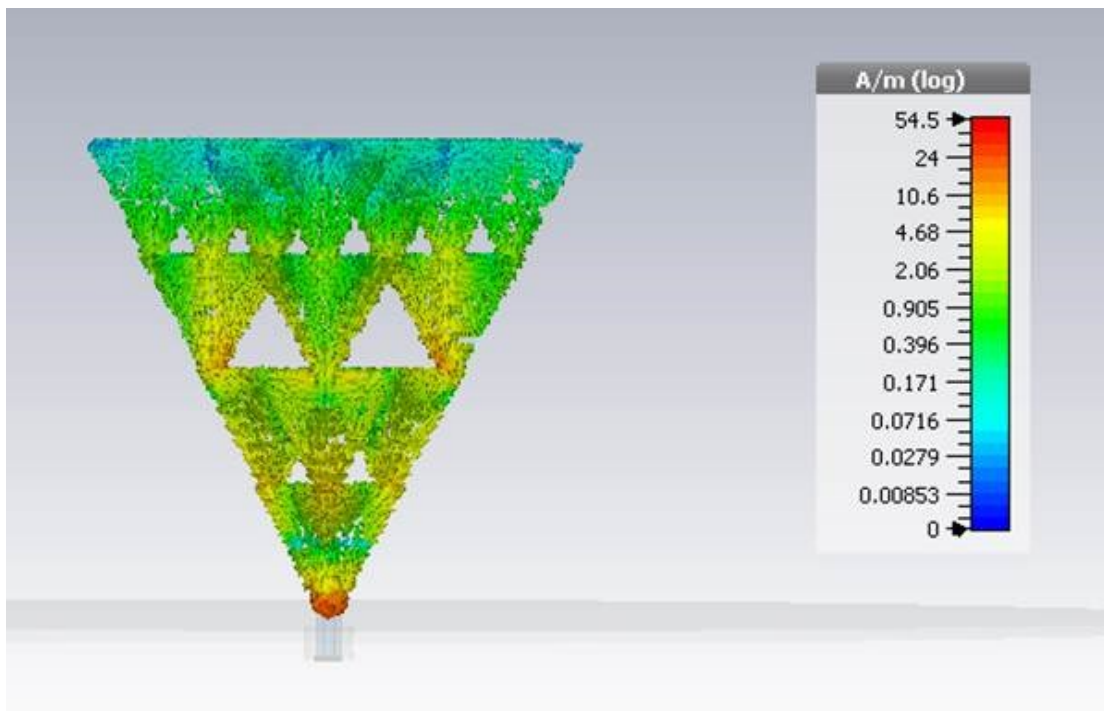


Figure 21: Visualization of surface current density of a Sierpinski gasket antenna using CST at 8.4 GHz

Due to this phenomenon, the surface roughness value on the lateral side of the antenna is more important than the surface roughness value on the top flat face of the antenna, where the surface current is at its minimum. The positioning of the surface current density has a great significance and has been exploited in depth in **Chapter 5** for designing a lightweight microwave component.

### 3.5.2 WET BLASTING

It is possible to reduce the surface roughness of the 3D printed structure in one step using polishing. However, in this work, the roughness was reduced in stages to examine the levels of roughness that affects the RF performance, due to which the staged reduction route was chosen. To achieve an intermediate reduction in surface roughness, while obtaining a consistent and repeatable surface finish the Sierpinski gasket antenna was first wet blasted using a Vixen Aquablast 1515. By wet blasting, all the loosely attached material particles from the powder bed were removed with the help of a highly accelerated, air-pressured, water-borne abrasive from the nozzle, as illustrated in **Figure 22** [27]. The sample was later dried with compressed air. The wet blasting process is also important for those RF components, where it is difficult to perform surface treatment on fully- or partly-enclosed inner faces of printed microwave components. One such example would be a horn antenna, where the maximum current density is enclosed inside the cavity, which can be wet blasted, but not polished, to reduce surface roughness. Although not producing as smooth a finish, the process of wet blasting also offers an alternative surface treatment option to polishing, by reducing the amplitude of surface roughness of the microwave component below its skin depth value, depending on the frequency of operation.

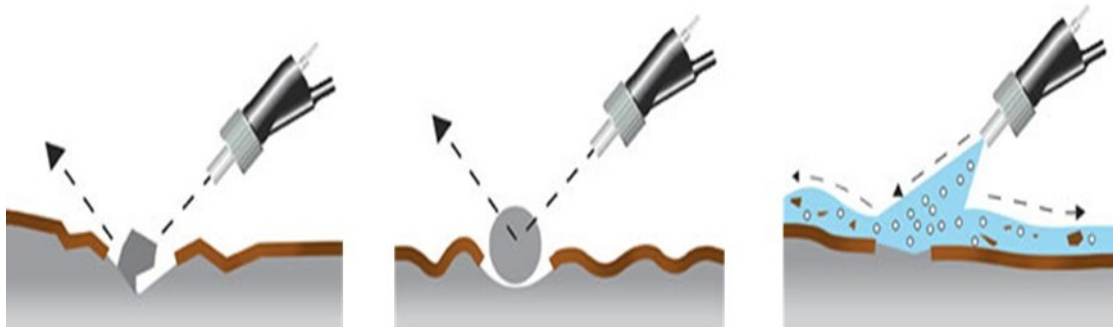


Figure 22: Process of wet blasting using abrasive media and compressed air to reduce the surface finish of the printed surface [27]

#### 3.5.2.1 POST WET BLASTING SURFACE ANALYSIS

Through 500x OM scans, shown in **Figure 23** it was concluded that all the loosely bound material particles, which were adhered to the faces of the antenna, were removed. The surface profile of both faces look almost identical, although the top, horizontal surface is still visibly slightly less rough, compared to its lateral counterpart.

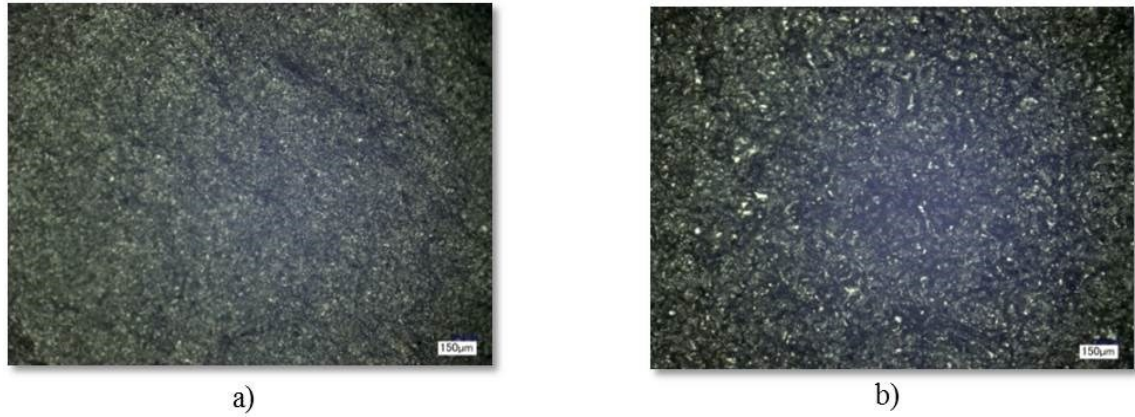


Figure 23: 500x OM scans of 3D metal printed Sierpinski gasket antenna a) along Z-direction (top surface of the antenna) and b) along XY- plane (lateral surfaces of the antenna) after wet blasting

Post wet blasting, the RMS value  $R_q$  of the antenna, along the Z-direction of the top face of the antenna, was found to be  $6.4 \mu\text{m}$  and  $11.47 \mu\text{m}$ , for the lateral surface as shown in **Figure 24** and **Figure 25**. Compared to the value of roughness after heat treatment, the process showed 20% improvement in the value of RMS surface roughness of the printed antenna along the lateral surface of the antenna after wet blasting. Also, as can be seen from the surface roughness figures that the value along both the lateral surface of the antenna as well along the top flat surface has been reduced. This is because wet blasting reduces the loosely attached particles uniformly along the antenna surface.

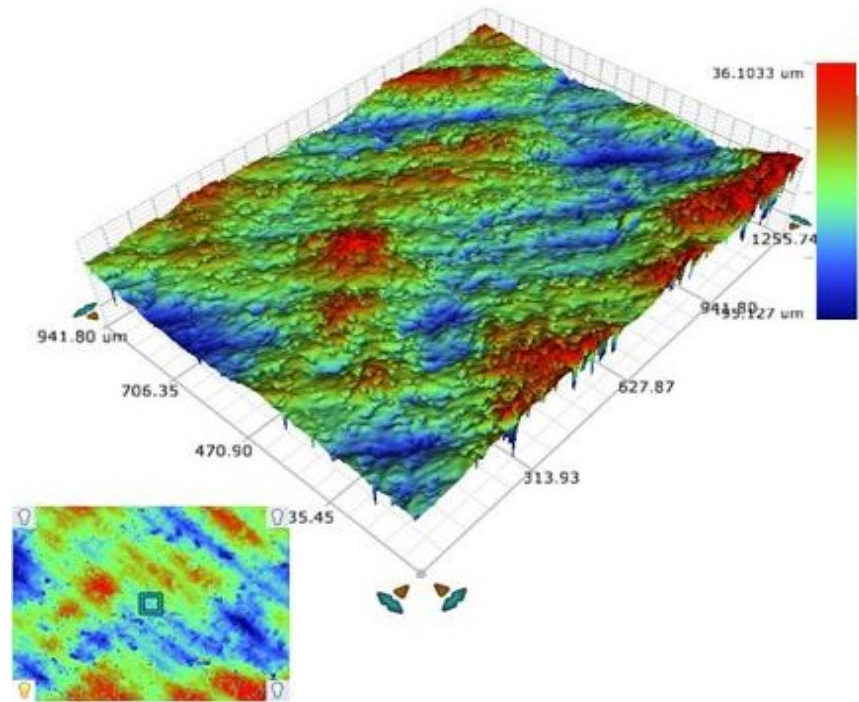


Figure 24: 5x WLI scan of 3D metal printed Sierpinski gasket antenna along Z- direction (top surface of the antenna) after wet blasting

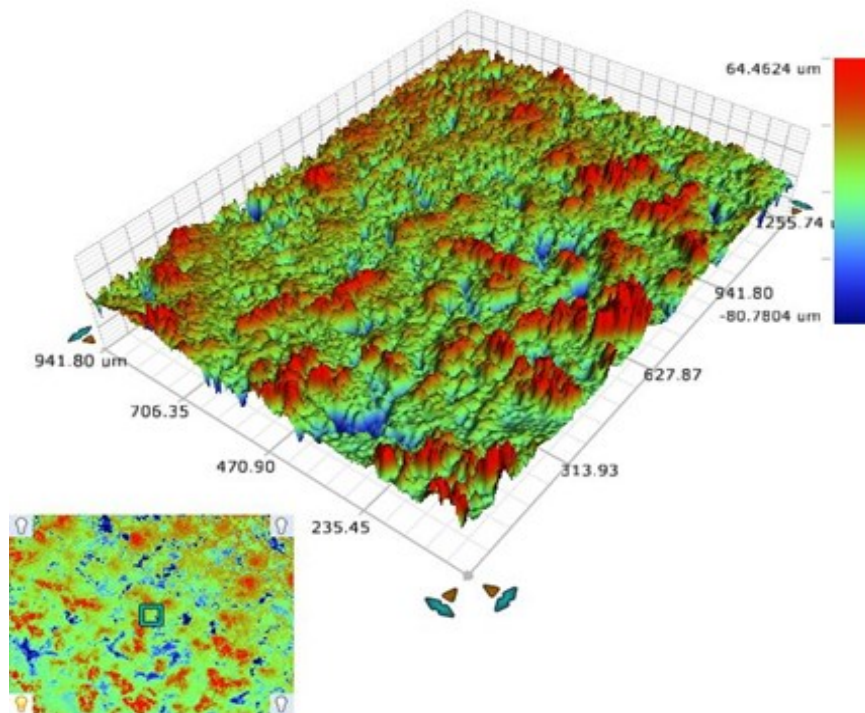


Figure 25: 5x WLI scan of 3D metal printed Sierpinski gasket antenna along XY- direction (lateral surface of the antenna) after wet blasting

### 3.5.3 POLISHING

Polishing can be used on 3D metal printed components to further improve the surface finish. In this case, the top and lateral surfaces of the antenna were polished using Buehler EcoMet™ 250 Grinder-Polisher. This method of polishing is a subtractive process that planarizes a rough surface by abrasion, assisted by continuous lubrication, most commonly water, which reduces deformation. The selection of the grinding surface is done in accordance with the following considerations, such as the amount of the material that needs to be removed, the durability of the grinding surface and the material type. In this case, for the post wet blasted antenna, with an RMS roughness of 11.47  $\mu\text{m}$  on the lateral side, initially polishing paper with a grit size of 500 was used, later increased to 1200 (higher value grit being the finer), to achieve a clean, bright, shiny surface finish.

Due to the complex structure of the 3D printed Sierpinski gasket antenna, it was impossible to perform polishing on the inner faces of the antenna. Instead, those surfaces were treated with the help of a bristle wheel, with a Tripoli (pre-polishing compound) in the bristle. After polishing the antenna, the antenna structure was dipped in a solution of ethanol, for its surface cleaning properties, to achieve a very smooth and glossy surface, visible to the naked eye.

#### 3.5.3.1 POST POLISHING SURFACE ANALYSIS

**Figure 26** shows 500x OM scans of the antenna surface along the Z-direction (top surface of the antenna) and along the XY-plane (lateral surface of the antenna) of the 3D metal printed Sierpinski gasket antenna after polishing. Both the surfaces have very similar surface profiles. Grooves on the surface, as can be seen in the figure are minute scratches, which have occurred while planarizing the antenna surface by abrasion while polishing.

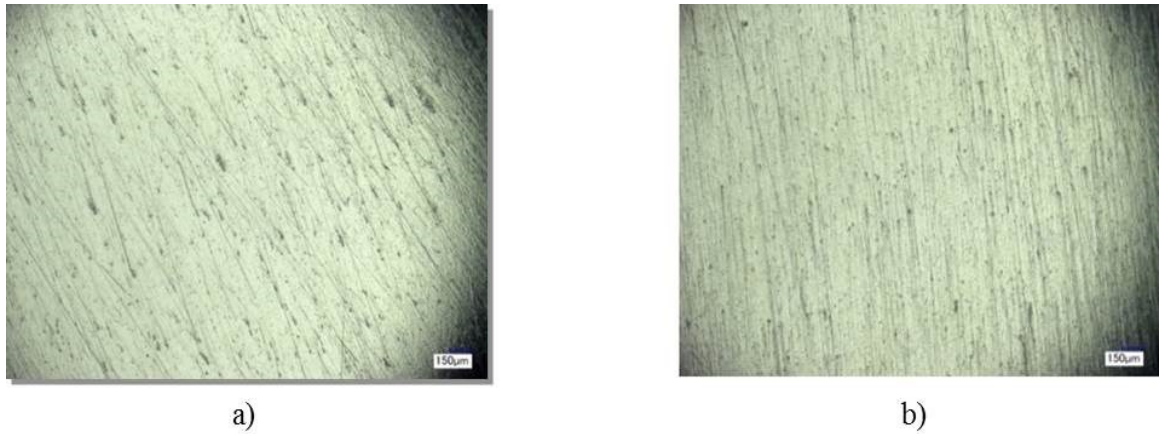


Figure 26: 500x OM scans of 3D metal printed Sierpinski gasket antenna along a) Z-direction (top surface of the antenna) and b) along the XY- plane (lateral surface of the antenna) after polishing

The rough surfaces along the antenna sides were removed using the Buehler EcoMet™ 250 Grinder-Polishers. A good, uniform finished roughness was achieved, of similar dimension to the automated surfaces after the polishing process. As can be seen in **Figure 27** and **Figure 28**, the RMS roughness of both the top flat surface, as well as the lateral surface of the antenna were almost in the same range. The  $R_q$  value on the top, flat surface was found to be  $0.33 \mu\text{m}$ , and that of the lateral surface to be  $0.25 \mu\text{m}$ . The improvement in the surface roughness numbers were significant, achieved by polishing.

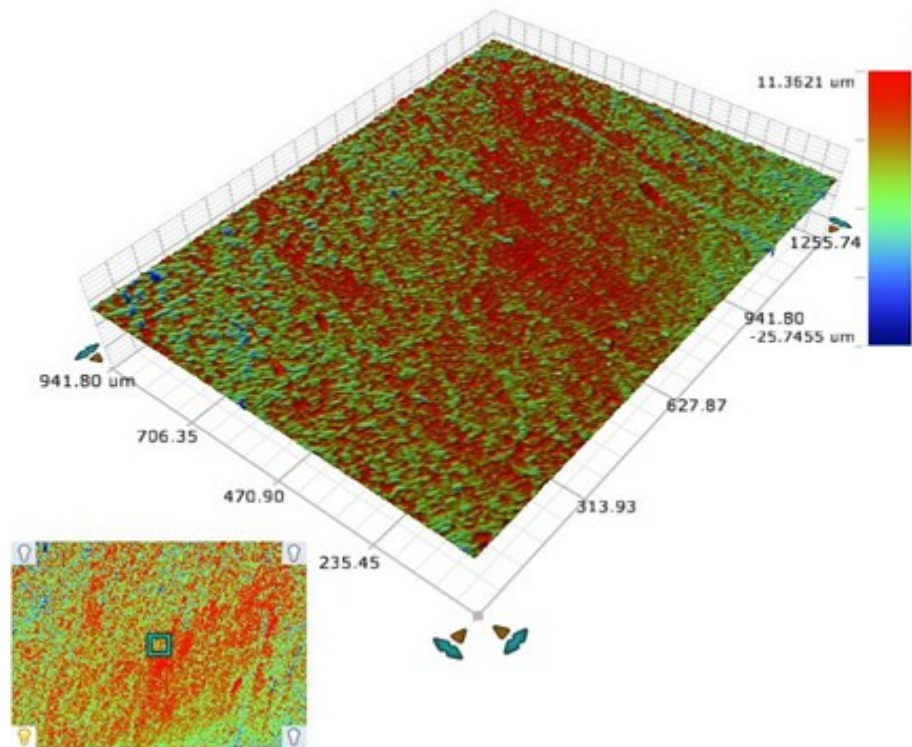


Figure 27: 5x WLI scan of 3D metal printed Sierpinski gasket antenna along Z direction (top surface of the antenna) after polishing

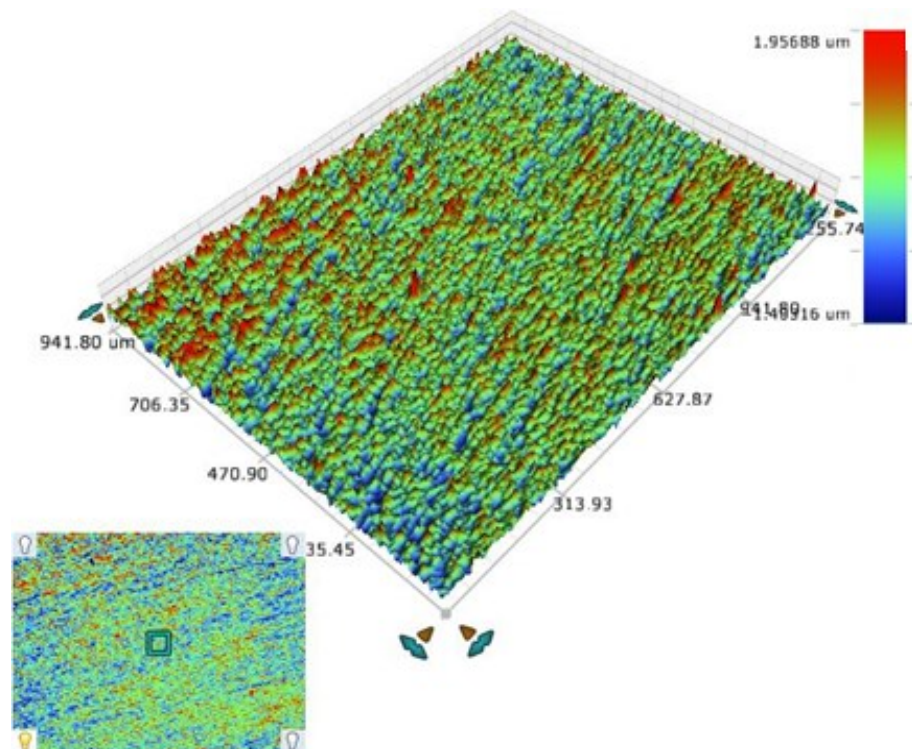


Figure 28: 5x WLI scan of the 3D metal printed Sierpinski gasket antenna along the XY-plane (lateral surface of the antenna) after polishing

### 3.6 SURFACE MORPHOLOGY

One of the most promising applications of 3D printing is exploiting its ability to manufacture parts with high accuracy, detailed resolution and excellent mechanical properties, such as durability and strength [19] [21]. However, there have been growing concerns regarding the rough surface finish, partly because removing it would add at least one more processing step. From the perspective of RF/microwave components, it is well known that if the surface roughness of an electromagnetic component is of the order of the skin depth, its performance will be significantly degraded [28]-[32]. The skin depth predicts how deeply a signal penetrates a material, and is dependent on the frequency of application, as well as the material's properties, such as resistivity and permeability. In [32], the authors evaluated the impact of surface roughness on two Ku-band 3D metal printed antennas, fabricated using EBM and experimentally compared their performance to a standard off-the-shelf horn antenna. Compared to the DMLS technique, EBM uses an electron beam as the energy source, which leads to faster construction, but lacks the DMLS quality of surface finish [33]. As a result, their reported measured surface roughness was much higher than their skin depth, for the chosen operating wavelength, due to which, a 1 dB loss on their transmission coefficient was reported, compared with the off-the-shelf standard horn antenna.

In this research, the realized gain and return loss  $S_{11}$  will be measured to see if the surface roughness from the DMLS system has any adverse effect on the performance of an antenna. Following this initial assessment, the surface roughness will be reduced gradually, in stages, using mechanical techniques such as wet blasting (shot peening) and polishing, while subsequently monitoring the surface morphological changes and their resultant impact on the RF performance of the antenna.

The morphological changes of the 3D printed Sierpinski gasket antenna were analysed using both Keyence VHX-5000 Optical Microscope (OM), for the roughness profile measurements, and Bruker Contour GT-K White Light Interferometer (WLI), to measure the surface roughness at various locations [34][35]. These roughness and RF measurements were all performed before and after any of the mechanical roughness reduction procedures were applied, to track RF performance changes as a function of reducing roughness.

The OM (500x) surface roughness profile of the 3D printed Sierpinski gasket antenna, without any post-processing, is shown in **Figure 29**, with the top, flat (given the notation here of Z-direction) surface in **(a)** and two images of the side or lateral surface (given the notation here of XY-direction) in **(b)** and **(c)**. It is immediately apparent that there are two distinct surface profile types. The flat, top surface is shiny and has a characteristic hatch line surface profile, caused by the lasing action of a 3D printer. In 3D printing, when the selected laser power is first exposed to the powder bed, the laser works in a vector scan mode, where it first scans the contour lines, outlining the area enclosed by the objects, corresponding exactly to the original CAD drawing. After that, the laser works in a raster scan mode, where the laser scans the area enclosed by the contour lines in one direction while switching ON and OFF. This continues line-after-line, inside the contour, while maintaining the hatching distance between lines, to ensure that the melting process has been completed correctly. This process is known as hatching and the streamline grooves that remain on the surface inside the contour are known as hatch lines [36].

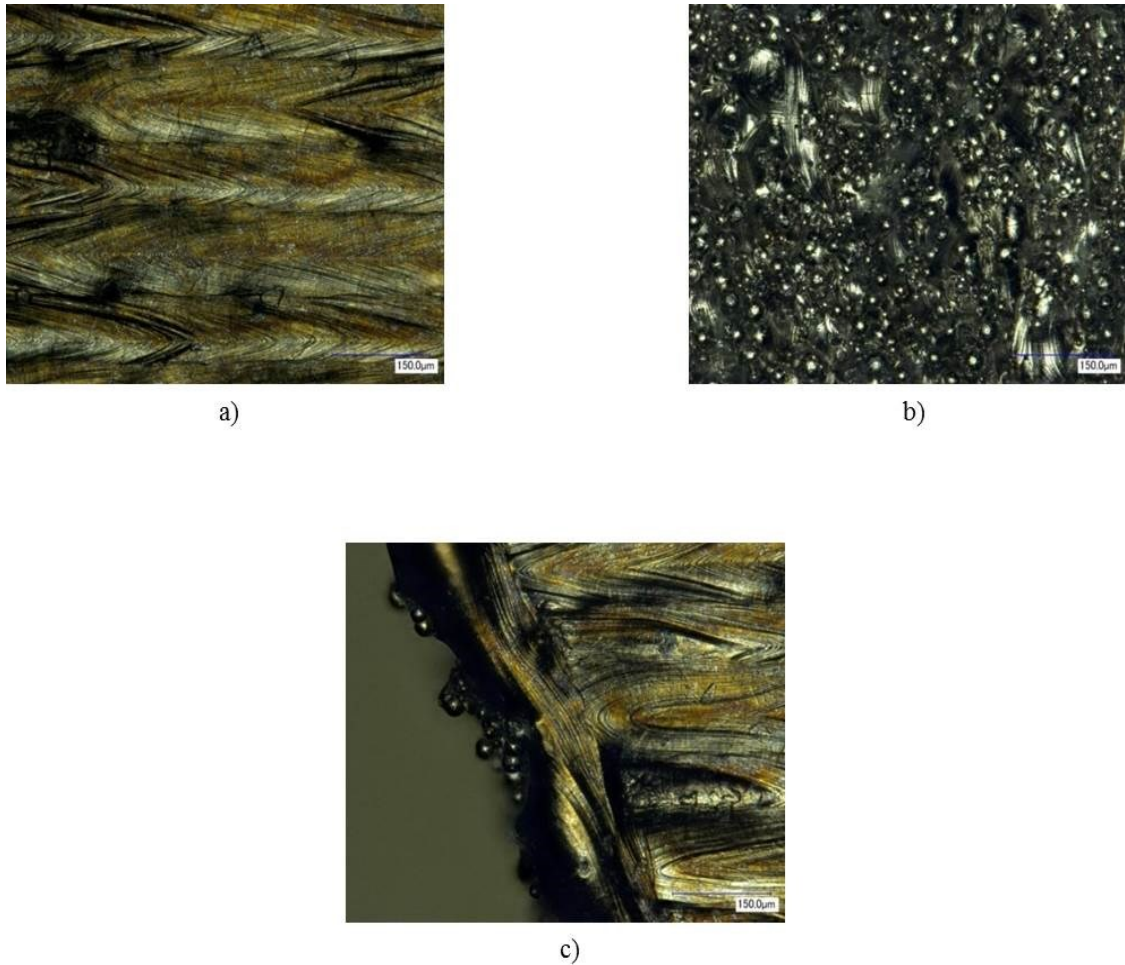


Figure 29: 500x OM scans of the 3D metal printed Sierpinski gasket antenna post heat treatment a) along the Z direction (top surface of the antenna), b) along the XY plane (lateral surface of the antenna) after heat treatment c) along the edge section of the lateral surface, showing both the flat top and side.

On the other hand, from the two images of the side or lateral surface in **Figure 29 (b)** and **(c)**, it is easy to see that the inclined lateral faces are rougher and have a spherical surface profile, again a characteristic of a 3D layered print. This surface profile can be explained by the fact that when the laser sinters metal powders, it creates melt pools (partially sintered particles). As the antenna structure builds up, the air surrounding the construction contains floating spherically shaped source powder, with Particle Size Distribution (PSD) here of 10 to 60  $\mu\text{m}$ , which sticks to the newly welded lateral (still hot) surface of the antenna. From the OM (500x) scans, it was found that agglomerates of material particles, stuck to the lateral surface of the antenna, vary in diameter, size and aspect ratio.

While the image in **Figure 29 (b)** is representative of an inner area of a lateral surface (a normal incidence aspect), the image in **Figure 29 (c)** on the other hand is taken from an edge section of a lateral surface (offering a side view of the surface, with clearly visible, bubble-like agglomerates). Around the edge section, the surface seems to be comparatively rougher, which was due to removal of support structures, as well as the powder melting and rolling over the edge of another surface. While the surface profiles appear to be quite different, once the post-processing is completed all surfaces will have a uniformly smooth profile as discussed later.

### 3.6.1 SURFACE ANALYSIS PARAMETERS

To numerically assess the surface roughness of the structure; three parameters are widely used, which are average surface roughness ( $R_a$ ), root mean square surface roughness ( $R_q$ ) and maximum peak to valley distance ( $R_z$ ). All the measurements are done with the Centre Line ( $C_L$ ) being the reference line, which is estimated and drawn in such a way that the area of the roughness profile curve under and over the  $C_L$  is the same as shown in **Figure 30**.

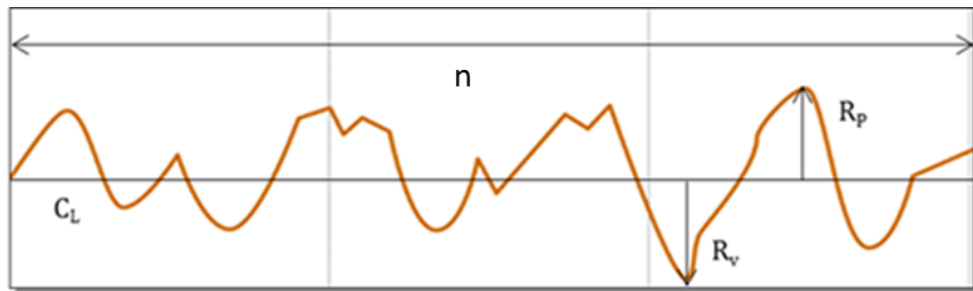


Figure 30: Surface roughness parameters

The roughness parameter,  $R_a$ , is then the arithmetic average of the total departure of the actual surface from the center line, measured within the number of sampling length ( $n$ ).

$$R_a = \frac{1}{n} \sum_{i=1}^n |y_i| \quad (1)$$

The geometric average roughness, also known as the RMS roughness, ( $R_q$ ) is the geometric average height of roughness-component irregularities from the  $C_L$ , measured within the sampling length.

$$R_q = \sqrt{\frac{1}{n} \sum_{i=1}^n |y_i|^2} \quad (2)$$

$R_q$  is more sensitive to peaks and valleys than  $R_a$ , as the amplitudes of the peak heights are squared.

The greatest height of the roughness profile  $R_z$  is the sum of the height of the highest profile peak and the depth of the deepest profile valley, relative to the mean line, within a sampling length  $L$ .

$$R_z = R_p + R_v \quad (3)$$

Where the maximum profile peak height,  $R_p$ , is the height of the highest peak from the mean line, and  $R_v$  is the maximum profile valley depth from the mean line defined over the sampling length.

A couple of points relating to this work are worth making now. First of all, the WLI software calculates the  $C_L$  based on calculated distances from the surface. However, each of the post-processing stages are subtractive, which means that each new run of the WLI not alone shows less deviation from the  $C_L$ , but also is based on a new  $C_L$ , corresponding to the post-processed surface. Also, it was difficult to take track of the scan position for all the measurement, due to which all the surface roughness measurements performed in the research were the average value of five WLI scans. Even though the deviation in the roughness values were small the average value of roughness measurement was necessary as the available WLI only scans, a small section of the area for the surface roughness measurements.

It should also be noted that a single post-processing surface stage would have been possible (polishing), but that the extra wet blasting stage was used here to allow analysis of the impact of roughness on the RF performance. Finally, while these processes are subtractive, in this work the subtraction means that the antenna is simply being brought closer to the original design geometry, as the extra material causing the roughness is a feature of 3D printing.

### 3.7 RF RESULTS AND ANALYSIS

The antenna was designed, optimized and simulated on CST software. The return loss,  $S_{11}$  and realised E-plane gain measurement were measured on a calibrated Rohde and Schwarz ZVB 20 VNA in a large room, where most reflecting surfaces are protected by absorbent foam. The Sierpinski gasket antenna was mounted on a modified Total Station for accurate angular measurements with the step size of  $10^\circ$  as shown in **Figure 31**. All the measurements, including the return loss and the realised E-plane gain measurements, were repeated every time the post-processing was performed on the antenna surface, to examine the impact of surface roughness on the RF performance of the antenna.

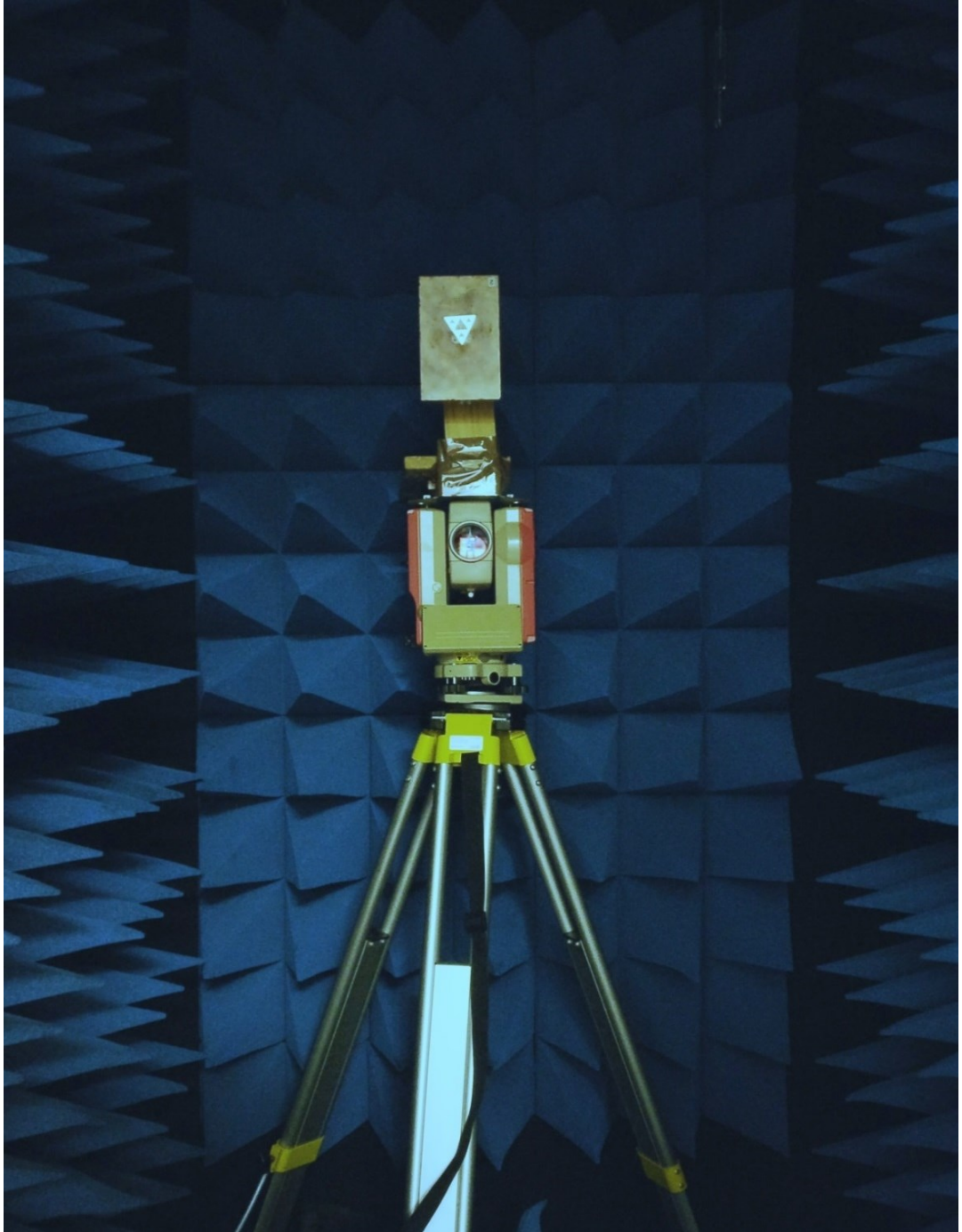


Figure 31: Antenna radiation measurement setup for E-plane gain measurement

### 3.7.1 MEASUREMENTS AFTER HEAT TREATMENT

As mentioned in **Section 3.4.1**, due to the “ring width effect”, the fundamental and the resonant frequency corresponding to the fabricated 3D printed antenna has been shifted towards higher frequency bands. For this reason, the antenna now resonates at the frequencies, of 8.4 GHz and 4.2 GHz, maintaining its multiband feature with responses below -10 dB, for both frequencies. Also, no extra matching circuitry has been employed to tune the antenna to its corresponding wavelength. The comparison measured and simulated return loss graph of the antenna, after heat treatment corresponding to the **Figure 32** is shown in **Figure 33**. The results show a good agreement between both the results.



Figure 32: 3D metal printed Sierpinski gasket antenna, after heat treatment

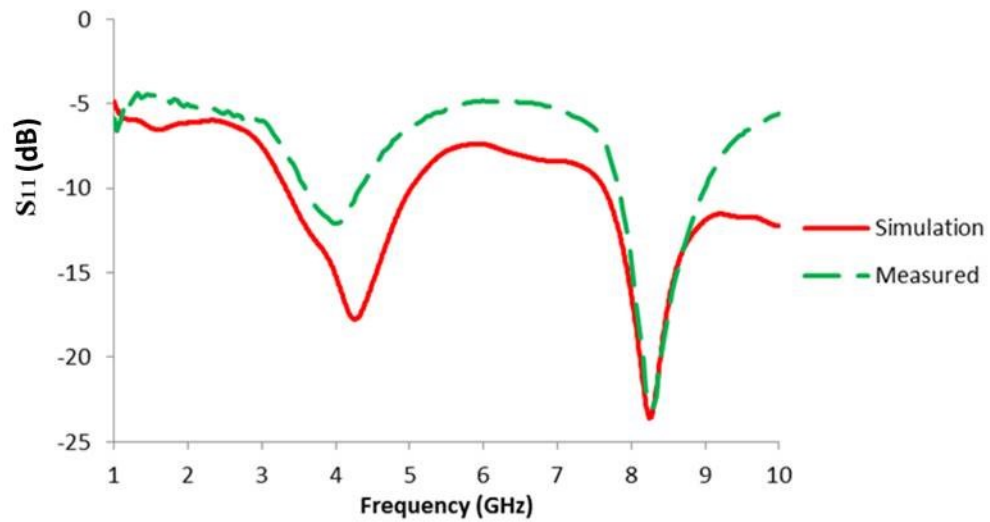


Figure 33: Simulated and measured return loss after heat treatment

While performing the simulations, no efforts have been made to apply surface roughness on to the antenna model in CST, as it was not possible to import the random surface roughness on the simulated model. Having said that, CST software allows strip-line, triangular grooves or spherical surface roughness's which can be used to relate its output to the measured results. However, in this research, the simulation file will consider a polished surface in all future comparisons, against which all gains and  $S_{11}$  values will be compared.

During the experiments, the radiation characteristics of the antenna were measured in the boresight direction. For measurements, Port 1 of the VNA is connected to the Antenna Under Test and operated as a receiving antenna, whereas other reference antenna connected to the port 2 of the VNA, served as a transmitting antenna. Both the receiving and transmitting antennas were separated by a distance of 4.2 m, maintaining the criterion for far-field distance. The measured and simulated E-plane gain patterns of the antenna at both frequencies, of 4.2 GHz and 8.4 GHz, are shown in **Figure 34**.

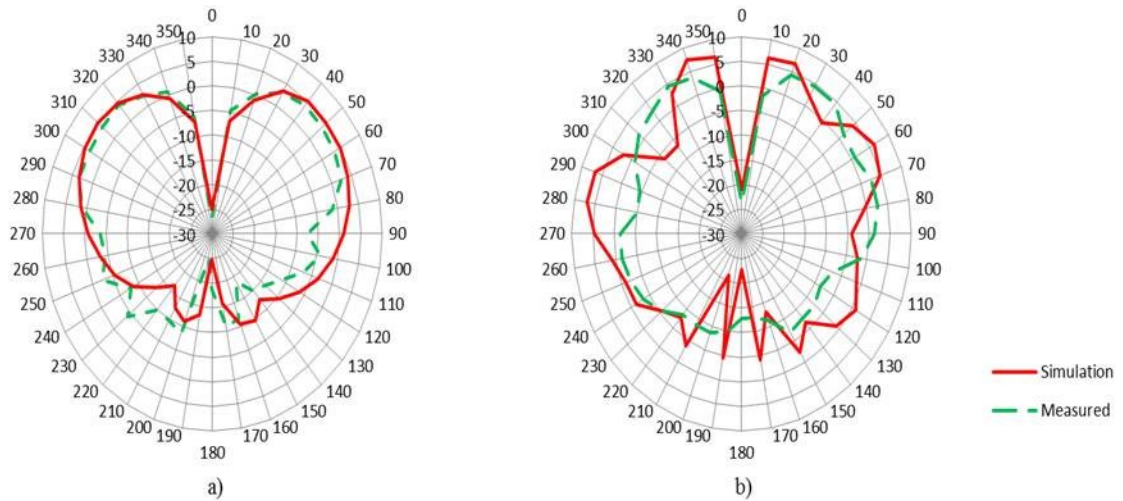


Figure 34: Simulated and measured gain radiation pattern a) 4.2 GHz b) 8.4 GHz

The maximum gain of the AUT was measured at an elevation of around 30-40 degrees with respect to the rectangular ground plane, as it is typical of a monopole antenna to have such a beam tilt, due to the finite ground plane effect [37]. It is possible to enhance the gain of the antenna with the inclusion of large ground plane. However, for fair comparison, the same finite ground plane has been used in the research, as the main motive of this research is to analyse the effect of the gradual reduction of the surface roughness on the performance of the microwave component.

The simulated gain at 4.2 GHz was found to be 5.07 dB compared to the measured gain of 4.07 dB, the losses were significant at 8.4 GHz, as expected, the measured gain was found to be 4.45 dB compared to the simulated gain of 6.64 dB. A summary of simulated and measured gain values as a function of surface roughness after heat treatment is presented in **Table 1**.

Table 1: Simulated and measured gain of Sierpinski gasket antenna after heat treatment, as a function of surface roughness

Post processing step	Roughness measurement along different planes ( $\mu\text{m}$ )		Simulated gain (dB)		Measured gain (dB)	
	XY-	Z-	4.2 GHz	8.4 GHz	4.2 GHz	8.4 GHz
After heat treatment	14.47	7.7	5.07	6.64	4.07	4.45

The influence of the surface roughness is the principle reason for the disagreement between the simulated and the measured gain, which is the figure of merit in this case. The losses at the higher frequency were more profound and would increase if the antenna is to be made to operate for smaller wavelengths, due to the skin effect, which is inversely proportional to the frequency. One of the reasons for such high losses due to the random surface roughness could also be explained from recently published work, which suggests that simple roughness measures alone are insufficient to understand RF performance as the proportion of smaller features (and not just their scale) can contribute to higher losses [38]. Although this is not considered further in this research work, but it could be a possible contributor to higher losses.

Further measurements were done by gradually reducing the surface roughness and measuring the gain of the antenna further for comparison with the corresponding simulated values.

### **3.7.2 MEASUREMENT AFTER WET BLASTING**

As illustrated in **Figure 35**, after the wet blasting process, all the loosely attached material particles from the powder bed attached to the antenna were removed and the antenna was left with intermediate rough surfaces. Once the surface analysis was performed, the antenna was mounted again onto the feeding circuitry as mentioned in **Section 3.4.5**, for RF measurements.



Figure 35: Sierpinski gasket antenna fabricated after wet blasting

During the  $S_{11}$  measurement, it was observed that the antenna still corresponds to the same fundamental and resonant frequency with dips below -10 dB as after the heat treatment phase. However, the higher order resonant frequency dip was reduced and was observed to be shifted a bit upwards. Initially, it was speculated that this might have happened due to an improper feed connection, worsening the reflection values. Repeating  $S_{11}$  measurements a few times confirmed that it was not due to improper feed connections, but due to the tapering of the antenna tip, during the process of wet blasting. As has already been mentioned earlier, the excitation point has a great significance in terms of the impedance bandwidth of the monopole and even a minute change to it can cause the frequency dip of the Sierpinski gasket antenna to shift. This assumption was confirmed not only by first physically examining the base diameter of the antenna, but also by then simulating the antenna model with the tapered tip on CST software. It was estimated that the base radius (ring width) of the antenna has been reduced to 0.6 mm, compared to its original value of 0.95 mm, immediately after heat treatment.

It is worth mentioning that the change in the  $S_{11}$  values, especially at 8.4 GHz, could also be related to the skin effect. The tapering of the tip means that the antenna had less surface

area over which the current could flow, which would also contribute to an upward shift in the resonant frequencies. The shift was more noticeable at the higher resonant frequency of 8.4 GHz, compared to the negligible change in the resonant dip at 4.2 GHz. The corresponding results confirmed the hypothesis as the results were in good agreement with each other as shown in the **Figure 36**.

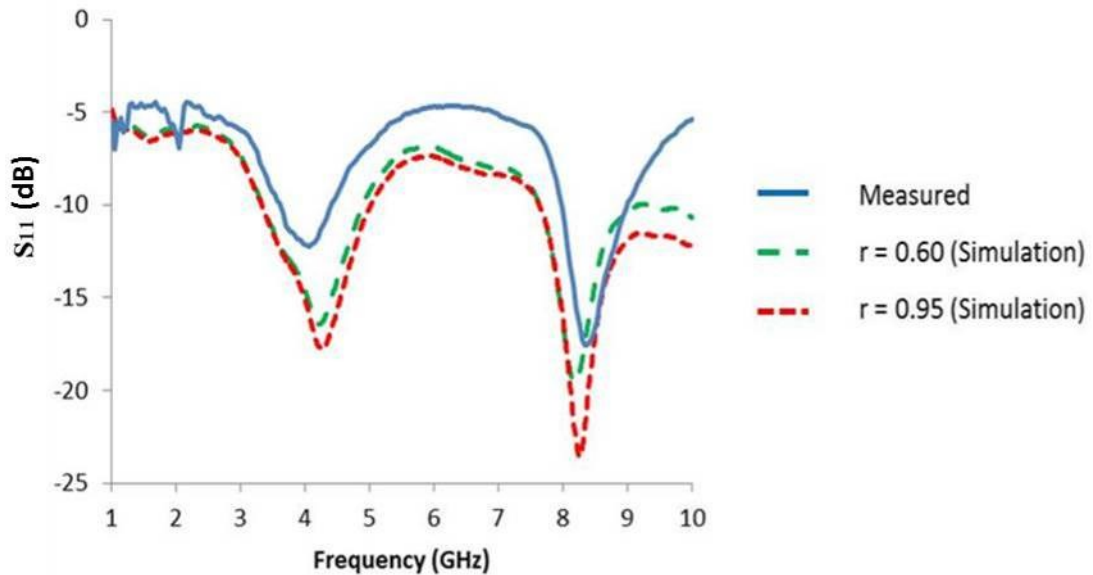


Figure 36: Comparison of simulated return loss with anticipated base radius of 0.6mm and the measured results obtained after antenna was wet blasted (all the dimension are in mm)

The E-plane gain measurement for the antenna, after wet blasting was performed, as shown in **Figure 37**. As can be seen from the figure, the gain, the figure of merit, was found to have improved once the antenna was surface treated, for both the chosen frequencies, which could be possibly because of the fact that the surface roughness of the antenna was of the order of the calculated skin depth of  $7.33 \mu\text{m}$  at the higher frequency of 8.4 GHz (electrical resistivity of Ti-6Al-4V is 0.000178 ohm-cm). The measured gain at 4.2 GHz was 4.77 dB (up from 4.07 dB) and was 5.8 dB (up from 4.45 dB) for 8.4 GHz, as presented in **Table 2**.

Table 2: Simulated and measured gain of Sierpinski gasket antenna as a function of reducing surface roughness, post wet-blasting

Post processing step	Roughness measurement along different planes ( $\mu\text{m}$ )		Simulated gain (dB)		Measured gain (dB)	
	XY-	Z-	4.2 GHz	8.4 GHz	4.2 GHz	8.4 GHz
After Wet blasting	11.47	6.4	5.07	6.64	4.77	5.8

This change in the gain after wet blasting confirmed the impact of surface roughness on the RF performance of the antenna. From the results obtained, it was clear that surface roughness increases the random scattering of electromagnetic waves, therefore increasing RF resistance, which further reduces the gain of the antenna.

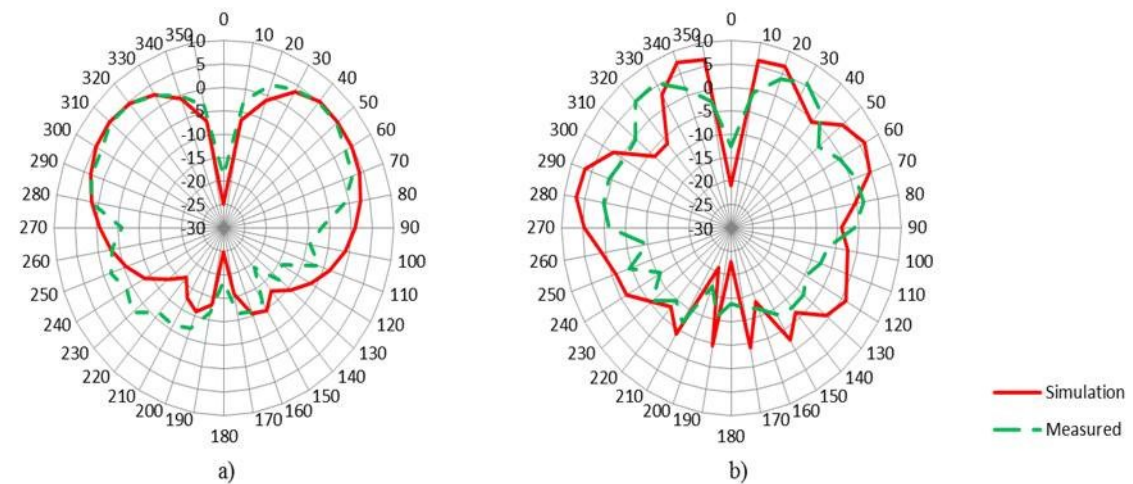


Figure 37: Simulated and measured E- plane realised gain radiation pattern a) 4.2 GHz b) 8.4 GHz

### 3.7.3 MEASUREMENT AFTER POLISHING

Once the polishing was performed, the antenna was reduced to a sharp-edged, shiny surfaced antenna with dimensions assumed to be equivalent to that of the modelled file, once the surface roughness was removed as shown in **Figure 38**.



Figure 38: Sierpinski gasket antenna after polishing

The  $S_{11}$  measurement results after polishing show a similar pattern, to the pattern observed after the wet blasting process. The high order resonance dip at 8.4 GHz of the antenna deteriorated further with respect to the earlier measurements. However, with a better understanding of the ring width effect, the simulation of the antenna was carried with an antenna base radius value of 0.1 mm. This value was chosen because the polishing process, which is a subtractive process, reduces the antenna base radius to a value of approximately 0.1 mm. As illustrated in **Figure 39**, the antenna still resonates at both frequencies, but with a lower dip in relation to the simulation results for the modelled antenna, which initially had a base radius value of 0.95 mm.

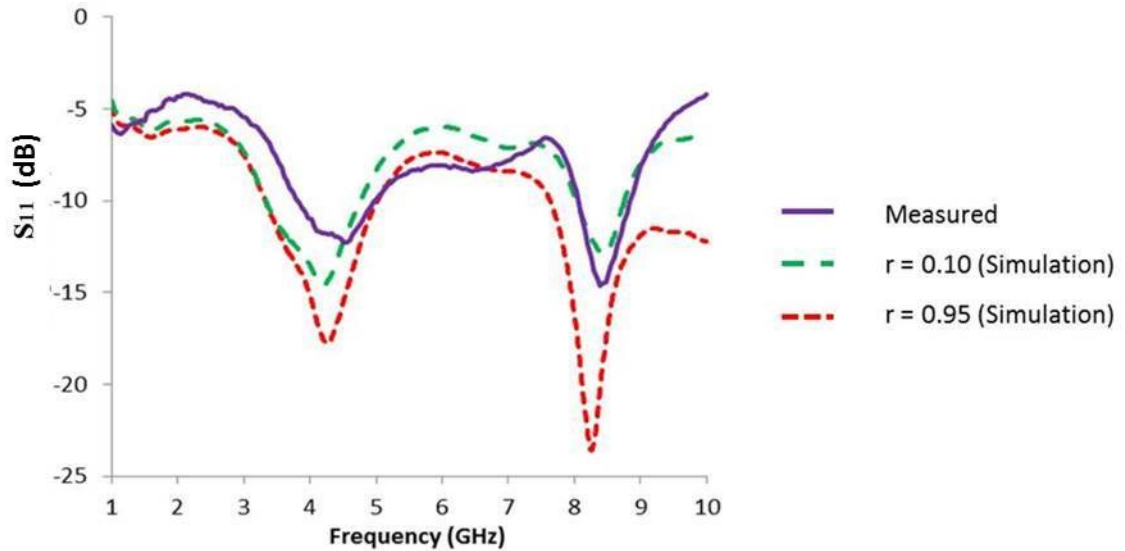


Figure 39: Comparison of simulated return loss with anticipated base radius of 0.10 mm and the measured results obtained after antenna was polished (all the dimensions are in mm)

However, this study gave us a clear understanding of the effect of surface roughness on the excitation tip and things one should consider prior to performing any surface smoothing process and its effect on the design.

In addition to the return loss measurements, the E-plane gain pattern was also performed on the polished 3D printed Sierpinski antenna. After the polishing was performed, the RMS surface roughness value  $R_q$  on the top, flat surface was found to be  $0.33 \mu\text{m}$ , and that of the lateral surface to be  $0.25 \mu\text{m}$ . The surface roughness at this point is much lower than the order of the skin depth of the titanium alloy (Ti-6Al-4V) for the chosen frequencies of application. After the polishing process was done, the measured antenna gain value comparatively matched the simulation gain, at both the resonant frequencies. The gain was measured to be 4.8 dB (up from 4.07 dB) and 6.24 dB (up from 4.45 dB) for both the corresponding resonant frequencies. A summary of simulated and measured gain values, as a function of surface roughness after polishing, is presented in **Table 3**.

Table 3: Simulated and measured gain of Sierpinski gasket antenna as a function of surface roughness, post polishing

Post processing step	Roughness measurement along different planes ( $\mu\text{m}$ )		Simulated gain (dB)		Measured gain (dB)	
	XY-	Z-	4.2 GHz	8.4 GHz	4.2 GHz	8.4 GHz
After Polishing	0.33	0.25	5.07	6.64	4.8	6.24

Figure 40 shows the comparison of the simulated and measured gain patterns after polishing for both the chosen frequencies.

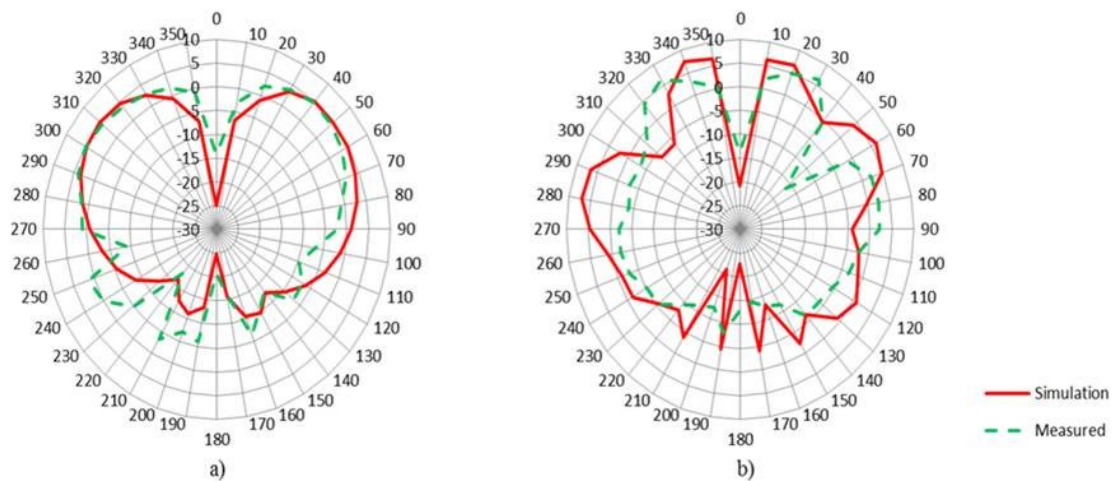


Figure 40: Simulated and measured gain radiation pattern a) 4.2 GHz b) 8.4 GHz

### 3.8 SUMMARY

From an RF design and realization perspective, 3D printing offers great advantages, as an efficient and easy method for printing complex geometries. The complex geometry antenna described in this work is a Sierpinski gasket antenna, created using a DMLS 3D metal printer.

The design restrictions and challenges were also identified, including the “ring width effect”, mounting issues of the Sierpinski antenna and its effect on RF performance. All of these issues underline the need for correct design and preparation, if 3D printing is to be a viable option towards the fabrication of complex-shaped microwave components.

To monitor the surface morphological changes on the surface of the antenna, OM and WLI are used. Finally, both the path loss and the return loss of the antenna are measured, to track the RF performance changes on the 3D metal printed antenna, as a function of reducing roughness. This change in the gain results after wet blasting and polishing confirmed the impact of surface roughness on the RF performance of the antenna.

From the results obtained, increased surface roughness increases the random scattering of electromagnetic waves; therefore, increasing RF resistance, which further reduces the gain of the antenna. The antenna RF performance was measured and found to be in good agreement with simulation results, in terms of bandwidth and radiation characteristics.

*\*\* Publications arise from this chapter have been presented in:*

*18th Research Colloquium on Radio Science and Communications for a Smarter World, Dublin, Ireland; March/2017.*

*2017 International Conference on Electromagnetics in Advanced Applications (ICEAA), Verona, Italy; September/2017 (Two papers).*

### 3.9 REFERENCES

1. F. Niesler and M. Hermatschweiler, “Additive manufacturing of micro-sized parts-trend of miniaturization is driver for 3D laser lithography”, *Laser Technik Journal*, vol. 11, no. 5, pp. 16–18, 2014.
2. EOS, “EOS M280”, [Accessed: 07th July 2015].
3. CST Microwave Studio 2016, *CST GmbH, Darmstadt, Germany*. 2016.
4. H.O. Peitgen, H. Jürgens, D. Saupe, “Chaos and Fractals: New Frontiers of Science”, 2<sup>nd</sup> ed., *New York: Springer-Verlag*, 2004.
5. R. Batra, P. L. Zade, D. Sagne, “Design and implementation of Sierpinski carpet fractal antenna for wireless communications”, *International Journal of Scientific Research Engineering & Technology (IJSRET)*, vol. 1, no. 4, pp. 043-047, 2012.
6. C. Puente-Baliarda, J. Romeu, R. Pous and A. Cardama, “On the behavior of the Sierpinski multiband fractal antenna”, *IEEE Antennas and Propagation Society*, vol. 46, no. 4, pp. 517 - 524, 1998.
7. M. Waqas, Z. Ahmed and M. Bin Ihsan, “Multiband Sierpinski fractal antenna”, *IEEE 13<sup>th</sup> International Multitopic Conference*, pp. 1 - 6, *Islamabad, Pakistan*. December/ 2009.
8. J. Romeu, J. Soler, “Generalized Sierpinski fractal multiband antenna”, *IEEE Transactions on Antennas and Propagation*, vol. 49, no. 8, pp. 1237–1239, 2001.
9. K. Siakavara, "Novel fractal antenna arrays for satellite networks: Circular ring sierpinski carpet arrays optimized by genetic algorithms", *Progress In Electromagnetics Research*, vol. 103, pp. 115-138, 2010.
10. Chatterjee, T. Mondal, D. G. Patanvariya, R. Prasad, K. Jagannath, “Fractal-based design and fabrication of low-sidelobe antenna array”, *AEU - International Journal of Electronics and Communications*, vol. 83, pp. 549-557, *January 2018*.
11. J. Anguera, J. P. Daniel, C. Borja, J. Mumburu, C. Puente, T. Leduc, K. Sayegrih and P. V. Roy, “Metallized foams for antenna design: application to fractal-shaped Sierpinski-carpet monopole”, *Progress In Electromagnetics Research*, vol. 104, pp. 239-251, 2010.
12. M. Alaydrus, “Analysis of Sierpinski Gasket Tetrahedron Antennas”, *Journal of Telecommunications*, vol. 5, no. 2, pp. 6-10, 2010.
13. C. Yana, L. Hao, A. Hussein, P. Young, “Ti–6Al–4V triply periodic minimal surface structures for bone implants fabricated via selective laser melting”,

- Journal of the Mechanical Behavior of Biomedical Materials*, vol. 51, pp. 61–73, 2015.
14. F. Yang, C. Chen, Q.R. Zhou, Y.M. Gong, R.X. Li, C.C. Li, F. Klampfl, S. Freund, X.W. Wu, Y. Sun, “Laser beam melting 3D printing of Ti6Al4V based porous structured dental implants: Fabrication, biocompatibility analysis and photoelastic study”, *Sci. Rep.* 7, 2017.
  15. M. Sherman, C. J. Sommer, F. H. Froes, “The use of titanium in production automobiles: Potential and challenges”, *The Journal of The Minerals, Metals & Materials Society*, vol. 49, no. 5, pp. 38-41, 1997.
  16. R. S. Electronics, “(Online) Chemtronics silver conductive adhesive epoxy, 0.25 oz tube,” (<http://ie.rs-online.com/web/p/conductive-adhesives/0496265/>), [Accessed 30 October 2015].
  17. V.H. Rumsey, “Frequency-Independent Antennas”, 1<sup>st</sup> ed., *Academic Press, New York*, 1966.
  18. R. G. Holfield, N. Cohen, “Self-similarity and the geometric requirements for frequency independence in antennas”, *Fractals - Complex Geometry, Patterns, and Scaling in Nature and Society*, vol. 07, no. 1, pp. 79-84, 1999.
  19. R. R. Bineli, A. P. G. Peres, A. L. Jardini, R. M. Filho, “Direct metal laser sintering (DMLS): Technology for design and construction of microreactors”, 6<sup>th</sup> *Brazilian Conference on Manufacturing Engineering, Brazil, April/2011*.
  20. W. D. Vree, “(Master’s Thesis) On the influence of build orientation on the mechanical properties of direct metal laser sintered (DMLS) Ti-6Al-4V flexures”, *Technical University of Delft, April/2016*.
  21. J. Kranz, D. Herzog, C. Emmelmann, “Design guidelines for laser additive manufacturing of lightweight structures in TiAl6V4” *Journal of Laser Application*, vol. 27, no. 1, pp. 1-16, 2015.
  22. 3ders, “(Online) Dissolvable support material used for 3D printing gearbox and Hilbert Cube”, (<https://www.3ders.org/articles/20120128-dissolvable-support-material-used-for-3d-printing-gearbox-and-hilbert-cube.html>), [Accessed: 5<sup>th</sup> November/2015].
  23. Z. N. Chen, “Experiments on input impedance of tilted planar monopole antenna” *Microwave and Optical Technology Letter*, vol. 26, no. 3, pp. 202-204, 2000.
  24. Vixen surface treatments, “(Online) Aquablast 1515”, (<https://www.vixen.co.uk/aquablast-1515.html>), [Accessed: 16<sup>th</sup> July 2016].

25. Buehler, “(Online) EcoMet™ 250 Grinder Polisher”, (<https://www.buehler.com/ecoMet-250-grinder-polisher.php>), [Accessed: 16<sup>th</sup> July 2016].
26. Stratasys Direct Manufacturing, “(Online) Getting the most out of metal 3D printing: Understanding design & process controls for DMLS”, *Metal 3D Printing*, pp. 1-14, 2016.
27. Vixen surface treatments, “(Online) What is Vapor Blasting? A Guide to the Vapor Blasting Process”, (<https://www.vixen.co.uk/wet-blasting/what-wetblasting-guide-vapor-blasting-process>), [Accessed: 21<sup>st</sup> July 2016].
28. S. P. Morgan, “Effect of surface roughness on eddy current losses at microwave frequencies”, *Journal of Applied Physics*, vol. 20, pp. 352-362, 1949.
29. C. L. Holloway, E. F. Kuester, “Power loss associated with conducting superconducting rough interfaces”, *IEEE Transactions on Microwave Theory and Techniques*, vol. 48, no. 10, pp. 1601-1609, 2000.
30. C. Scogna, M. Schauer “Performance analysis of stripline surface roughness models”, *Proceedings of the IEEE International Symposium on EMC Europe, Hamburg, Germany, September/2008*.
31. Y. Ning and W. Jiang, “The electromagnetic characterization of conducting rough surfaces at millimetre wave frequencies”, *International Conference on Microwave and Millimetre Wave Technology, Nanjing, China, April/ 2008*.
32. C. Garcia, R. Rumpf, H. Tsang, J. Barton, “Effects of extreme surface roughness on 3D printed horn antenna”, *IET Electronics Letters*, vol. 49, no. 12, pp. 734 - 736, 2013.
33. J. T. Tuomi, R. V. Bjorkstrand, M. L. Pernu, M. V. Salmi, E. I. Huutilainen, J. E. Wolff, P. K. Vallittu, A. A. Makitie, “In vitro cytotoxicity and surface topography evaluation of additive manufacturing titanium implant materials,” *Journal of Materials Science: Materials in Medicine*, vol. 28, no. 3, pp. 53, 2017.
34. Bruker, “Contour GT K,” (<https://www.bruker.com/products/surface-and-dimensional-analysis/3d-optical-microscopes/contourg-t-k/learn-more.html>).
35. Keyence, “Digital Microscope – VHX-5000 series,”
36. D. Manfredi, F. Calignano, M. Krishnan, R. Canali, E. P. Ambrosio, S. Biamino, D. Ugues, M. Pavese, P. Fino, “Additive manufacturing of Al alloys and Aluminium matrix composites (AMCs)”, *Light Metal Alloys Applications*, W. A. Monteiro, Ed., *InTech*, Chapter 1, 2014.

37. R. F. Hahn, J. G. Fikioris, "Impedance and radiation pattern of antennas above flat discs", *IEEE Transactions on Antennas & Propagation*, vol. 21, pp. 97-100, 1973.
38. N. Clark, S. Hefford and A. Porch, "Effect of build orientation and surface finish on surface resistance in microwave components produced by selective laser melting", *Proceedings of 47<sup>th</sup> EuMC, Nuremberg, Germany, 2017*.

# 4 CHAPTER 4

## A NOVEL APPROACH TOWARDS INTEGRATING A SIGNAL FEED TO A 3D METAL PRINTED MONOCONE ANTENNA

### ABSTRACT

The previous chapters highlighted mechanical issues and the RF impact that can arise in connecting an antenna to a feeding source. In this chapter, this issue is addressed successfully as follows: 3D printing technique is utilized to integrate an N-type feed onto a 3D metal printed monocone antenna, to create a single monolithic structure. 3D printing can produce fine detail and, through appropriate design and post-processing, robust components, with low surface roughness. These qualities also suit the production requirements of complex RF components, in this case in realizing both the monocone structure and also the integrated feed. A monolithic antenna structure can offer at least similar or, more usually, better mechanical properties over conductive glues and even solder. It also can reduce the assembly time and resources required for construction, while guaranteeing a more consistent connection. Finally, it is of particular use if the antenna is either difficult to manufacture or difficult to attach to the feeding circuitry, due to its geometry or dimensions, for example in the case of spiral or fractal antennas.

DMLS was used to fabricate this antenna, from Maraging Steel, MS1, on an EOSINT M280 system. The feed production was not straightforward and some of the challenges are presented here, along with the approaches taken to overcome them and to produce a working prototype. The measured RF results for the 3D printed antenna are found to be in a good agreement with the CST simulation results. The radiation pattern was measured over the frequency range of 4.6-8.2 GHz, for which voltage standing wave ratio (VSWR) values were less than 2.

### 4.1 INTRODUCTION

With the recent interest in fabricating all-metal 3D RF/microwave components, there have been issues regarding feeding the 3D printed microwave component. In **Chapter 3**, it was demonstrated for a 3D metal printed Sierpinski gasket antenna, that was very difficult to mount the antenna onto the feeding circuitry, as the complex geometry and

metal of the antenna made it extremely difficult to attach the feed circuitry to a connector. In order to maintain a position perpendicular to the ground plane, a laboratory clamp was used, after which the antenna had to be glued using a conductive epoxy. This had further complications in that the final fixed position itself was not always reliable in the medium-to-long term, as the glued joint between the antenna and the feed often proved to be fragile. Moreover, antenna structures made from metals like iron, steel, aluminium, etc., are even more challenging to solder to the attaching feed, as they are unreactive to soldering and thus do not bond unless initially plated with copper. One such problem was also faced by Belvin in her thesis [1]. She reported similar problems to correctly position the SMA feed onto a 3D polymer printed antenna, using a soldering iron, as the heated solder was unable to bond to the metal-coated polymer. For this reason, it was challenging to position the feed circuitry correctly.

Conductive epoxy adhesive typically has a volume resistivity  $0.001\Omega\text{-cm}$ , has been used in the previous chapter, and achieved an acceptable RF performance. In comparison to soldering, connections made through conductive epoxy adhesives form mechanical and chemical bonds on the applied surface, whereas soldering makes metallurgical bonds. Consequently, soldering joints are more conductive and possess higher tensile strength. Also, conductive epoxies possess poorer thermal fatigue resistance, making them unsuitable for high-temperature applications such as automotive or some other electronic deployments. Epoxies also require curing times of approximately 24 hrs @  $25^{\circ}\text{C}$  to make a robust connection, often even more time in the author's experience, which further delays the testing of the component.

Although conductive epoxies can be used as an alternative to soldering to connect the antenna onto the feed, the situation becomes more challenging in the case of this 3D monopole antenna, which needs to be glued in a position that is perpendicular to the ground plane. Even then, the final fixed position itself may not be reliable long term, if the glued joint between the antenna and the feed is fragile as discussed in **Section 3.4.5**.

The alternative option proposed in this research is to use AM to integrate an antenna feed onto the printed antenna and thus eliminate the previously mentioned problems. A key point to note here is that, the geometry of the monocone antenna in this research was chosen also because the geometry of the monocone replicates the last tetrahedron apex of

the complex shaped Sierpinski gasket antennas. Even though the antenna used in this research is a monocone antenna, the integration of a feed can be replicated on any 3D monopole antenna design, including the 3D fractal shaped Sierpinski gasket antenna, as presented in **Chapter 3**. The proposed antenna will, therefore, be fabricated as a single piece of metal, with high precision. Furthermore, with this method, the expectation is to reduce any losses which could occur due to discontinuities in the joints caused by soldering.

The antenna designed possesses a measured wide band frequency range from 4.6-8.2 GHz. A short description of wideband monopole antennas is presented in **Section 4.2**, followed by a detailed discussion of this design, including mechanical and manufacturing of the 3D metal printed monocone antenna in **Section 4.3**. The surface roughness analysis of the monocone is conducted in **Section 4.4**, while **Section 4.5** describes the RF characterization of the proposed antenna.

## 4.2 MONOCONE ANTENNA

Due to the increasingly high demand for high wireless transmission rates, low power consumption and low-cost due to their compact size, wideband antennas have gained prominence and have become very attractive in modern wireless communication systems. Monopole antennas are a good option for these applications, but usually, have very limited bandwidth. To achieve better control of the impedance bandwidth, and to make the monopole antennas wideband, an additional impedance matching circuitry, such as stubs, are required [2][3]. In addition, some geometrical forms, such as triangular, concave and convex shapes, are also inserted or truncated around the corners of monopole antennas to achieve wideband properties [4][5]. The truncation can be done either in the upward or downward directions, where the lower frequency is dictated by the antennas height, whereas the higher frequency is imposed by the finite size of the connectorized feeder [6]. The monopole antenna that increases the impedance bandwidth due to its conical shape, by merging a cone with a circular cylinder at a junction, is known as a conical monopole or monocone antenna [4].

Monopole antennas are categorized as i) planar or 2D monopole and ii) 3D monopole antennas. In research literature, both types of antennas have been explored. In this

research, an alternative solution to mounting a 3D antenna onto the feeding circuitry is presented, with a secondary aim to minimize the losses, which occur due to discontinuities in the joints.

### **4.3 ANTENNA DESIGN AND MANUFACTURING**

The proposed 3D monocone antenna with an integrated feed was fabricated using DMLS, on an EOSINT M280 machine, with Maraging Steel, MS1, as the material of choice. One of the contributing factors for the antenna to be fabricated out of Maraging Steel, MS1, rather than choosing any other available 3D printing material in the research centre, was due to its ability to be sintered with the minimum achievable layer thickness, i.e. 20  $\mu\text{m}$  with the available system. The minimum layer thickness has a further effect on the surface roughness of the component as discussed in detail later. Apart from that, the chosen material also has excellent mechanical characteristics, which gives the monolithic antenna high strength properties that are important when dealing with the delicate N-type female connection feed [7]. The screw threads were designed on the feed, in order to provide sufficient friction. These embedded threads prevent the linear motion of the antenna feed, so that the feed does not slip, when linear force is applied onto the feed, to position it into the N-type flange connector.

The monocone antenna with integrated feed and embedded screws was modelled on CST. The 3D modelling design file from CST was later exported into the industry standard STL file format, which is compatible with the software used by all forms of AM printing machines, to slice CAD data appropriately in a layer-by-layer format to form a 3D component with a high level of detail. The results obtained through the simulations were then compared with the measured results of the proposed antenna model.

Mechanical considerations such as the requirement of support structures, build orientation and minimum wall thickness were investigated and these parameters were assigned values that would ensure successful fabrication. For example, the build orientation played an important role in influencing the construction time, as well as in deciding the requirement of the support structure in the modelling file. As the antenna possesses geometry with a very delicate feed design, the monocone antenna was printed upside down, with an orientation of 90° with respect to the building platform. Fabricating the

antenna in this orientation also had the advantage of satisfying the maximum overhanging angle condition, required to print an antenna with minimal support structures employed during the build, and later removed using Wire-EDM. The proposed antenna is a compact monocone, as shown in **Figure 41**, where the antenna feed is connected to the lower end of the monocone and placed perpendicularly above the ground plane.

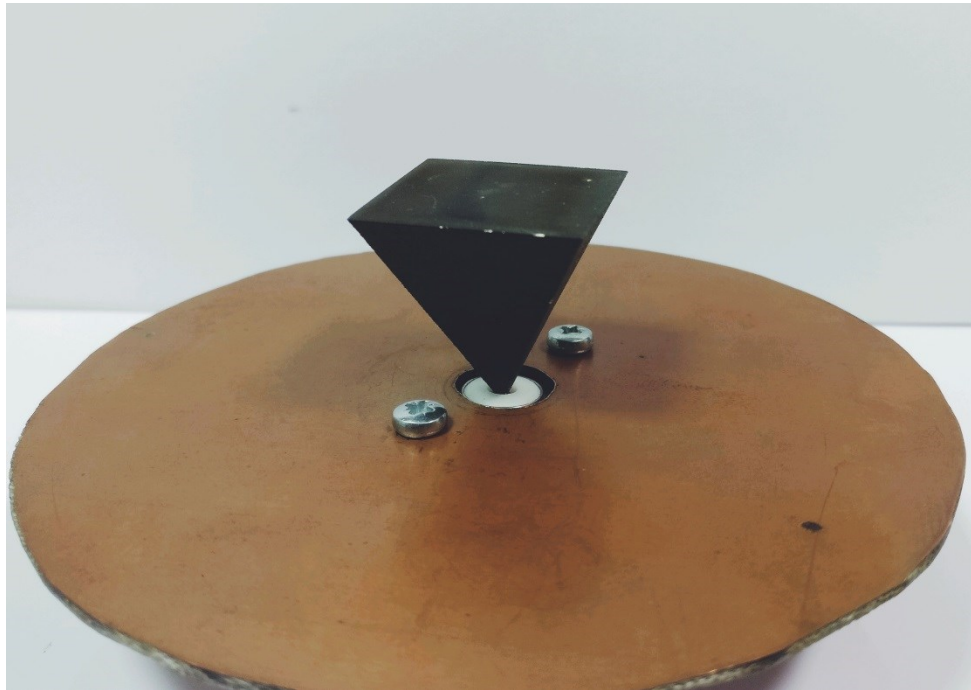


Figure 41: 3D monocone antenna with an integrated feed

The sketch of the 3D monocone antenna with the feed is illustrated in **Figure 42**. The dimensions of the antenna are listed in **Table 4**. The realized rectangular monocone antenna feed has the same dimensions as those of an N-type female feed, in order to be compatible with the N-type flange connector. The total height of the antenna along with the feed is 43 mm. A copper clad PCB ground plane, with a diameter of 120 mm and with 1 mm thickness, was used as a finite ground plane.

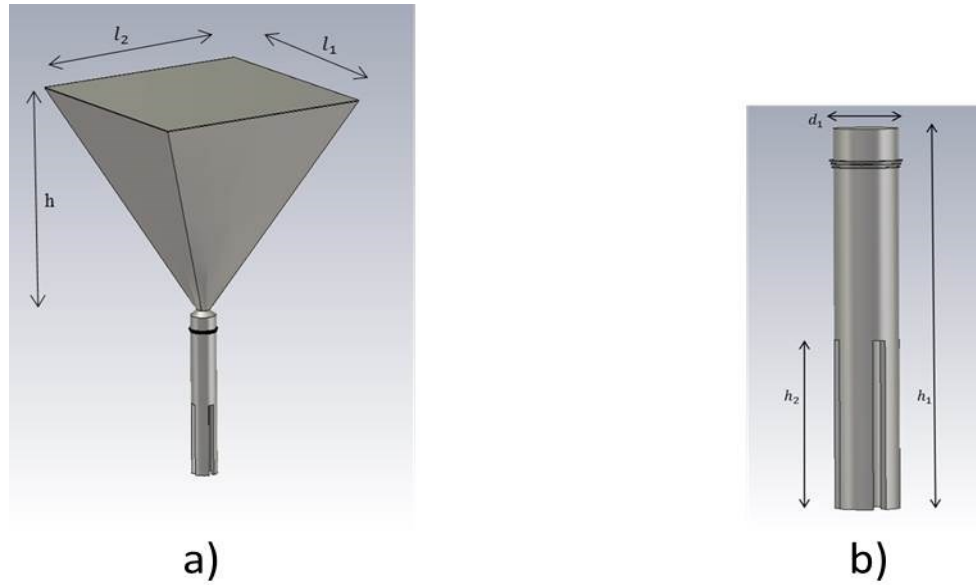


Figure 42: 3D model illustration of the (a) monocone antennas with an integrated feed, (b) N-type female feed

Table 4: Dimensions of antenna and integrated feed

S.no	Parameters	Dimensions (mm)
1	$l_1$	25
2	$l_2$	25
3	$h$	25
4	$h_1$	18
5	$h_2$	8
6	$d_1$	1.46

The thin walls of the N-type feed do not lend themselves to easy fabrication via AM. The dimensions of the feed were chosen to match an N-Type feed connector, which has a wall thickness of 0.5 mm. This decision was arrived at, taking also into account the industry standard guidelines for printing minimum wall thickness using Maraging Steel MS1 as the printing material, which is 0.3-0.4 mm [8].

**Figure 43** shows an experimental prototype of the lattice monocone, with a disfigured, unacceptable integrated feed finish, printed at a thickness below the industry-prescribed minimum wall thickness, i.e. 0.25 mm. Two experiments were run simultaneously; one was to determine the minimum thickness required to successfully print the intrinsic feed above the apex of the monocone geometry. Another was to utilize the 3D printer to fabricate lattice shape structures. Lattice structures are recognized for their advantages in

providing lightweight, stiff and shock-resistant constructions. The successful fabrication of this component later paved a path for research work detailed in the next chapter on the 3D printing of lightweight microwave components. Deeper discussion on the antennas with lattice structures is beyond the scope of this chapter and hence will not be discussed any further.

As illustrated in the **Figure 43**, the delicate feed could not be printed along with the antenna structure and hence collapsed during the build. Once it was observed that the print job had failed, the machine was stopped and the build was taken out of the chamber.



Figure 43: Experimental prototype and monocone antenna with an integrated feed

The final build dimension of the wall thickness of the feed was chosen to be 0.4 mm, to achieve the 3D antenna with an acceptable feed finish, as shown in **Figure 44**. Even though the printed screw threads were the part of the feed circuitry and were fabricated on the outer periphery of the feed, they were not successful as they merged together, due to their small dimension, of radius 0.10 mm and their minute pitch distance of 0.3 mm. The pitch distance of 0.3 mm between the screw threads was chosen as a best estimate to tighten the connection.

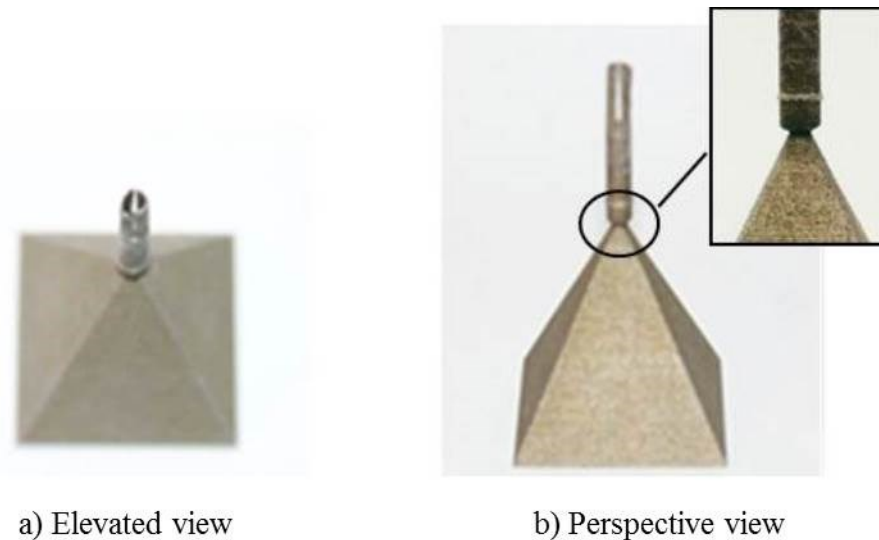


Figure 44: Photographs of 3D monocone antenna with an integrated feed, (a) elevated view (b) perspective view

The screws were only designed to provide a better grip with the flange connector. However due to their minute dimensions, an unsatisfactory finish was achieved. The poor finish of the screws did not affect the performance of the antenna, as the screws were printed on the outer part of the feed, which has no role to play in the electromagnetic behaviour of the antenna. Even though no mechanical testing has been performed on the 3D metal printed integrated feed to evaluate its strength, visual inspection and manual flexing confirmed a similar mechanical strength of the printed feed in comparison to an off-the-shelf N-type connector.

#### 4.4 SURFACE ROUGHNESS ANALYSIS

3D printing has great potential in the production of microwave components, however, there have been concerns regarding its inherent rough surface finish. With 3D metal printing technology, there are many reasons due to which the surface roughness occurs on the printed structure such as laser intensity, Particle Size Distribution (PSD), layer thickness, melt pool, build orientation, removal of support structures. Some of them are discussed in detail in **Section 3.5**. These factors can be categorized under two groups, where some of them are considered to be avoidable, while the rest be non-avoidable.

Two of the avoidable factors for surface roughness are build orientation of the component and the material layer thickness, depending on the availability, from which the structure has been built. The influence of build orientation on the surface roughness of 3D metal printed antenna will be discussed in detail in **Chapter 6** of this thesis. While layer thickness also affects surface roughness, on the other hand, it also has an impact on the construction time of the build. From my previous research work described in Chapter 3, where I manufactured a Sierpinski gasket antenna using Titanium alloy, with a PSD of 10-60  $\mu\text{m}$ , the surface roughness of the lateral side of the Sierpinski gasket antenna was found to be 14.47  $\mu\text{m}$ , when the structure was built with a layer thickness of 30  $\mu\text{m}$ . On the other hand, in this research, where the monocone antenna has been fabricated with Maraging Steel, MS1, with a PSD of 10-60  $\mu\text{m}$ , and a material layer thickness of 20  $\mu\text{m}$ , the surface roughness of the lateral side of the printed component was found to be 4.97 $\mu\text{m}$ . The surface roughness values obtained are in accordance with the data sheet values, provided by the manufacturer, for the print thickness value selection for both materials [8][9].

This surface roughness was investigated using WLI, as shown in **Figure 45**. The investigation proves the importance of the print thickness and material selection on the surface roughness of the microwave component. This has been one of the reasons that all further components described in this thesis has been fabricated using Maraging Steel as the conductive material (apart from the one mentioned in the next chapter, which are fabricated using Titanium alloy, but are the polished to achieve a roughness value  $<0.5$   $\mu\text{m}$ ), with a material layer thickness of 20  $\mu\text{m}$ , which was not an option if the material selection was Titanium on an EOS M280 system.

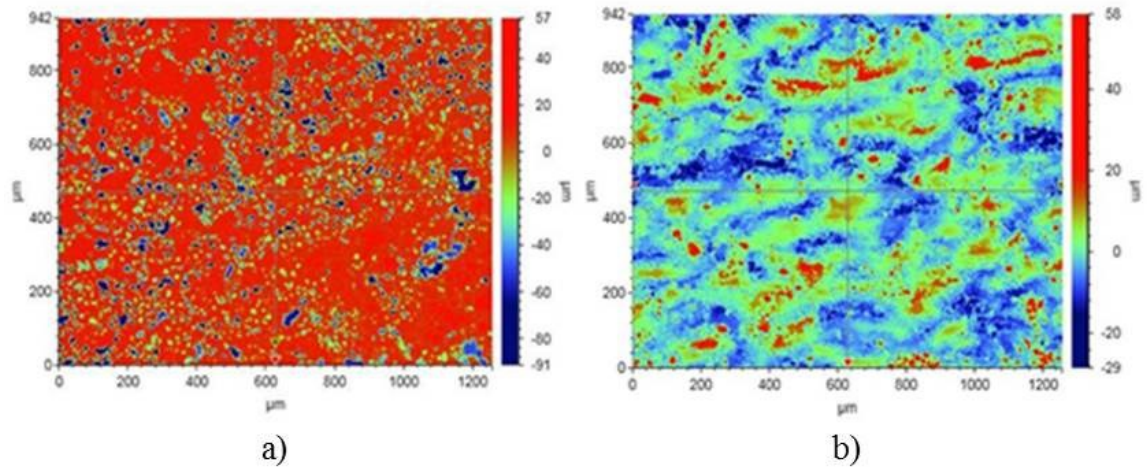


Figure 45: 5x WLI scan for surface roughness measurement of the lateral side of 3D metal printed monocone antenna fabricated using two different materials (a) Titanium alloy (Sierpinski gasket antenna), (b) Maraging Steel

The selection of the layer thickness in the printing of the structure is an option to reduce the surface roughness, and could prove to be significant, especially when there is no possibility of using surface treatment techniques. Although the surface roughness is in the range of  $4.97\ \mu\text{m}$ , compared to the calculated skin depth of  $3.89\ \mu\text{m}$  (at the highest operational frequency of  $8.4\ \text{GHz}$  and  $4.89\ \mu\text{m}$  at  $5.8\ \text{GHz}$ ), no further efforts were made to improve the surface finish of the printed antenna using surface treatment processes. The decision was also taken keeping in view the geometry of the monocone antenna attached to an integrated feed, which makes the component impossible to be polished, especially at the lateral side using Buehler EcoMet™ 250 Grinder-Polishers. Also, from the datasheet value provided by the manufacturer, for the surface roughness of the component post-wetblasted and from past experience of wetblasting Maraging Steel material, no significant improvement would have been made to the surface roughness values of the component.

## 4.5 RF RESULTS

A comparative return loss,  $S_{11}$  (in dB), graph between the measured and simulation results, is shown in **Figure 46**. The results indicate the wide band nature of the proposed antenna and illustrate that both results are in reasonable agreement with each other, in terms of overall bandwidth. The impedance bandwidth results prove that there is no ill effect of printing a feed as a single component along with an antenna, and this technique

could potentially become a viable option in the near future, in replacing the mounting process of an antenna and minimizing the errors due to an imperfect feed connection.

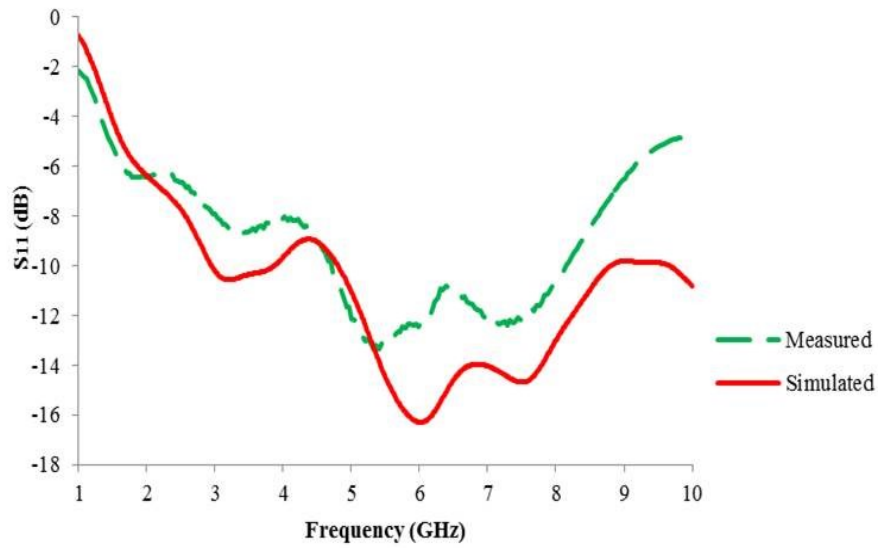


Figure 46: Simulated and measured return loss of 3D monocone antenna with an integrated feed

**Figure 47** presents the simulated and the measured VSWR as a function of frequency. The magnitude of VSWR is well matched and is below 2 over the whole bandwidth, representing a good match with each other.

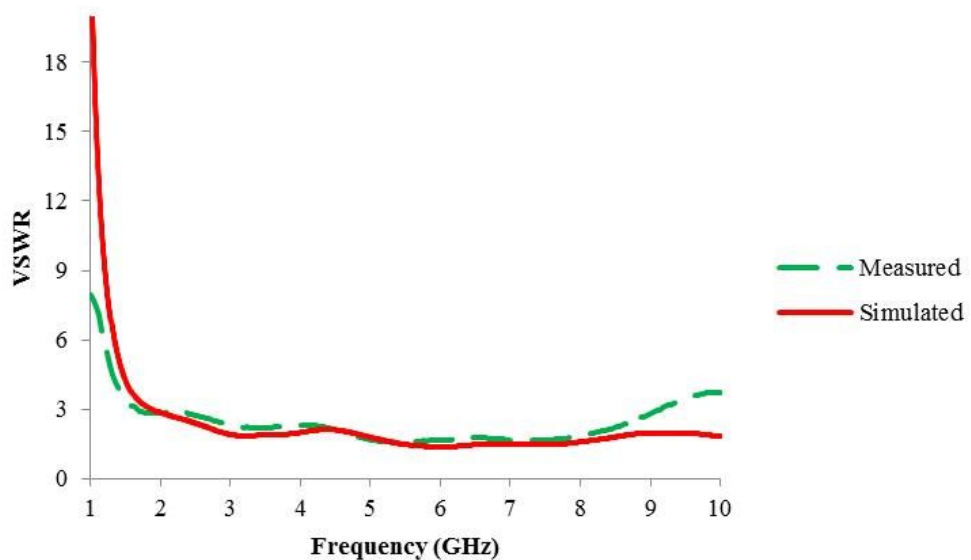


Figure 47: Simulated and measured VSWR

In addition, to the return loss measurement, the realised E-plane gain measurements of the antenna were also performed, at three different frequencies, a) 4.75 GHz b) 5.2 GHz c) 5.8 GHz, as illustrated in **Figure 48**. The simulated and measured gain is frequency dependent at 4.7 dB ( $\pm 1$  dB) over the whole bandwidth.

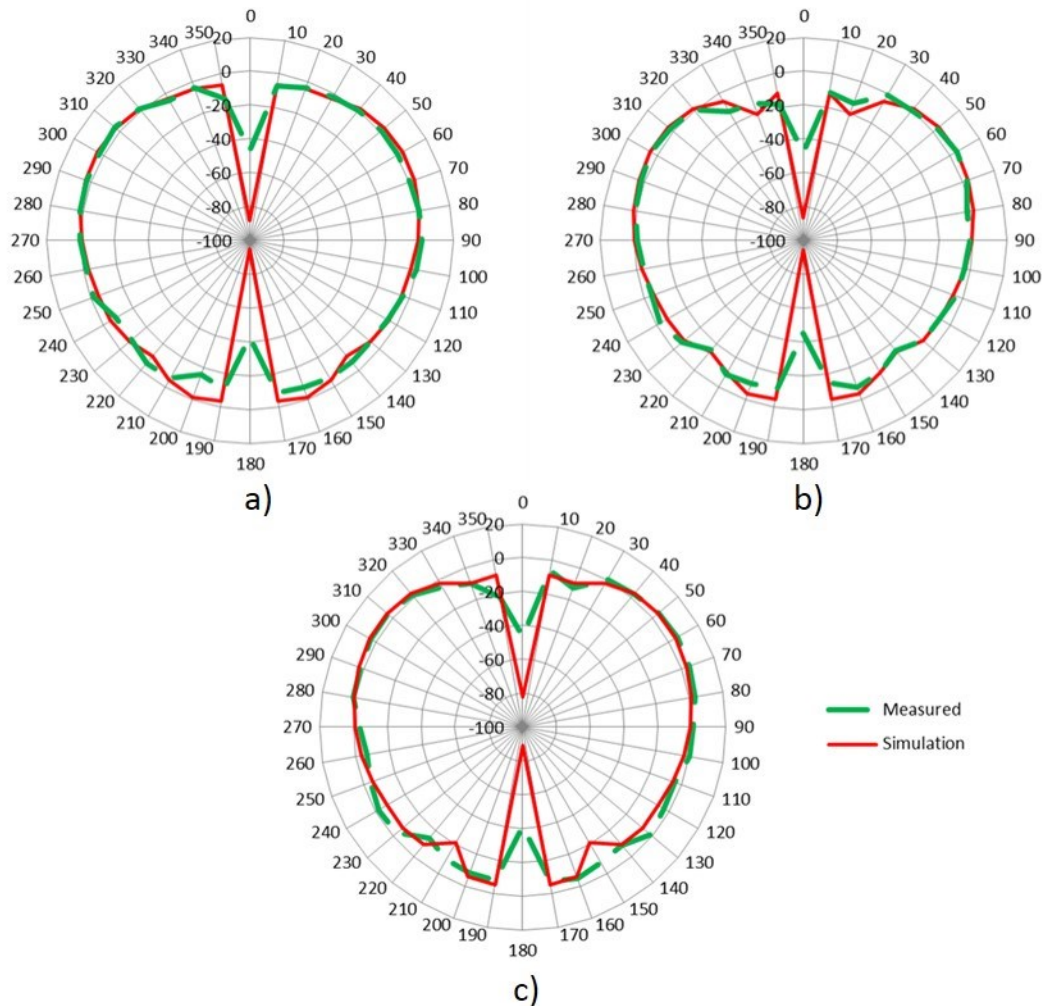


Figure 48: Simulated and measured gain radiation pattern a) 4.75 GHz b) 5.2 GHz c) 5.8 GHz

The discrepancies between the measured and simulated gain of the 3D proposed antenna, can arise due to the fact that the friction fit, which lead to impedance mismatch as the design is still not perfect. One more reason for the difference between the measured and the simulation values could also be due to the effect of surface roughness, whose values were almost comparable to that of the skin depth of the microwave component.

## 4.6 SUMMARY

A compact 3D monocone antenna with an intricate, integrated N-type feed has been modelled, simulated and fabricated, as a single component via 3D printing. The study proposes a novel alternative approach by printing a feed with any antenna using the DMLS process. The impedance bandwidth results have proven that there are no ill effects of printing a feed in conjunction with an antenna. This approach can help antenna designers in replacing the mounting of an antenna by using solder or epoxy glue and in minimizing the errors due to an imperfect feed connection and also remove one extra step of mounting an antenna on to the feeding circuitry. This also yields a far more robust component than conventional methods. In this chapter, for the first time, lower print layer thickness has been used for the fabrication of microwave components, to avoid the surface roughness. Comparative WLI results prove the surface roughness, being dependant on print layer thickness, can be reduced with the usage of a lower print layer thickness, minimizing its effect on the electromagnetic component.

With the successful outcome of integrating a signal feed onto a 3D metal printed antenna, the next task was to exploit the potential of DMLS in the fabrication of lightweight structures. The detailed research work on this topic has been carried out in the next chapter.

*\*\* Publication arises from this chapter has been presented in:*

*Proceedings of 47<sup>th</sup> European Microwave Conference (EuMW), Nuremberg, Germany, October/2017.*

## 4.7 REFERENCES

1. K. Belvin, "(Master's Thesis) Examining 3D Printed antennas for spaced based applications", *University of New Mexico, May/ 2015*.
2. S. M. Naveen, R. M. Vani, P. V. Hunagund, "Compact wideband rectangular monopole antenna for wireless applications", *Wireless Engineering and Technology*, vol. 3, pp. 240-243, 2012.
3. S. T. Choi, K. Hamaguchi, R. Kohno, "A novel microstrip-fed ultrawideband triangular monopole antenna with wide stubs", *Microwave and Optical Technology Letters*, vol. 51, no. 1, pp. 263-266, 2008.
4. I.H. Choi, S. S. Choi, J. K. Park, H. W. Song, H. S. An, "Design of a compact rectangular mono-cone antenna for UWB applications", *Microwave and Optical Technology Letters*, vol. 49, no. 6, pp. 1320-1323, 2007.
5. M. Hayouni, F. Choubani, M. Denden, T. H. Vuong, J. David, "A novel compact ultra-wideband rectangular shaped antenna", *Progress in Electromagnetics Research Symposium Proceedings, Marrakesh, Morocco, March/ 2011*.
6. S. Bories, C. Roblin, and A. Sibille, "Ultra-wideband monocone antenna for UWB channel measurements", *XXVIII URSI Convention on Radio Science and FWCW Meetings*, pp. 1-3, Oulu, Finland, Oct/ 2003.
7. RS Components Ltd., "(Online) N type connector, female, contact part: gold plating, 50  $\Omega$  Radial", (<https://jp.rs-online.com/web/p/n-connectors/2956898/>), [Accessed: 10<sup>th</sup> June 2017].
8. EOS, "(Online) EOS Maraging Steel MS1 - Material Data Sheet", ([http://ip-saas-eos-cms.s3.amazonaws.com/public/1af123af9a636e61/042696652ecc69142c8518dc772dc113/EOS\\_MaragingSteel\\_MS1\\_en.pdf](http://ip-saas-eos-cms.s3.amazonaws.com/public/1af123af9a636e61/042696652ecc69142c8518dc772dc113/EOS_MaragingSteel_MS1_en.pdf)), [Accessed 15<sup>th</sup> January 2016].
9. EOS, "(Online) EOS Titanium Ti64 - Material Data Sheet", ([http://www.crpm.co.za/wp-content/uploads/2017/07/M280-Titanium\\_Material\\_data\\_sheet\\_10-11\\_en.pdf](http://www.crpm.co.za/wp-content/uploads/2017/07/M280-Titanium_Material_data_sheet_10-11_en.pdf)), [Accessed: 15<sup>th</sup> January 2016].

# 5

## CHAPTER 5

# IMPROVING THE STRENGTH-TO-WEIGHT RATIO OF 3D PRINTED ANTENNAS: METAL VERSUS POLYMER

## ABSTRACT

The research presented in this chapter compares the weight and structural strength of several versions of the same 3D metal printed antenna, to the equivalent metal-coated 3D polymer printed antenna. In this chapter, a metal antenna has been fabricated, which weighs lighter than its metal-coated 3D printed polymer equivalent antenna, while also possessing much higher structural strength. The RF performance was confirmed to be similar to the CST simulation results, for each antenna. Mechanical testing has also been conducted, to compare the strength-to-weight ratio of each of the metal and polymer printed structures.

## 5.1 INTRODUCTION

As discussed in previous chapters, the fabricating material used for 3D printing can either be polymer or metal. When the physical RF component structure is polymer printed using non-conducting thermoplastics, such as ABS or PLA, it must then be uniformly metallized or covered with conductive paint, in order to make the printed component electromagnetically functional. Uniform metal-coating or selective coating, adds an extra processing step over standard polymer printing, to achieve acceptable electromagnetic performance from the component. One of the major advantages which metallized 3D polymer microwave components offer, is that they are inherently lightweight compared to the equivalent metal components, making them of value in sectors where weight is at a premium. However, they also suffer from disadvantages, such as the lack of mechanical strength, as well as unsuitability for high-power or high-temperature applications. Due to

the metal coating thickness of just a few microns, they are vulnerable to even small abrasions over their relatively thin metalized surface, which can lead to an undesirable electromagnetic performance from the component.

In that regard, recent interest has been to fabricate all-metal lightweight microwave components, which would possess all the benefits of 3D polymer printing, such as realizable conformal shapes, while also offering the possibility of still being lightweight, through careful design. One such attempt in this regard has been done in [1], as mentioned in **Chapter 2**, where the authors have used the perforation technique to fabricate a lightweight horn antenna. The same technique, if applied to another antenna type, could possibly obstruct the free flow of surface current, degrading the performance of the microwave component. While the technique to reduce the weight of the structure depends on the design, in this work, an attempt has been made to keep the surface current as unaffected as possible.

The aim of the research, presented in this chapter is to exploit the potential of DMLS in manufacturing microwave components that have all of the desired electromagnetic properties, but with higher strength-to-weight ratios, than polymer counterparts. The detailed design of the 3D metal antennas and their weight comparison with the polymer equivalent are presented in **Section 5.2**. The mechanical strength test results are included in **Section 5.3**, while **Section 5.4** describes their RF characterization.

## 5.2 ANTENNA FABRICATION

Two of the foremost advantages of 3D printing lies, first of all in its ability to manufacture complex structures which are difficult or in some case impossible to manufacture using conventional manufacturing techniques. Secondly, in its ability to fabricate lightweight structures, with the help of non-solid interior structures, and sometimes with the help of unit cell lattice structures. The repeating unit lattice is a 3D periodicity, open-cell, cellular structure, which contains straight struts of uniform thickness and consistent joint angles arranged in a symmetrical fashion. Such structures offer features such as high strength accompanied by a relatively low weight [2]. For example, **Figure 49** shows the three different lightweight heat sinks produced during the course of this research, with various lattice sizes designed along the fins of the heat sinks, to increase the surface area of the

component. The same feature has been used in this work in the fabrication of a lightweight metal antenna.

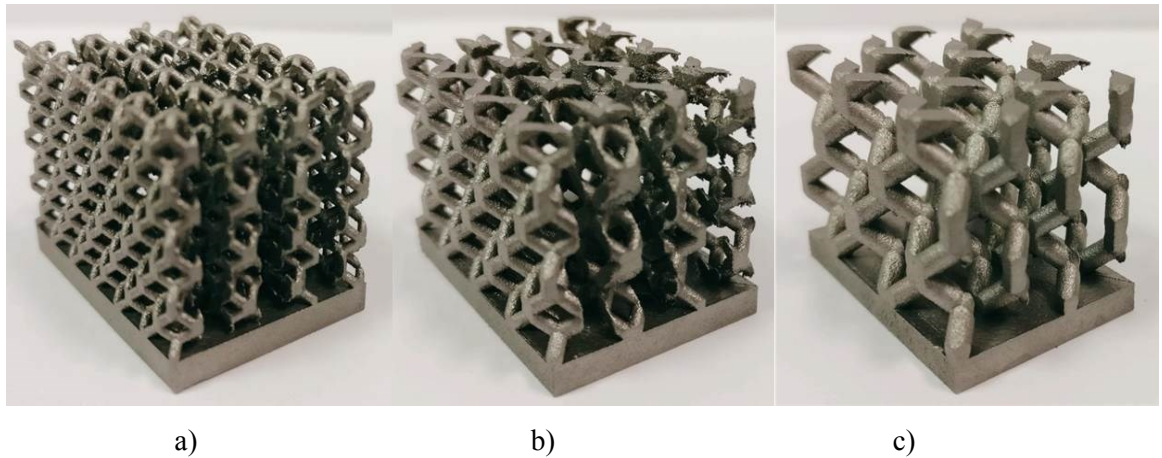


Figure 49: 3D metal printed lattice structures heat sinks, fabricated with varying unit cell length dimensions along the fins a) 5mm, b) 7.5 mm, and c) 12 mm

This work considers an alternative approach to microwave antennas production, with improved structural strength, by printing lightweight all-metal antennas, all with similar RF performance. Four versions of the same antenna were printed; one polymer and three metal, all with identical external dimensions and thus RF performance. Considering the minimum skin depth required for an antenna to be electromagnetically functional, and exploiting the potential of the DMLS technique to print very thin walls, two lighter weight metal antennas were manufactured, keeping their overall outer structural dimensions unchanged, but with non-solid internal structures. All 3D metal printed antennas in this work, were fabricated in a titanium alloy (Ti-6Al-4V), on a DMLS EOS M280 system. The printed antennas are first iteration Sierpinski gasket antennas, having a large side length of 32.3 mm, corresponding to a half-wavelength frequency of 5.35 GHz. As for previous work on the 2<sup>nd</sup> iteration Sierpinski gasket antenna, here also the selection of antenna and frequency of operation were done merely as a proof of concept, largely to show the ability of AM to produce lightweight, complex-geometry microwave components. However, as before the same structure can be designed for different wavelengths.

It is worth mentioning here that the selection of Sierpinski gasket antenna could be considered a bit odd. However, the weight reduction technique presented in this chapter

could be replicated for other 3D inverted cone antennas as well, including the monocone antenna presented in **Chapter 4**. The approach could be used in future for fabricating spatially smaller lightweight inverted cone antennas for wide band applications [3]-[5].

Also, the selection of the titanium alloy for the fabrication of the antennas was done as the material had the advantage of keeping the overall weight of the antenna low, in comparison to an antenna fabricated from steel, as titanium itself as a material is approx. 45% lighter than steel. Also, and by extension, titanium itself possesses a high strength-to-weight ratio, which would further increase the structural yield compression strength of the entire antenna structure.

The solid, hollow and metal-coated polymer antennas were modelled and simulated for RF performance using CST. However, the lattice structure, due to its complex geometry, could not be successfully modelled in this manner and was instead designed (only, no RF simulation) using Materialise Magics 19.01 [6], which is better-equipped than CST to generate lattice structures. The design file was then exported in .STI format, which is widely acceptable, by all forms of 3D printing machines.

The limitations of 3D printing were always kept in mind, which include the design limitations imposed on the lattice structures, the minimum wall thickness required, the need to include escape holes and also the need for support structures required due to the minimum overhanging angle demand and to dissipate excess heat.

### **5.2.1 SOLID METAL PRINTED ANTENNA**

The first antenna produced was a solid metal antenna. Also, just like the 2<sup>nd</sup> iteration Sierpinski gasket antenna, in this work also, external support structures were added for all-metal antenna mentioned in this research while printing as a precaution, as shown for example in **Figure 50**, to reduce the droop risk while being printed.

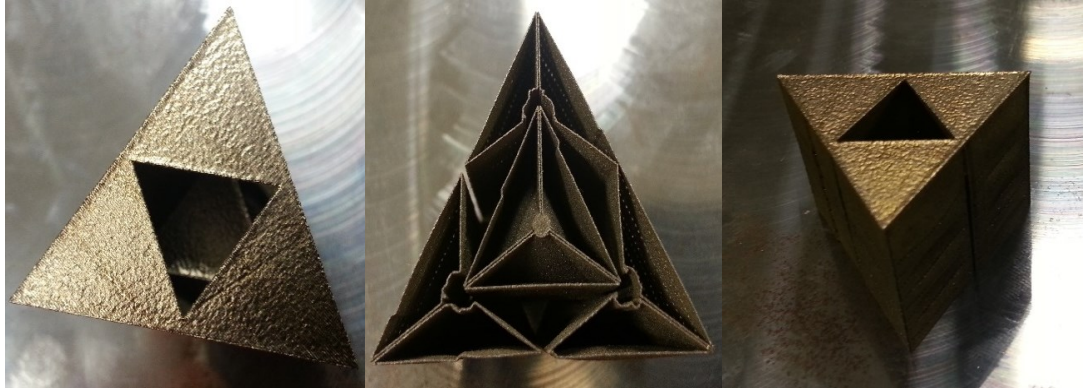


Figure 50: 3D metal printed first iteration solid Sierpinski gasket antenna with build support

Once the solid antenna was post-processed (Wire-EDM and heat treatment) and surface treated using techniques such as wetblasting and grinding-polishing, as explained in detail in **Section 3.5**, the solid metal antenna weighed 10.57g. The weight of this antenna will serve as a reference, against which all other antennas weights and performances will be compared.

In this research, the read side or the “reflective shiny side” of a Compact Disk (CD) with a diameter of 120 mm, and with 1.2 mm thickness was used as an immediate ground plane to all four monopole antennas, as shown in **Figure 51**. The performance of this antenna design with a CD as ground plane was simulated and measured and compared with the same results for an alternative copper clad FR-4 PCB ground plane. Both ground planes were found to be exactly same.



Figure 51: 3D metal printed solid antenna with CD as ground plane

The selection of a CD as a ground plane was done primarily to exploit the thin layer of aluminum beneath the polycarbonate layer coating. The positioning hole being in the middle of the CD was also well suited to mounting an off-the-shelf N-type connector centered in the ground plane, to be used as a feed to the monopole antenna. Using a CD as a ground plane, also allowed this part of the testing to be a controlled parameter, and allowed rapid prototyping, as each antenna was readily furnished with an identical ground plane configuration. In this research, an assumption was made that the polycarbonate layer, the top layer of CD, has minimum impact on the electromagnetic performance. Also for fair comparison, all the antennas manufactured in this chapter used a CD, as a ground plane.

### 5.2.2 HOLLOW METAL PRINTED ANTENNA

In the case of the 3D Sierpinski gasket antenna, where the majority of the surface current flows along the outer periphery of the antenna, designing an antenna with a hollow interior would have negligible effect on its RF performance, compared to the performance

of the solid antenna discussed earlier. The next antenna after the first iteration Sierpinski gasket solid antenna was the first attempt at a hollow equivalent antenna.

In the antenna design process, three considerations were added to the design brief, all related to successful printing of the antennas. The first consideration was the wall thickness of the 3D printed antenna structure, which should be kept at a minimum given the weight reduction goal. Therefore, a 1 mm wall thickness (the same for all surfaces) was chosen as the best design target for the hollow antenna, bearing in mind the overall structural strength, as the structure needs to be strong enough to prevent breaking during the printing process, especially in this case, where the interior of the antenna is hollow. Choosing the wall thickness value of 1 mm will not affect the performance of the antenna, as the value is much greater than the skin depth for the alloy at the frequency of operation.

The second consideration, which is a direct consequence of all hollow structures in 3D printing, related to removing unused powder from within the hollow structure. 3D printing of a hollow structure has the complication of trapping unsintered material powder inside hollow interiors. To avoid such a scenario, escape holes are recommended in order to get the ‘trapped’ unsintered Ti-6Al-4V powder out of the model, partly because the unsintered powder is not only recyclable but also in this case, if trapped inside the antenna, would add unnecessarily to the weight. However, having escape holes can disrupt the flow of surface current, which would further result in a change in the radiation characteristics of the proposed antenna. Therefore, CST was deployed to simulate the current flow through the antenna and played an important role in deciding the position of escape holes. From the CST simulations, it was observed that the majority of the current flow was through the triangular surface areas connected to the apex of the tetrahedrons as shown in **Figure 52**. For this reason, escape holes were designed on the top flat surface of each tetrahedron, where the current density was at its minimum. Also, in order to keep the RF attenuation to a minimum due to conductor losses, the escape holes were limited to only one per tetrahedron; with an opening diameter of 1 mm.

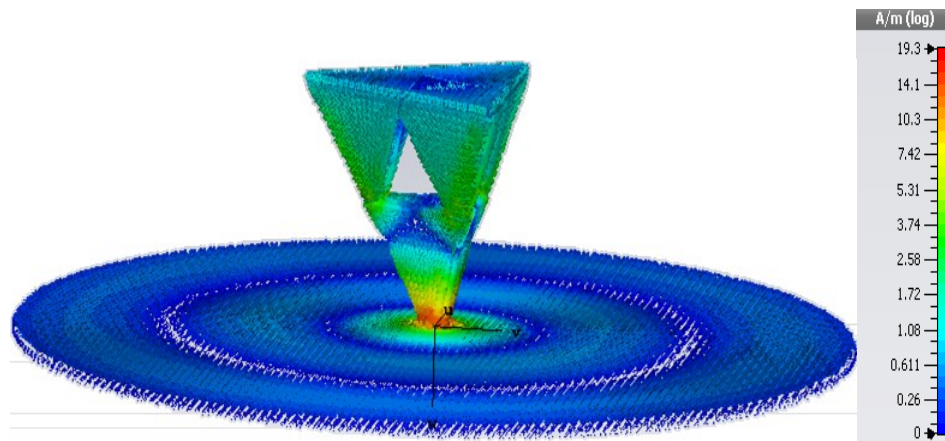


Figure 52: CST simulation of surface current distribution along the surface of antenna

The third and most important consideration related to printing the hollow tetrahedron, is that during printing there is a risk of drooping of the top flat surface of the individual tetrahedrons, due to the lack of any supportive base beneath them (inside the hollow). In order to overcome this problem, the hollow space beneath the flat surface was re-designed, so that the upper surface of the hollow space is not parallel to the outer flat surface, but instead slopes inwards at an angle of  $45^\circ$  from all tetrahedron sides towards a point in the centre. This makes an internal apex in the hollow void and the metal of the upper flat surface slightly thicker and thus stronger, from the sides towards the centre, as shown in **Figure 53**. Adding an internal support structure of this kind, by increasing the surrounding wall thickness to the hollow structure, would have negligible effect on the RF performance of the antenna.

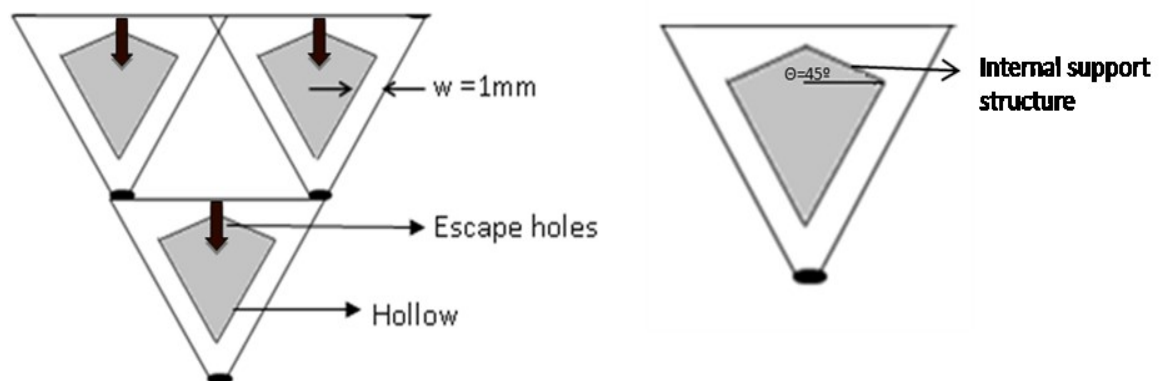


Figure 53: Illustration of hollow antenna with internal support

After the post-processing, the hollow metal antenna weighed 8.75g, approximately 17.2% lighter than the solid metal antenna. The hollow antenna, mounted on an N-type connector, is shown in **Figure 54**, with the escape holes clearly visible on the top.



Figure 54: 3D metal printed hollow antenna with CD as ground plane

### 5.2.3 INNER LATTICE METAL PRINTED ANTENNA

The next antenna aimed to further improve the strength-to-weight ratio compared to the available lightweight polymer antenna, is an inner lattice structure antenna, as shown in **Figure 55**. Materialise Magics 19.01 software was used to design the inner lattice structure sandwiched within an outer skin. The lattice design was chosen to be rhombic dodecahedron with 30% relative density, and with a unit cell length of 6 mm. This design was chosen due to its less dense structure, long side length and the ability to be successfully printed with an outer surface that exceeds the RF skin depth. Also, the lattice design chosen is self-supportive and can be easily fabricated without any need of support structures. As the research work presented in this chapter is merely a proof of concept, there is no intention to analyse different lattice structures, to further reduce the weight of the component or to enhance the strength, as that would be beyond the scope of this research. However, there is huge potential to further lighten the weight or to enhance the

strength, by examining other lattice structures and optimizing the unit cell parameters for lattice generation.



Figure 55: 3D metal printed inner lattice antenna with CD as ground plane

With the interior lattice offering strength, it was possible to reduce the outer antenna wall thickness to 0.5 mm, compared to the strength-defined minimum wall thickness of 1 mm, used for the first hollow antenna. The thickness of 0.5 mm was chosen due to prior experience with thin printed structures. However, the data sheets suggest that the minimum wall thickness that can be printed using Ti-6Al-4V is 0.3-0.4 mm. The actual fabrication thickness was a little higher, at 0.5mm, and was a reasonable compromise to successfully print a structure with an inner lattice, to reduce the weight without risking the structural integrity during printing [7]. Similar to the hollow antenna, this inner lattice antenna also required the inclusion of escape holes needed to get the trapped metal powder out of the 3D printed structure. However, in this antenna the escape hole diameter was 2 mm. Increasing the diameter was essential, as it would otherwise have been too difficult to remove the unsintered powder from the more complex internal geometry. Increasing the diameter from 1 mm (hollow antenna) to 2 mm also has a slight impact on

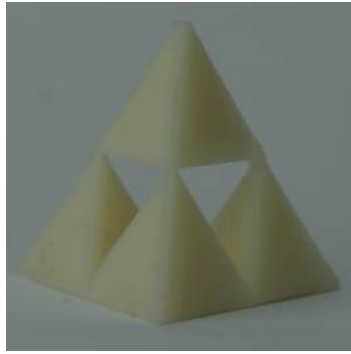
minimizing the weight of the component, but not on its RF performance, as the escape holes were placed at the top faces, where the current density was at its minimum.

Following the surface treatment steps such as wet-blasting and grinding-polishing, the antenna weighed 6.01g, which was 43.1% lighter than the solid metal antenna.

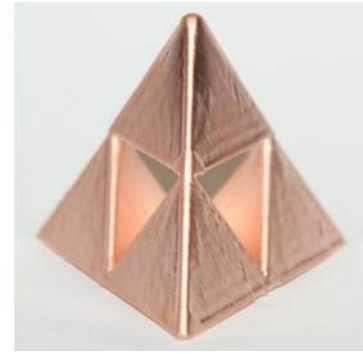
#### 5.2.4 METAL-COATED POLYMER PRINTED ANTENNA

Similar to the DMLS technique just described, FDM is also an AM process, which builds polymer parts in a layer-by-layer fashion using computer-aided design (CAD) files, again converted into the same .STI file format usable by the 3D printer. During the printing, the polymer fabrication material takes the form of plastic threads, or filaments, which are unwound from a coil and fed through an extrusion nozzle. The nozzle then melts the filaments and extrudes them onto a base, called a build platform. Both the nozzle and the base are computer controlled, which translates the dimensions of an object into X, Y and Z coordinates for the nozzle and base. Once a layer has been completed, the base is lowered with every print, to make room for the next layer of plastic to form a 3D structure. The printing filaments used for this research was ABS. The first iteration Sierpinski gasket antenna printed using FDM with ABS, as shown in **Figure 56a**.

ABS, as the fabricating material, is commonly used in fabricating microwave components partly because it is lightweight and partly because it is cost-efficient, compared to the other material options available for 3D polymer printing. Apart from that, ABS also has other useful properties, such as good chemical resistance, especially important when the 3D structure has to be metal-coated, and it also possesses excellent adhesion to metal-coatings [8]. While ABS is commonly used because of the above mentioned advantages, it is also true that there are other fabricating polymers available, which possess higher tensile strengths compared to ABS. One such polymer is ULTEM 1010, which is a high-strength, high resistant, 3D printing thermoplastic [9]. However, as research is more focussed on highlighting the proof-of-concept of lightweight metal printed components.



a)



b)

Figure 56: 3D Polymer printed antenna a) post printing b) post metal-coating

Once the FDM fabrication process had been completed, the next step was to make the component electromagnetically functional through the electroless plating method. For this research work, electroless plating on the polymer printed component was done in close collaboration with RepliForm Inc. [10], by providing them with the specification for the amount of metal coating to be done on the printed component.

The process was very instructive. It was learned that the plating is not directly performed on the polymer printed part, which was first treated for surface porosity, which, if not done could present an obstacle later in the printing/coating process. There are different sealing options for FDM printed parts, including dipping, vapor smoothing, and epoxy impregnation. The first two methods are fast and easy, and do a reasonable job of sealing. However, dipping will not work on sparsely built parts and can also degrade the part, by rounding the corners. Moreover, vapor smoothing does not consistently seal and even rounds the edges. Therefore, in order to maintain the sharp edges of the polymer printed structure, epoxy impregnation was chosen. The sealing process is straightforward and required the FDM parts to be immersed in the epoxy resin followed by placement in a vacuum chamber, to help infiltrate the epoxy into the part. The entire process takes about three hours to complete and offers air- and water-tight sealing of the FDM manufactured parts. Sealing by this method also increases the thermal resistance, so the parts have better performance in high temperature and furthermore protects the ABS, by offering chemical resistance.

Once the process of sealing the FDM parts was done, the next step was the plating process. In order to make the FDM part into a functional microwave component, a simple application of a metal coat of thickness of its skin depth value would be enough. This can be achieved either by applying a simple conductive spray over the FDM part or by the more difficult electroplating method. However, both these methods are manual and provide an uneven metallic coating over the entire surface, which not only further leads to an undesirable electromagnetic performance, but also influence the weight of the component [11] [12]. For this reason, electroless plating was chosen over the other coating methods, in order to have a uniform metal-coating thickness of 15-20  $\mu\text{m}$  on the inside and outside surface of the proposed complex antenna configurations. The uniform relatively thin coating from electroless coating was also important to keep the weight of the polymer antenna at a minimum, as coating with the other two methods would have resulted in a lumpy and uneven surface, with extra coating needed to guarantee the minimum thickness would be met everywhere, thus also adding excessive weight.

The process of electroless plating involved the sealed FDM parts being dipped in a resin so that the coating sticks. Following that, the printed part was run through a room temperature electroless nickel/copper line, to make the component conductive. This initial strike of electroless copper or nickel is required before electroplating was done to provide a conductive surface on which the copper was then electroplated. Once this step was over, the component was then placed in an electroplating tank to apply the performance coating. The effective coating conductivity of the electroplated copper has been verified to be  $5.61 \times 10^7 \text{ S/m}$ . Given that only 15-20  $\mu\text{m}$  of copper was enough to make an antenna functional, for the calculated skin depth, the process of electroplating did not take long. One alternative solution to electroless plating is the direct plating method, which according to the recent publication [13], is even capable of depositing a layer of silver spray over the component with a thickness as small as 1  $\mu\text{m}$ . The technology to achieve this uses compressed air and a double nozzle paint spraying gun, simultaneously spraying oxidizing (metallic ions  $\text{Ag}^+$ ) and a reducing agent onto the polymer printed structure, resulting in a compact, dense and adherent silver film on the surface of the printed part. The technology is extremely useful for plating microwave components for higher frequencies, where skin depth is quite small, especially for the deposition of Silver as the conducting material.

**Figure 56b** illustrates the polymer antenna post metal-coating. Once this whole process had been completed, the polymer antenna was weighed and found to be 6.63g, which is 37.2% lighter than the solid metal antenna. Once weighed, the antenna was carefully connected to the feeding circuitry as shown in **Figure 57**.



Figure 57: 3D metal-coated polymer printed antenna with CD as ground plane

A 3D model illustration of all the fabricated antennas with their interior structure is shown in **Figure 58**. The weight comparison of the 3D printed antennas is given in **Table 5**.

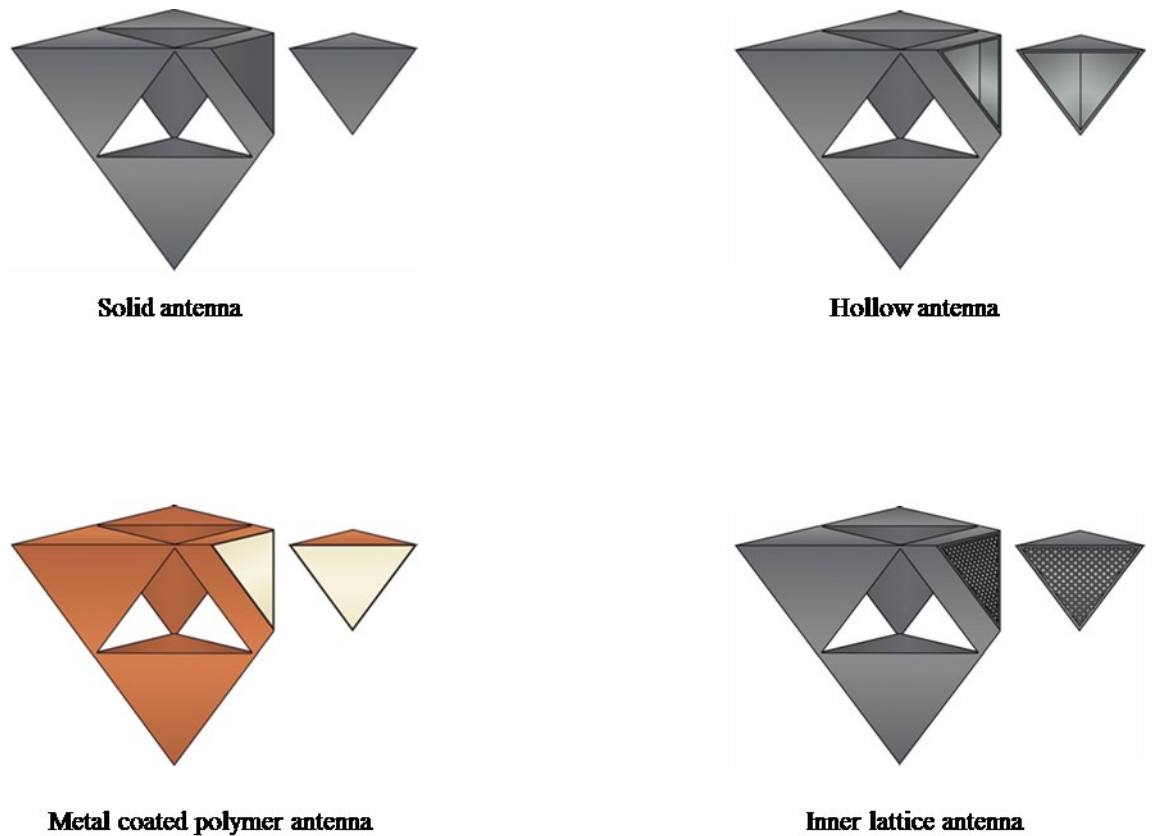


Figure 58: 3D model illustration of the antennas fabricated with their interior structure

Table 5: Mechanical comparison of 3D printed components

S.no	Antenna type	Weight (g)	Weight decrease (%)
1	Solid	10.57	Ref.
2	Hollow	8.75	17.2
3	Lattice	6.01	43.1
4	Polymer	6.63	37.2

At this stage, there are two points which are worth mentioning. Firstly, the better weight performance of the titanium lattice antenna over the polymer would not occur if steel had been used instead, which was the other printing material choice of this work. Secondly, no efforts have been made in this research, to reduce the weight of the polymer antenna any further by designing lattice or hollow structures inside. It should be also mentioned, however, that doing this would further deteriorate the structural strength of the polymer antenna.

### 5.3 MECHANICAL TESTING

3D polymer components, due to their potential for low cost and ease of manufacture of complex parts, are becoming more prevalent in many varied applications. Even many traditionally all-metal, microwave components can now be manufactured out of polymer and used for diverse microwave applications, by applying a thin layer of (conductive) metal coat over them, of thickness defined by their skin depth. However, these applications also include load-bearing applications, which require the 3D printed component to have the necessary strength properties to perform properly and safely.

In order for lightweight 3D printed antennas to be useful for some microwave engineering applications, some of their other mechanical properties, apart from their weight, may also be required. In the case of this research, the compression yield strength is quantified, so various strength-to-weight ratios will be eventually available for selection, depending on the particular application requirement. The main focus of the mechanical testing is in comparing the strength-to-weight ratios of the proposed lightweight structures. As destructive testing was used to determine the compressive strength, instead of compressing the printed antennas, testing has been performed on four representative 3D printed cube types, each of size 10 mm x 10 mm x 10 mm. As illustrated in **Figure 59**, each cube mimics as much as possible their equivalent antenna's mechanical properties. For this reason, the internal lattice is a rhombic dodecahedron with 30% relative density, and a unit cell length of 6 mm; the wall thicknesses are all identical to the antennas the cube represents.

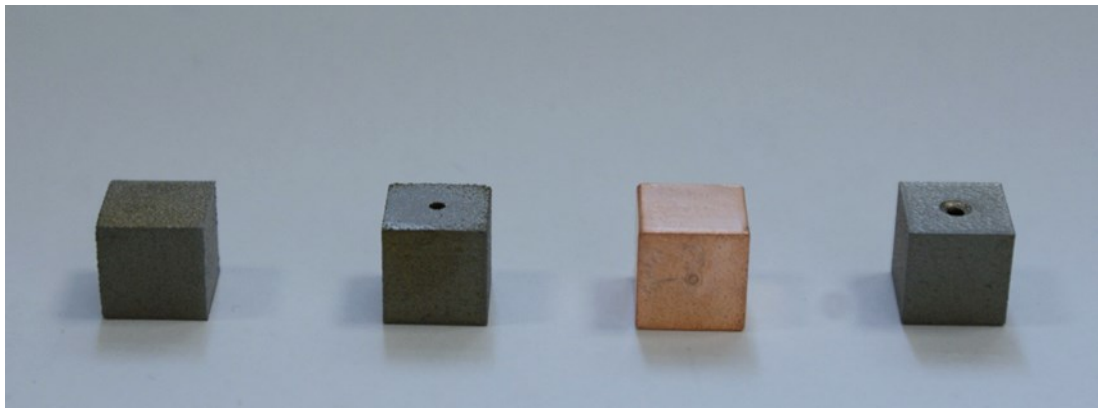


Figure 59: 3D printed cubes for mechanical testing, arranged according to their weight, left to right: solid, hollow, polymer and lattice

For this experiment, Testometric's FS150CT [14] calibrated material testing equipment has been used. The equipment is specifically designed to test large or high load samples, and to determine the mechanical properties, where the structure (specimen) must be carefully centred with respect to the testing machine heads, allowing two opposing forces to be directed towards each other, so that the cubic structure between the plates is compressed and the related mechanical properties in compression are determined. The procedure is followed until all the cube structures are compressed.

Due to the uniformity of the given solid metal printed cube (solid structure), its compression strength can be calculated by the formulae given below.

$$\text{Compression Strength} = \frac{\text{Maximum load applied to the specimen}}{\text{Area}} \quad (4)$$

However, even though hollow and inner lattice printed cubes were fabricated with a Titanium alloy, Ti-6Al-4V, with identical outer dimensions; their compressive strength will be different from the solid metal example and also they cannot be directly calculated using the above formula, due to the change in the inner cross-sectional area of the metal cubes, even though they have a similar outer face. The weight of the cubes and their measured (and not calculated) strength-to-weight ratio are detailed in **Table 6**.

Table 6: Mechanical properties comparison of 3D printed cubes

S.no	Cube type	Weight (g)	Strength-to-weight ratio (MPa/g)
1	Solid	10.57	350.5
2	Hollow	8.75	298.8
3	Lattice	6.01	165.7
4	Polymer	6.63	33.7

It can be clearly seen that the inner lattice structure has much higher structural strength compared to its polymer counterpart, even if their weights are marginally similar.

## 5.4 RF RESULTS

The antennas discussed in this chapter were designed, optimized and simulated on CST software. As the simulation plots for all the antennas were the same, only one graph has been used to compare with the measured antennas plots. The  $S_{11}$  and measured E-plane

gain radiation pattern of the antenna were measured on a Rhode and Schwarz ZVB 20 VNA. The simulated and measured  $S_{11}$  comparison graph of lightweight antennas is shown in **Figure 60**.

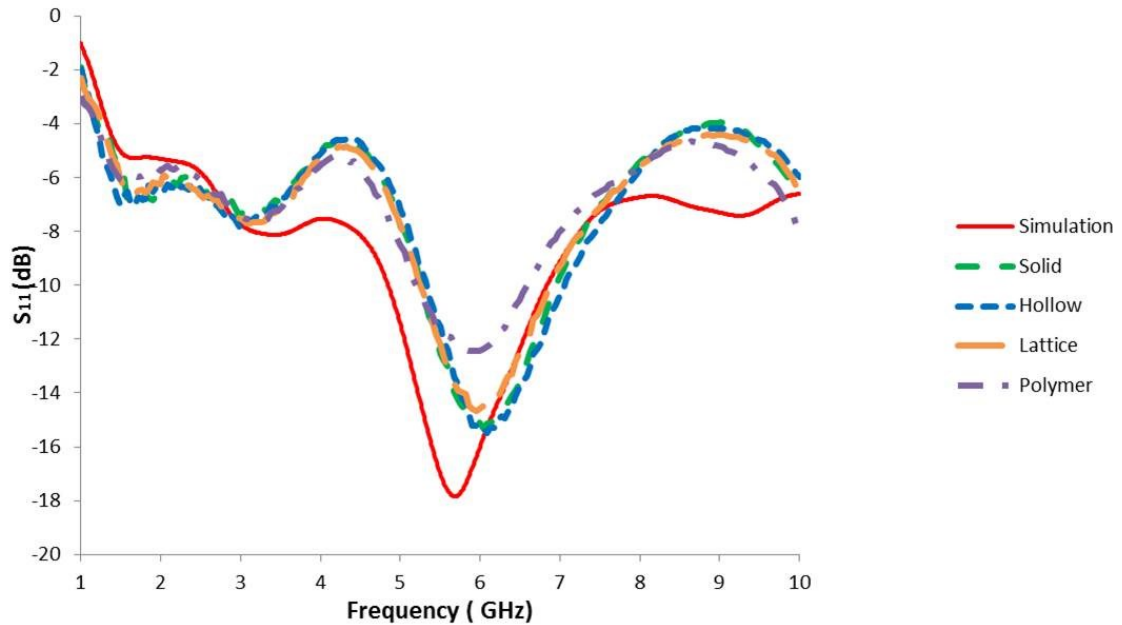


Figure 60: Simulated and measured return loss comparison graph of antennas

The difference between the simulated and measured graphs can be explained by small variations in the conductive base radius around the feed of an antenna. As explained earlier, the “ring width” effect is due to the manufacturing base radius of 0.75 mm, which was required for successful printing of the antenna. Due to this, the simulation antenna resonant dip corresponding to 5.35 GHz shifted towards higher frequency bands, in the manufactured antennas, to 5.8 GHz. Further shift of the measured results is due to the application of conductive epoxy around the feed of the monopole, due to which all the metallic antenna showed the same resonance shift to 6.03 GHz. On the other hand, in the case of the polymer antenna, where the resonant frequency has shifted to 5.8 GHz, this was due to both the application of conductive glue, as well the fact that the polymer antenna was fabricated initially with identical dimensions to those of the metal antennas. However, due to the subsequent application of epoxy resin and then a conductive metal-coating of a few microns, the combined new height of the antenna increased by up to 3 mm, causing a shift in the resonant frequency, corresponding to the increased wavelength. Although the shifts in the resonant frequencies for the antennas are quite small, this should nonetheless be considered prior to the antenna design and fabrication.

In addition to the return loss measurement, the antenna gain measurements were performed on the metal-antennas, at their resonant frequency of 6.03 GHz, and for the polymer printed antenna at 5.8 GHz. The measured results in **Figure 61** show good agreement to the simulation results. The measured and simulated gain of all 3D printed antennas were found to be 4.8 dB ( $\pm 0.5$ dB).

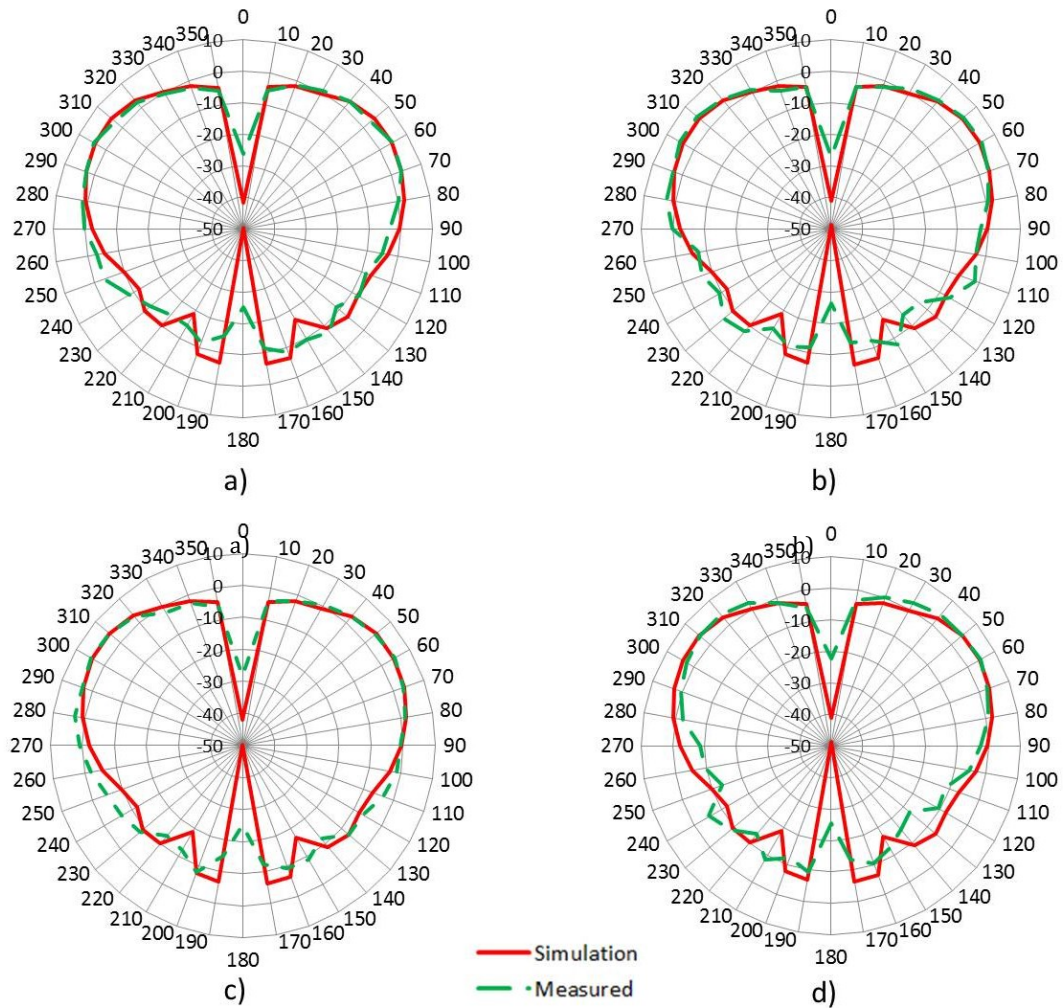


Figure 61: Simulated and measured realized E-plane gain of 3D printed antennas a) Solid b) Hollow c) Lattice d) Polymer

## 5.5 SUMMARY

In this research, three 3D metal printed antennas were investigated, with a view to reducing antenna weight, while considering also their compression strength and maintaining the same RF performance. In contrast to the polymer antennas, which are well known in industry, due in part to their lightweight properties, in this chapter, a metal

printed inner lattice antenna has been proposed, possess high strength-to-weight than the metal-coated polymer 3D printed antenna produced here.

The manufactured antennas are all relatively small, with a total vertical height of only 28 mm. However, this design can scale in every respect linearly, with the resonant frequencies changing with the length change. As the design scales linearly, the weight increase for each antenna and the weight difference between antennas will also scale linearly.

*\*\* Publication arises from this chapter has been published in:*

*IEEE Antennas and Wireless Propagation Letters*

## 5.6 REFERENCES

1. G-L Huang, S.-G Zhou, C.-Y.-D. Sim, T-H. Chio, T. Yuan, “Lightweight perforated waveguide structure realized by 3-D Printing for RF applications”, *IEEE Transactions on Antennas & Propagation*, vol. 65, pp. 3897 – 3904.
2. D. Manfredi, F. Calignano, M. Krishnan, R. Canali, E. P. Ambrosio, S. Biamino, D. Ugues, M. Pavese, P. Fino, “Additive manufacturing of Al alloys and Aluminium matrix composites (AMCs)”, *Light Metal Alloys Applications*, W. A. Monteiro, ed., *InTech*, Chapter 1, 2014.
3. S. Bories, C. Roblin, and A. Sibille, “Ultra-wideband monocone antenna for UWB channel measurements,” *XXVIII URSI Convention on Radio Science and FWCW Meetings*, pp. 1-3, Oulu, Finland, Oct/ 2003.
4. A. Alshabo, P. J. Vial, M. Ros, D. Stirling, M. A. B. Sidik, “Measurement of ultra-wideband channel sounding using a vector network analyzer”, *TELKOMNIKA (Telecommunication, Computing, Electronics and Control)*, vol. 13, no. 3, pp. 859-869, 2015.
5. H. Choi, S. S. Choi, J. K. Park, H. W. Song, H. S. An, “Design of a compact rectangular mono-cone antenna for UWB applications”, *Microwave and Optical Technology Letters*, vol. 49, no. 6, pp. 1320-1323, 2007.
6. Materialise.Magics, “(Online) Materialise Magics 19.01”,
7. EOS, “(Online) EOS Titanium Ti64 - Material Data Sheet”, ([http://www.crpm.co.za/wp-content/uploads/2017/07/M280-Titanium\\_Material\\_data\\_sheet\\_10-11\\_en.pdf](http://www.crpm.co.za/wp-content/uploads/2017/07/M280-Titanium_Material_data_sheet_10-11_en.pdf)), [Accessed: 15<sup>th</sup> January 2016].
8. United Plastic Components, “(Online) ABS (Acrylonitrile-Butadine-Styrene)” (<http://www.upcinc.com/resources/materials/ABS.html>), [Accessed: 21<sup>st</sup> September 2016].
9. Stratasys, “(Online) ULTEM 1010- High-Strength, Heat Resistant FDM Thermoplastic”, (<http://www.stratasys.com/materials/search/ultem1010>), [Accessed: 21<sup>st</sup> May 2018].
10. Repliform Inc., “(Online) (<http://www.repliforminc.com/index.html>)”, [Accessed: 1<sup>st</sup> October 2016].
11. J. Tak, D.-G. Kang, J. Choi, “A lightweight waveguide horn antenna made via 3d printing and conductive spray coating”, *Microwave and Optical Technology Letters*, vol. 59, no. 3, pp. 727-729, 2017.

12. H. Yao, L. Fang, R. Henderson, "Evaluating conductive paint performance on 3-D printed horn antennas", *IEEE Radio and Wireless Symposium (RWS)*, pp. 191-193, CA, USA, 2018.
13. A. Jammes, E. d. Gayets, K. Staelen, "Silver Metallization of 77 GHz 3D Printed Horn Antennas", *12<sup>th</sup> European Antenna & Propagation Conference (EuCAP)*, London, UK, April/2018.
14. Testometric, "(Online) 150KN FS Machines", [Accessed: 08<sup>st</sup> May 2017].

# 6 CHAPTER 6

## INVESTIGATION OF THE INFLUENCE OF BUILD ORIENTATION ON THE SURFACE ROUGHNESS OF 3D METAL PRINTED X-BAND HORN ANTENNA

### ABSTRACT

The research presented in this chapter proposes an alternative approach to avoid the inherent surface roughness of the printed microwave component. The design challenge has been to minimize the surface roughness at the high current density area of a 3D metal printed X-band horn antenna (8.2-12.4 GHz), by simply varying the build orientation of the component. Build orientation is investigated by printing the antenna at three different orientations of 45°, 90° and 180°, with respect to the building platform. The results indicate that build orientation has indeed an impact on the surface roughness, though not sufficiently high enough to affect its transmission coefficient in the X-band. The horn antennas are fabricated with Maraging Steel, MS1, using the DMLS technique. The variations in the microstructural surface roughness due to the build orientation have been analysed and measured using OM and WLI.

This investigation proves that there is no significant effect of the orientation on the gain of the antenna while working in the X-band. However, there is a variation in surface roughness and the impact of orientation would be significant if working at higher frequencies.

### 6.1 INTRODUCTION

3D metal printing microwave components is an emerging, as well as an attractive technology for various reasons already mentioned in this work, although there have also been concerns regarding the roughness of the surface finish, which is a feature of all metal printed components, as also discussed earlier. From earlier research work, it is known that if the amplitude of the surface roughness of an EM component is greater than the skin depth, its performance will be significantly degraded, mainly through signal loss [1]. For

example, in **Chapter 3**, the RF performance of 3D metal printed antenna has been improved through gradual reduction in surface roughness using surface treatment techniques. The findings of the research work concluded the negative impact of unintentional surface roughness on the performance of a 3D metal printed antenna. However, one important point to be noted here is that it is difficult to perform some surface treatments, such as polishing, on the fully- or partly-enclosed inner faces of printed microwave components, for example, in the inner cavity of a horn antenna, where the maximum current density occurs.

Surface roughness on a metal printed part depends on various factors such as laser intensity, PSD, material melt pool, print layer thickness, build orientation, removal of support structures, etc. In **Section 4.4**, the difference in the surface roughness value on the printed microwave component due to layer thickness has been detailed. The selection of material layer thickness of the printed part is an option to limit the surface roughness, which in this case for Maraging Steel has been chosen to 20  $\mu\text{m}$ . Similarly, the selection of the build orientation is also an option to limit surface roughness. The research presented in this chapter explores this approach to limit the surface roughness on the high-current density areas of the printed component, namely by emphasizing the selection of the best build orientation. The effect of the surface roughness due to the build orientation is investigated by printing a horn antenna prototype at three different orientations, of 45°, 90° and 180°, with respect to the build plate. The reason behind the different values in surface roughness due to different orientation angles is due to the “Staircase Effect” [2]-[5]. The impact on surface roughness due to the staircase effect increases when a component has overhang angles or cantilevered sections. Thus, roughness increases gradually as the angle of the component, with respect to the build plate, decreases. Due to this effect, the component built with an orientation perpendicular to the base plate may appear to be smoother than the same component’s surface built with an overhang (or at any off-normal angle). One important point here is that, even though the print layer thickness influences surface roughness, it cannot be changed during the printing process [6].

The selection of the orientation angles, in this chapter, was done to make a fair comparison, as with these selected angles, no extra support structures were required in the inner cavity in any of the three-horn antennas during the print, a place where the maximum current density lies. This eliminated the possibility of any additional surface roughness due to (later-) removed support structures.

## 6.2 ANTENNA FABRICATION

**Figure 62** shows photographs highlighting the different fabrication orientations of the three, otherwise identical, X-band horn antennas. The antennas were fabricated using DMLS technology on an EOSINT M280 system, with Maraging Steel, MS1, as the conducting material with 20  $\mu\text{m}$  layer thickness.

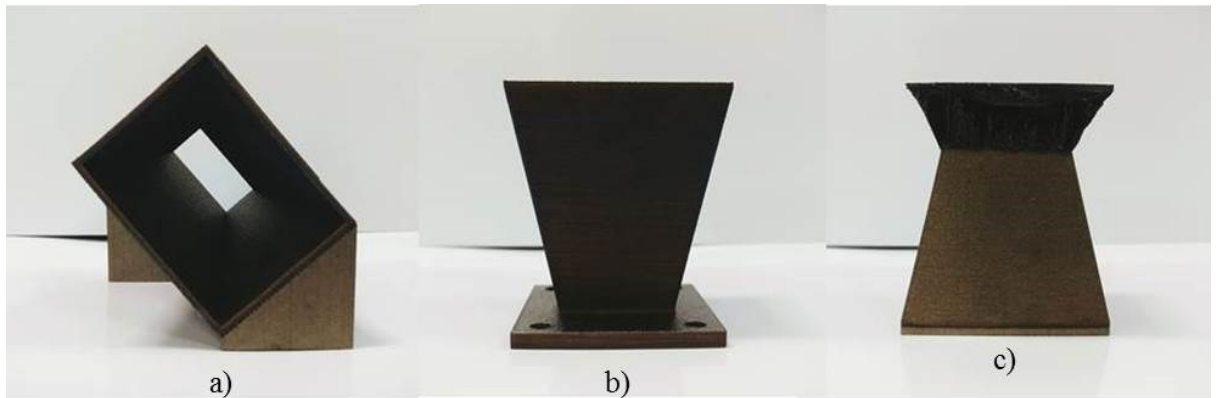


Figure 62: 3D metal printed horn antenna with support structures, constructed using different possible build orientations a) 45°, b) 90°, c) 180°

Apart from the impact on surface roughness, build orientation also has a huge impact on the construction time required to complete the entire build, as well as on the amount of support structure required for the cantilevered sections. It also influences the requirements of the support structure in the modelling file, during the file pre-processing stage. The orientation also affects the mechanical properties of the printed components, such as tensile strength and fatigue limit [4]. However, the focus of this research is to analyse the effect and highlight the importance of the selection of an appropriate build orientation on the surface roughness of the 3D printed antenna. For this reason, the other mechanical properties affected by the change in orientation, will not be considered in this work.

## 6.3 BUILD ORIENTATION AND ITS EFFECT ON SURFACE ROUGHNESS

A 3D printing machine builds a structure with many different surface finishes, depending on the orientation with respect to the build plate. In that regard, the relationship between the printing methods, build orientation and critical surfaces, where the current density of the electromagnetic component is maximum, should be considered for the better

performance of the EM component. For some designs, it will also be possible to reduce surface roughness through post-processing techniques.

However, this research is focused on RF components where it is difficult to perform surface treatment on fully- or partly-enclosed inner faces. One such example would be a horn antenna, such as the one studied here, where the total electric field is enclosed inside the cavity, as shown in **Figure 63**, which can be wet-blasted, but not polished, to reduce surface roughness.

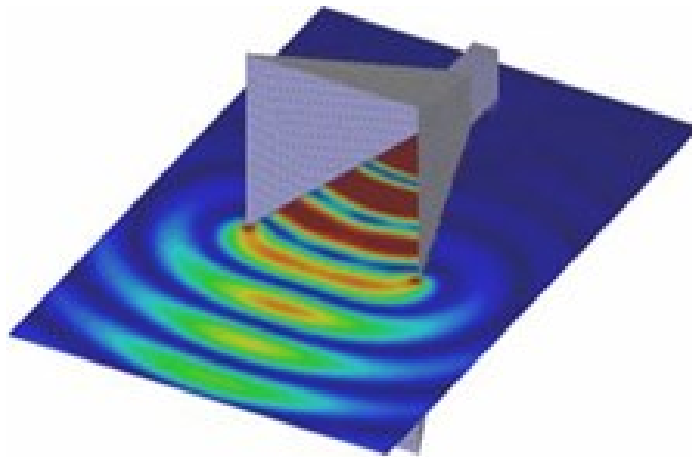


Figure 63: CST simulation of total electric field of a horn antenna.

Once all the antennas were printed, in order to analyse the effect of orientation on the surface morphology of the antenna, all three horn antennas were sectioned in half, to access the internal walls of the antennas structure for surface morphology measurement of the cavity, as shown in **Figure 64**.

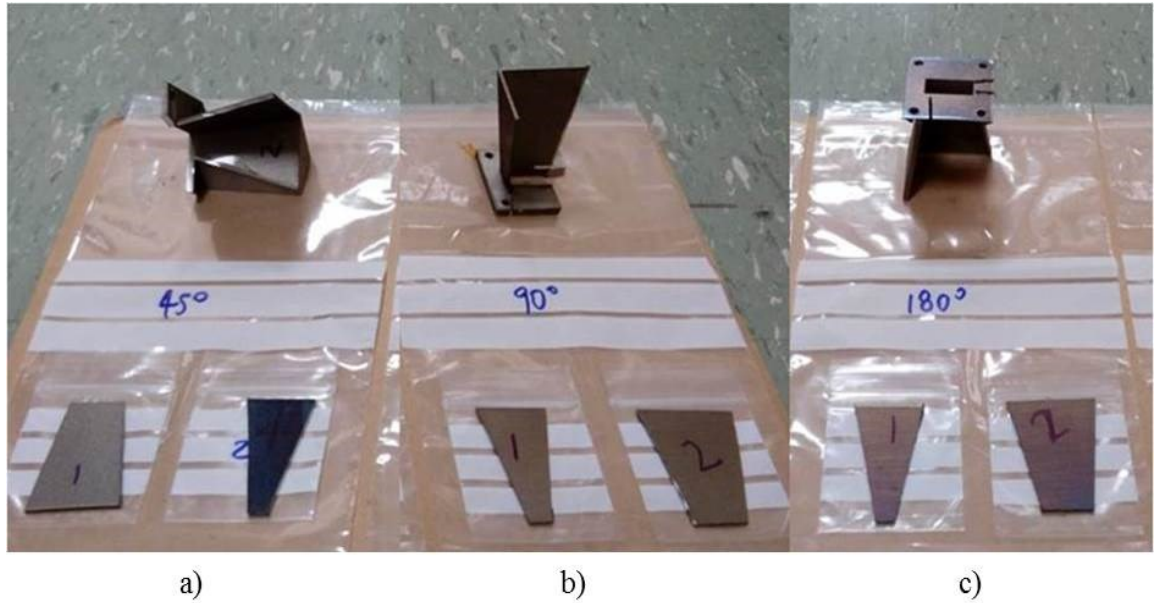


Figure 64: Horn antennas printed using DMLS sectioned in half for the surface measurement. The antennas were printed with three different orientations a) 45°, b) 90°, c) 180°

WLI (5x) and OM (400x) scans of the inner cavity of the three horn antennas are shown in the **Figure 65** for three different orientations. The effect of orientation on the surface of the parts can be explained by the layering process of DMLS. The best surfaces should be obtained from either the horizontal or vertical (normal to the build plate) surfaces. The worst surfaces should occur when the component printed has an overhang angle, for example, as is the case here for one of the three antennas, where the antenna is printed at an angle of 45°. The overhanging surface gathers poorly sintered particles, due to the directional nature of the laser, affecting greatly the surface roughness and morphology of the printed component. The OM images clearly illustrate these effects of orientation on the surface finish of the horn antenna. It should also be taken into account that the angles mentioned are for a horn antenna. However, the surfaces which were printed were built were at angles of +60°, -60° and 45° with respect to the building plate.

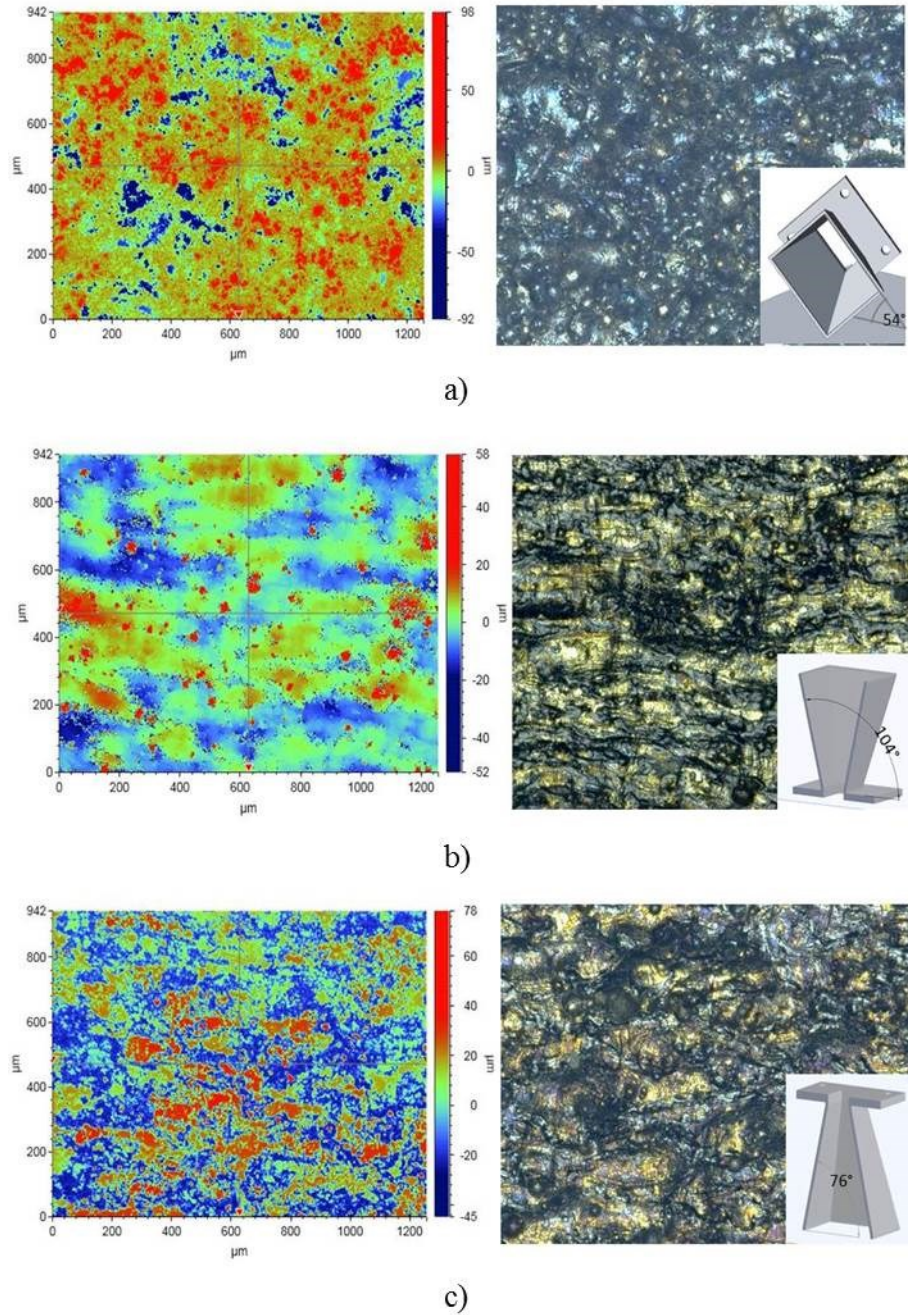


Figure 65: WLI (5x) and OM (400x) scans of the inner cavity of the horn antennas, built with three different orientations a) 45°, b) 90°, c) 180°

As the surface roughness parameter  $R_q$  (RMS surface roughness) does not give detailed morphology information, the  $R_z$  value was also measured using WLI (5x), which accounts for the maximum peak to valley distance over a given scan length. Also, as mentioned earlier in **Chapter 3**, in order to get an accurate value for surface roughness, the roughness values presented in **Table 7** are averages calculated from a minimum 5 WLI (5x) scans performed on the surface of the antenna.

Table 7: Surface roughness measurements of the inner cavity of the horn antennas, built with three different orientations

S.no	Antenna built orientation	$R_z$ ( $\mu\text{m}$ )	$R_q$ ( $\mu\text{m}$ )
1	45°	165±18	11±0.75
2	90°	84±6	6.5±0.43
3	180°	103±12	8±0.33

The results show a clear and expected roughness trend due to build orientation; with the overhanging face orientation exhibiting almost twice the  $R_z$  and peak-to-valley distance compared with the normal build orientation. This phenomenon can be explained by the unsintered particles attaching to the overhanging surfaces, along with the Staircase Effect as illustrated in **Figure 66**. This is because the laser penetrates into the powder bed and fuses particles to the downward surface of the overhanging face resulting in a poor and rough surface, whose impact increases with the angle of overhang subtended with respect to the build platform [7]. It is also worth mentioning here that in **Figure 66**, the steeper angle results in a smaller overhang, due to which, the staircase effect is less than that for a shallow angle.

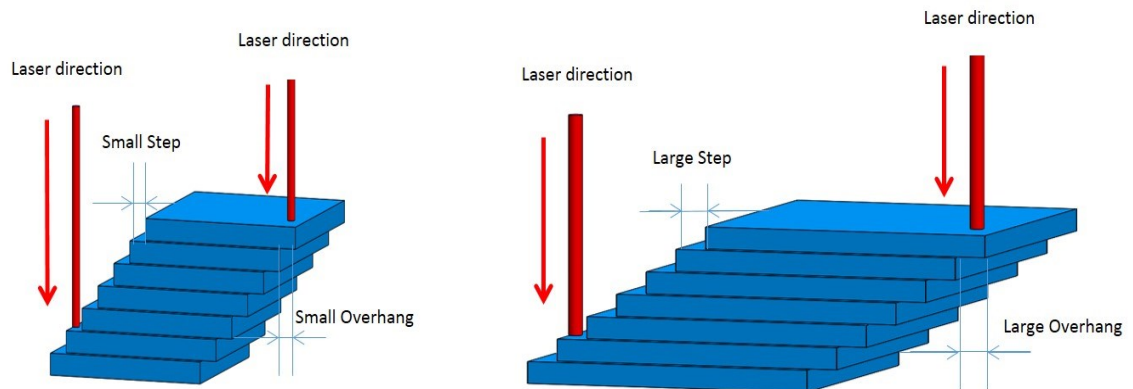


Figure 66: Effect on the surface finish of the 3D printed component due to build orientation and the staircase effect

## 6.4 RESULTS

The antennas performances were measured for both the  $S_{11}$  and the E-plane gain radiation pattern using a Rhode and Schwarz ZVB 20 VNA. **Figure 67** shows the return loss comparison against simulation results for a classical horn, with no surface roughness obtained through CST, and the measured results of these three horn antennas, built in

three different orientations and all three having been energized using a WR-90 waveguide ( $22.86 \times 10.16 \text{ mm}^2$ ). Even though the return loss profile is quite similar, it should be noted that neither the simulation nor the measured results showed the expected wideband response which would be expected from a horn antenna. This is due to the fact that the antenna is energized using a waveguide WR-90, with an N-type co-axial feed, instead of a waveguide feed, and so the impedance response of the antenna is highly dependent on the positioning of the co-axial feed. This phenomenon was confirmed with the simulation results as well, when the antenna model was energized using the waveguide output and N-type co-axial feed. One important point here to be noted is that, as confirmed by the optical images earlier, the roughness on the antenna surface has a random profile, for this reason no efforts were made to incorporate surface roughness in the CST simulation model of the antenna. Therefore, the simulation results are for an ideal antenna, with no surface roughness and shall be considered as a reference, against which the various measurements will be compared.

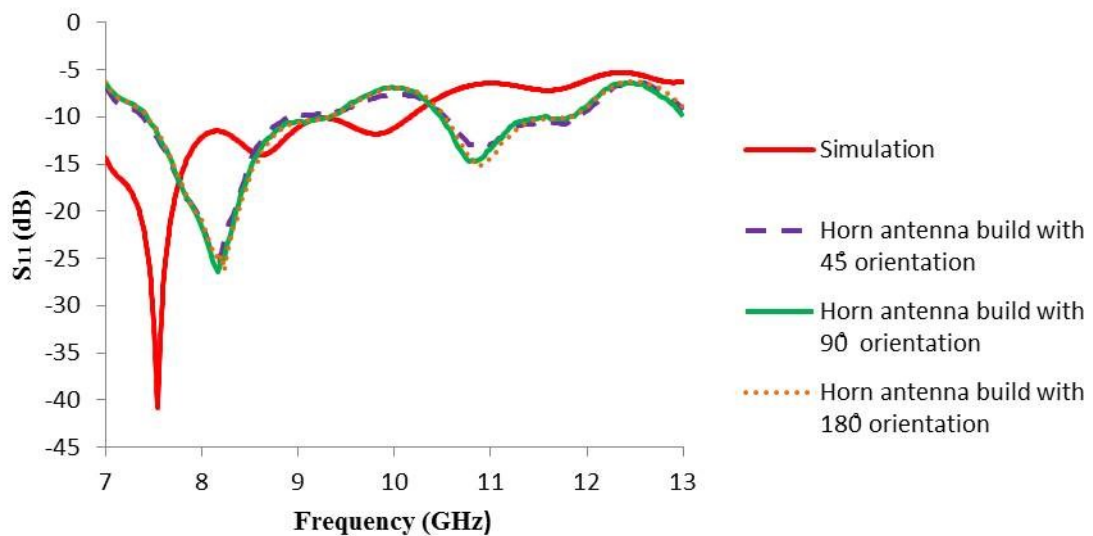


Figure 67: Return loss comparison graph

In addition to the return loss measurements, the E-plane gain of the antennas was also measured. From  $S_{11}$ , the value of return loss at the frequency of 12.4 GHz was -6.4 dB, which is not below the value of -10 dB, reference value, usually accepted by the antenna design research community as an acceptable return loss/transmission property at a given frequency. Assuming there would be a minimum effect of it on the performance of the antenna, the gain measurements were performed at 12.4 GHz, where the impact of the

surface roughness would be more significant than at lower frequencies in the X-band. **Figure 68** shows the 2D realized gain comparison graph between the simulation results and the measured horn antenna results, for each of the printed orientations.

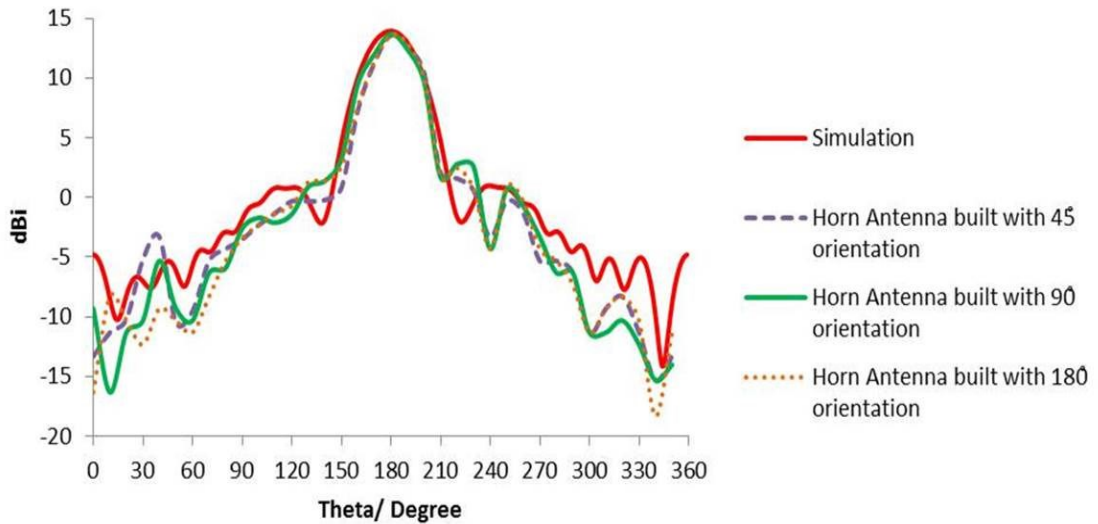


Figure 68: 2D realized gain comparison graph

In the measurement it was realized that all the antennas had the gain  $\pm 0.5$  dB compared to the simulation results of 13.9 dB, which proved that the antennas printed with different orientations did not have any significant degrading effect on the performance of the X-band horn antennas. However, as the skin depth for the operating frequency is lower than the measured amplitude surface roughness, the result would degrade further if the antenna were fabricated to work for higher frequencies. Due to the limited RF resources (the maximum VNA frequency was 20GHz), measurements beyond the selected frequency were not possible. In some future research, it would be interesting to see the impact of surface roughness at higher frequencies, caused by different orientations.

## 6.5 SUMMARY

In this research, a 3D metal printed horn antenna has been investigated, for variations in the surface roughness due to the build orientation and the consequent RF impact. Three horn antennas have been built, with different build orientations using DMLS technology with Maraging Steel on an EOS M280 system. The results obtained showed significant difference in the measured  $R_z$  values of the surface roughness, which accounts for the maximum peak-to-valley distance over a given scan length. The surface roughness's of

the antennas, with three different orientations, were measured and it was found that, due to the staircase effect, the surface roughness value is dependent on several factors such as the overhang angle, upward facing, and general part build orientation of the component. However, the measured antenna results proved that there is no significant effect of the orientation on the gain of the antenna, at the frequency of operation, but changes could be significant when working at higher frequencies, where the magnitude of surface roughness is more dominant. Nonetheless, the research could be of use to future antenna designers, who wish to utilize 3D printing, especially at high current density surfaces, by changing the orientation of the print.

Having a better understanding of the 3D metal printing for the fabrication of complex, lightweight components, as well as finding ways to minimize the impact of the surface roughness on the microwave component, the next chapter focusses on utilizing 3D printing technology towards improving the performance of state-of-the-art antennas.

*\*\* Publication arising from this chapter has been presented in:*

*12<sup>th</sup> European Antenna & Propagation Conference (EuCAP), London, UK, April/2018*

## 6.6 REFERENCES

1. C. L. Holloway, E. F. Kuester, “Power loss associated with conducting superconducting rough interfaces”, *IEEE Transactions on Microwave Theory and Techniques*, vol. 48, no. 10, pp. 1601-1609, 2000.
2. A. Townsend, N. Senin, L. Blunt, R.K Leach, J.S Taylor, “Surface texture metrology for metal additive manufacturing: a review”, *Precision Engineering*, vol. 46, pp. 34-47, October/ 2016.
3. F. Calignano, D. Manfredi, E.P. Ambrosio, S. Biamino, M. Pavese, P. Fino, “Direct fabrication of joints based on Direct Metal Laser Sintering in Aluminum and Titanium alloys”, *Proceedings of 24th CIRP Design Conference*, pp. 129-132.
4. H.J. Yang, P.J. Hwang, S.H. Lee, “A study on shrinkage compensation of the SLS process by using the Taguchi method”, *International Journal of Machine Tools & Manufacture*, vol.42, pp. 1203-1212, 2002.
5. W. D. Vree, “(Master’s Thesis) On the influence of build orientation on the mechanical properties of direct metal laser sintered (DMLS) Ti-6Al-4V flexures”, *Technical University of Delft*, April/2016.
6. D. Milan, Z. Ivana, H. Pavel, H. Ondřej, “Accuracy of holes created by 3D printing (DMLS)”, *28<sup>th</sup> DAAAM International Symposium on Intelligent Manufacturing & Automation*, Zadar, Croatia, November/2017.
7. R. I. Campbell, M. Martorelli, H.S. Lee, “Surface roughness visualisation for rapid prototyping models”, *Computer-Aided Design*, vol.34, no. 10, pp. 717-725, 2002.

# 7

## CHAPTER 7

# 3D PRINTED PERIODIC STRUCTURES IN A HORN ANTENNA FOR SIDE-LOBE REDUCTION USING DIRECT METAL LASER SINTERING

## ABSTRACT

The research presents a novel 3D metal printed X-band (8.2-12.4 GHz) horn antenna with side-lobe reduction, achieved by selectively printing pyramidal periodic structures on the inner faces of the antenna's E-plane. The 3D pyramidal periodic structures result in the suppression of the surface current and hence reduce the side-lobes of the horn antenna. The placement of the periodic structures has been optimized using commercially available electromagnetic simulation software, CST, not only for reducing side-lobes, but also for successful 3D metal printing. The beam efficiency of the proposed antenna was measured to be 98.5% at the selected frequency of 12.4 GHz, with an improvement of 8% over the 90.4% simulated beam efficiency of the conventional horn antenna without any periodic structures. The antenna was fabricated on EOS M280 DMLS system using Maraging Steel, MS1.

## 7.1 INTRODUCTION

Horn antennas, due to their wide-bandwidth, ease of excitation, high gain, easy and robust construction have been used widely in most communication systems. Despite being so popular, horn antennas still suffer from a few drawbacks; and one of these is their large side-lobes, which happen due to the non-smooth phase of the wavefront at the horn antenna's aperture.

To address this problem, a lot of research has taken place, which includes corrugated horn, Gaussian corrugated horn and trifurcated horns [1]-[6]. The approach taken by all of these is to reduce the side-lobe level, by avoiding field scattering at the antenna's

aperture, resulting in a low energy level in the undesired side-lobes. Although they provide a solution to the problem, these antennas suffer from the disadvantage of being heavy, large and are difficult to manufacture, especially when it comes to fabricating a smaller aperture horn.

Recently, the use of metamaterials and Electronic Band Gap (EBG) structures has also gained attention in this regard. The chosen EBG structure on the inner walls of horn antennas suppresses the surface waves over a wide frequency range [7][8]. In addition to this technique, a novel graphene-based method has also been proposed in [9], to reduce and control the side-lobe level of the traditional pyramidal horn antenna at microwave frequencies. The purpose of EBG structures and graphene sheets is to act as a high impedance surface, thus, hindering the electromagnetic energy from reaching the horn aperture edges and diminishing the diffraction pattern, and minor lobes from the main radiating beam.

This research proposes a novel approach to 3D printing horn antennas, with the help of periodic structures, leading to the successful reduction of the E-plane side-lobe level by 10-20 dB. The results and the complex fabrication of the periodic structure inside the horn antenna should be of interest both in terms of measurement and fabrication for future antenna designers, who wish to design and fabricate the horn antennas with reduced level of side-lobes for different areas of application utilizing AM.

The rest of the chapter is organized as follows. In **Section 7.2**, the conventional horn antenna and periodic structures are discussed. The fabrication of the proposed antenna is described in **Section 7.3**, followed in **Section 7.4** by a comparison between the simulation results obtained through CST and the measured results. Finally, the summary along with future work that can be done is presented in **Section 7.5**.

## **7.2 HORN ANTENNA & PERIODIC STRUCTURE CONFIGURATION**

### **7.2.1 HORN ANTENNA**

The horn antenna employed in this research is an X-band standard gain horn antenna with a nominal 10 dB gain as shown in **Figure 69**. The horn antenna has an aperture of 41.8 x 32.26 mm<sup>2</sup> and a flare length of 42.2 mm, and is energised using a WR-90 waveguide (22.86 x 10.16 mm<sup>2</sup>). The mechanical specification of the horn has been kept identical to

an off-the-shelf horn antenna from Pasternack Enterprises [10]. The antenna was modelled and simulated on CST and the simulation results were matched with the datasheet results provided by the manufacturer, as the benchmark for the results and showed good correlation between them.

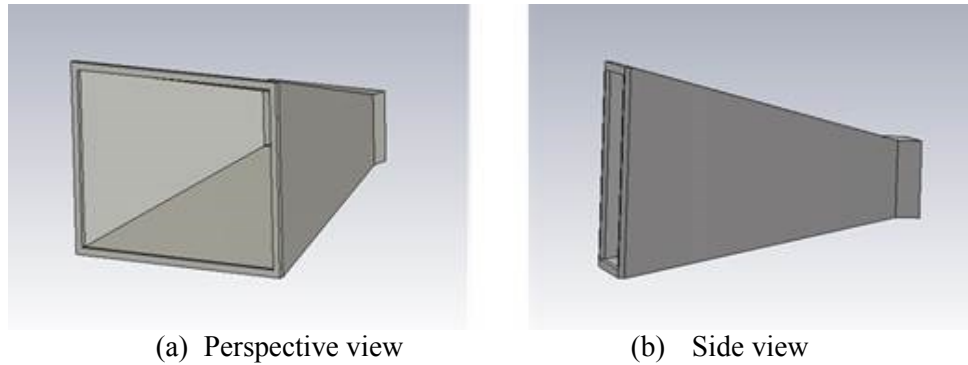


Figure 69: A standard gain horn antenna in (a) Perspective view and (b) Side view

### 7.2.2 PERIODIC STRUCTURES

In the course of this research, many simulations were performed on different shapes of periodic structures, to minimize the impedance at the surface of the horn, with the primary aim of reduced side-lobes. In this regard, simulations were carried out on the well-researched mushroom-shaped EBG structure in [7], where the authors have used circular patch, mushroom-like EBG structures, to suppress the antenna side lobes. Even though their concept was proven to work, the research carried out was limited to simulations only, due to the manufacturing constraints posed by conventional construction techniques. Moreover, their design could not be 3D printed, as it violates the 3D printing over-hanging rules. For this reason, 3D, pyramidal structure was chosen to be the best suited shape not only in terms of reducing side-lobes, but also to ensure successful printing requirements of the 3D printer. The proposed pyramidal structures are self-supporting while being 3D printed, which means they reduce the possibility of metal drooping.

Moreover, with the advent of 3D printing, it is also desirable to push the limits of 3D printing for mechanical reasons to consider different shapes of periodic structures, which can be successfully 3D printed, to enhance the performance of existing antennas. The research on the shape of periodic structures proposed here has already been carried out and patented [3], where the author proposed a V-shape corrugation over conventional

rectangular teeth corrugation in a horn antenna, as the shape is readily adaptable to unfurlable antennas for mm-wave space applications. The heights of the slots were chosen so that the corrugated surface impedance is capacitive and operates in a cut-off mode to achieve side lobe reduction.

From the literature review and the simulations performed in this regard, it was analysed that side lobes are prominent due to diffraction of electromagnetic energy along the aperture of the horn. Therefore, in this research, pyramidal periodic structures have only been positioned along the aperture to prevent the diffraction at the edges, as an attempt to improve the E-field pattern of the horn antenna. One more noteworthy point here is that the radiation pattern along the E-field is independent of the structural density along a row, which means that the stacked row of tetrahedrons would perform similarly, if individual rows were replaced by a wedge of a similar dimension instead. However, it should also be taken into account that the pyramidal periodic structure along the inner face of the horn antenna not only adds to more complex geometry while 3D printing, but also adds to the structural efficiency by using less material during the print, compared to the model using wedges. A similar computation study in this regard, was done in [11], where the authors have computed the radiation pattern of the wedge shaped corrugated horn antenna with the conventional horn antenna. The results showed considerable amount of side lobe reduction, with the first null reduced to almost extinction just by placement of 5 cavity-backed, wedge shaped corrugations, near the aperture of the horn antenna.

**Figure 70** shows the perspective view of 58 proposed pyramidal periodic structures on one face of the E-plane horn antenna. Four rows of periodic structures gradually increased in height towards the aperture of the horn, separated with a constant corrugation density of 2.5 mm. The height of the different rows of periodic structure has been parametrically optimized and is presented in **Table 8**.

The purpose of varying the height of the corrugation is to electrically modify the surfaces of the horn, minimizing the diffraction pattern to reduce unwanted sidelobes of the horn antenna.

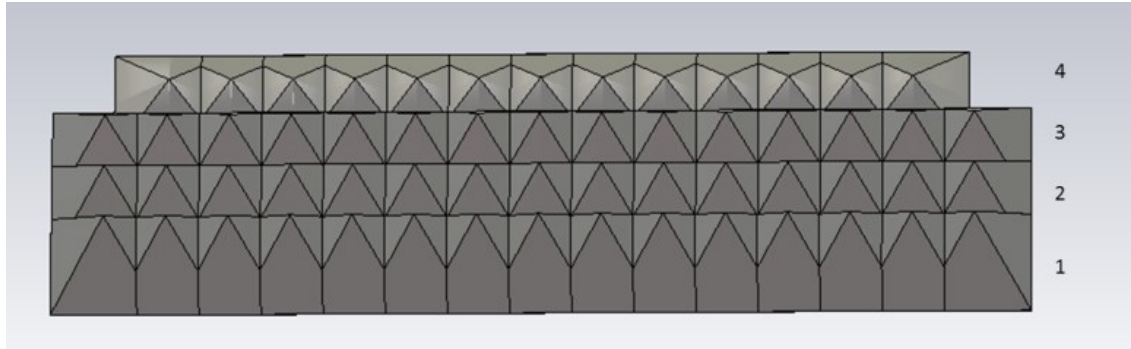


Figure 70: Row formation of pyramidal periodic structure

Table 8: Variation of height of periodic structures on the basis of rows

Row no.	Height (mm)
1	4.25
2	4.00
3	3.75
4	2.00

One interesting point here is that, for the V-shape corrugation where the depth of the slots ranges between 0.3125 and 0.625 of the operating wavelength, whereas for the rectangular slots between rectangular corrugations, the corresponding depth range is 0.25 to 0.5 of the operating wavelength [3]. In this research, where the shape of the periodic structure is pyramidal, the simulations on CST were performed not only to determine the optimized value for heights of the periodic structures in different rows, but also to determine the number of rows required. The optimized value corresponds to minimum loss in the gain value of the antenna, with maximum suppression to the side lobes by diminishing the diffraction phenomena happening at the aperture.

### 7.3 ANTENNA FABRICATION

The photograph of the proposed fabricated horn antenna with periodic structures is shown in **Figure 71**. The antenna has been fabricated as a monolithic component using DMLS technology on an EOSINT M280 system, with Maraging Steel, MS1, as the conducting material. To successfully print the horn antenna with periodic structures, many mechanical considerations, such as the requirement of support structures, build orientation, minimum wall thickness, and material layer thickness were taken into account and these parameters were assigned values which would lead to successful

fabrication. For example, the build orientation was 90 degrees, as in previous experimentation, this yielded the lowest value of surface roughness. Similarly, the material layer thickness was 20 microns, as this value would lead to low surface roughness.

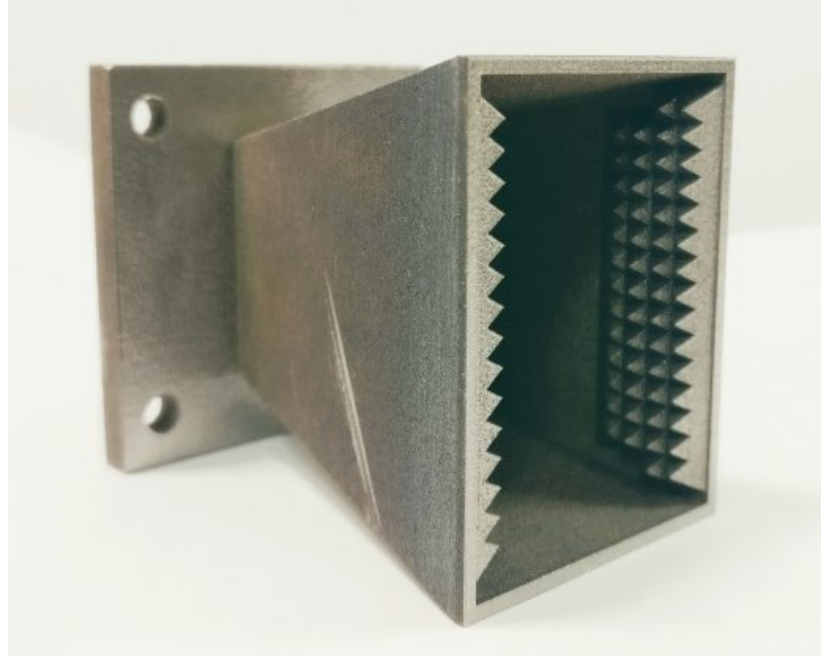


Figure 71: Proposed horn antenna with periodic structures

From the conclusion of chapter 3 and 4, the proposed antenna was fabricated on Maraging Steel, MS1, as the conducting material, with the 90° orientation with respect to the build platform, to avoid the Staircase Effect, in the inner cavity of the horn, which would increase the surface roughness of the microwave component. However, this approach may be conservative, as the earlier work at the frequency of operation of 12.4 GHz, showed that surface roughness of the given amplitude does not have a significant effect on the performance of the antenna. For this latter reason, no further efforts have been made to reduce the component's surface roughness, by the application of surface treatment techniques, such as wet blasting and polishing, as explained in detail in **Chapter 3**.

## 7.4 RF RESULTS

After fabrication, the antennas performances were measured for both the  $S_{11}$  and the E-plane gain radiation patterns. **Figure 72** depicts the  $S_{11}$  comparison of simulation results

between a classical horn and the proposed antenna, with periodic structures obtained through CST, against the measured results.

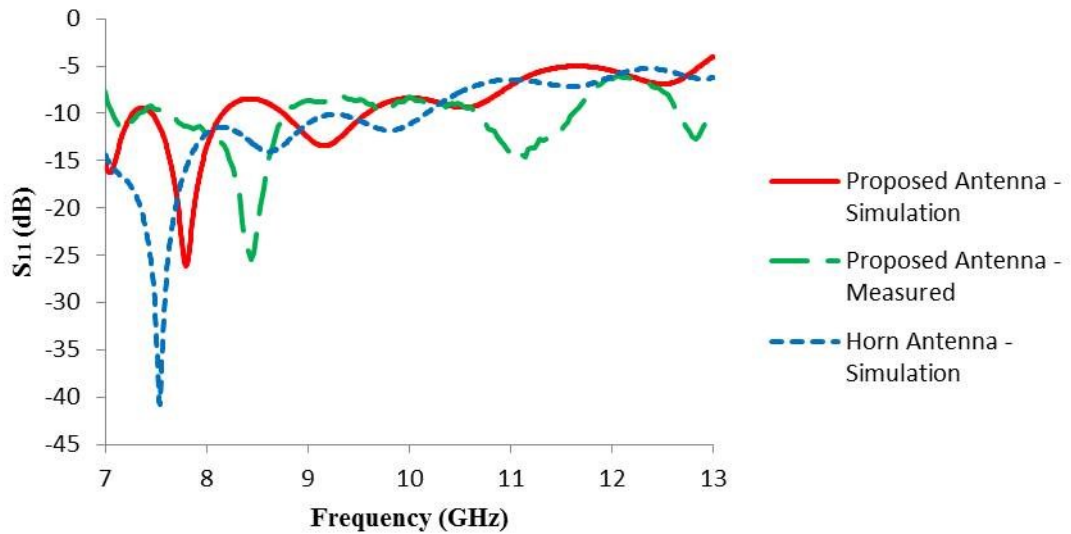


Figure 72: Simulated and measured return loss

As shown in **Figure 72**, the proposed antenna provides a similar impedance matching profile to that of the classical horn. From the graph, it can also be concluded that adding these periodic structures near the aperture of the horn antenna doesn't have any degrading effect on the antenna's  $S_{11}$  performance. To further tune the impedance matching of the horn antenna in [8], the authors have added a conducting metal wedge inside the horn antenna. However, no efforts have been made in this research to improve the antenna impedance bandwidth any further. In this research CST played a vital role, not only in determining the height and of the periodic structures, but also in determining the frequency of maximum suppression. In this regard, the maximum suppression of 10-20 dB on the E-plane side-lobes was realized at 12.4 GHz as shown in **Figure 73**. As can be seen in the corresponding graph, for the horn antenna with a periodic structure in place, the maximum side suppression was achieved at the 12.4 GHz frequency compared to the several other frequencies in the X-band.

Also, even though in this research, the results have been optimized at an individual frequency of 12.4 GHz, there is ample room for research to be done to tune the antenna for wide frequency bands.

A similar study was done in order to determine the number of rows and the heights of the periodic structures where it was realised that periodic structures with same heights doesn't correspond to the optimized results. As shown in **Figure 74**, by gradually increasing the height of the periodic structures towards the aperture of the horn, the first null of the main lobe has been suppressed by a minimum of 10 dB compared to the horn with periodic structures of constant height. As the proposed antenna is the first of its kind, it would be interesting to measure if this proposed antenna is an improvement on the commercially available corrugated horn antennas.

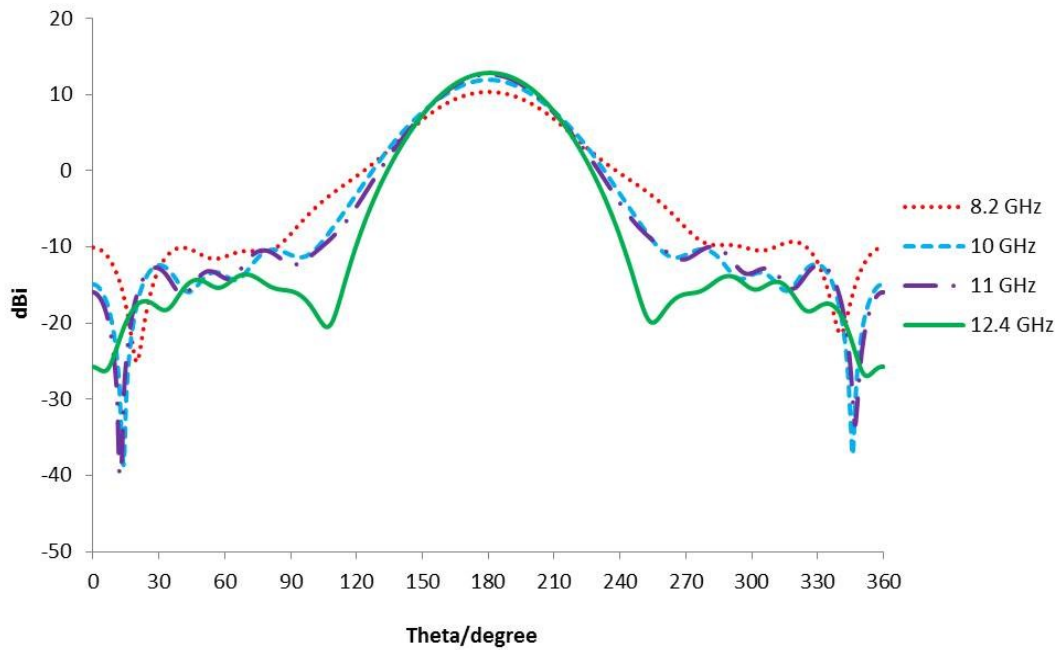


Figure 73: 2D realised comparison simulation gain, for different frequencies in X-band

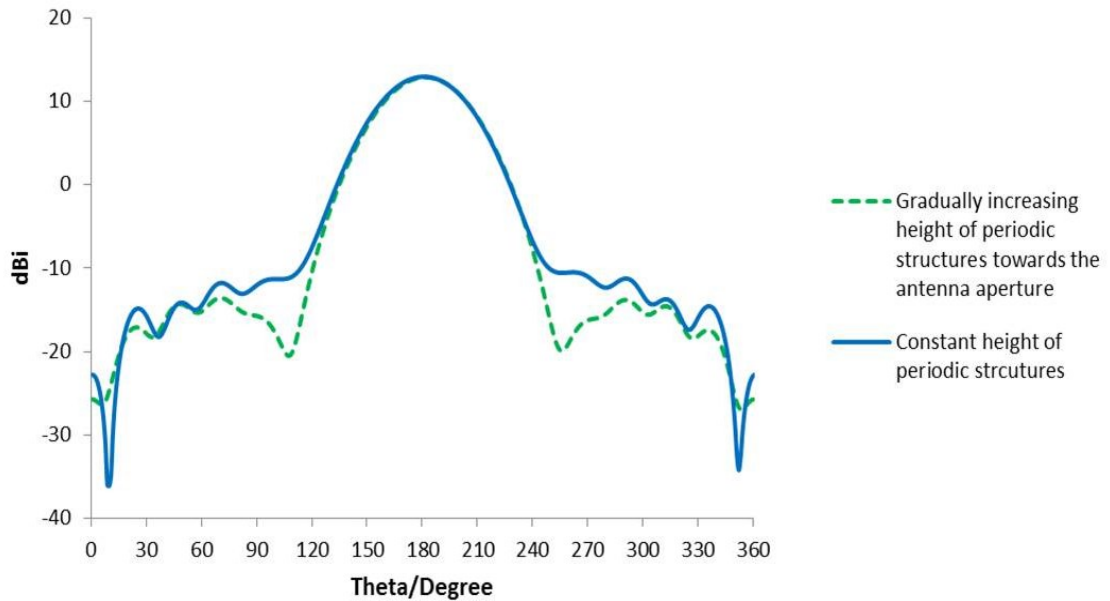


Figure 74: 2D realised gain comparison simulation gain of horn antenna, with varying periodic structure height to the one with constant height along the rows

In the final measurements, the antenna was fabricated with varying periodic structures, towards the horn aperture. As can be seen from **Figure 75**, even though the proposed antenna had a 1 dB loss over the conventional horn antenna without any periodic structures, side lobes were reported to be suppressed by 10-20 dB along the radiation pattern. No comparisons were made with the fabricated conventional horn antenna, but can be compared to the radiation results achieved in **Chapter 6** for a horn antenna at 12.4 GHz. The results achieved through the proposed antenna in this chapter showed an improvement to the counterpart where the simulation results matched the measured results very well. Subsequently, the beam efficiency of the fabricated antenna was measured to be 98.4%, increased from 90% for the conventional antenna without any periodic structures. The 2D and 3D comparison gain radiation pattern are presented in **Figure 75** and **Figure 76**.

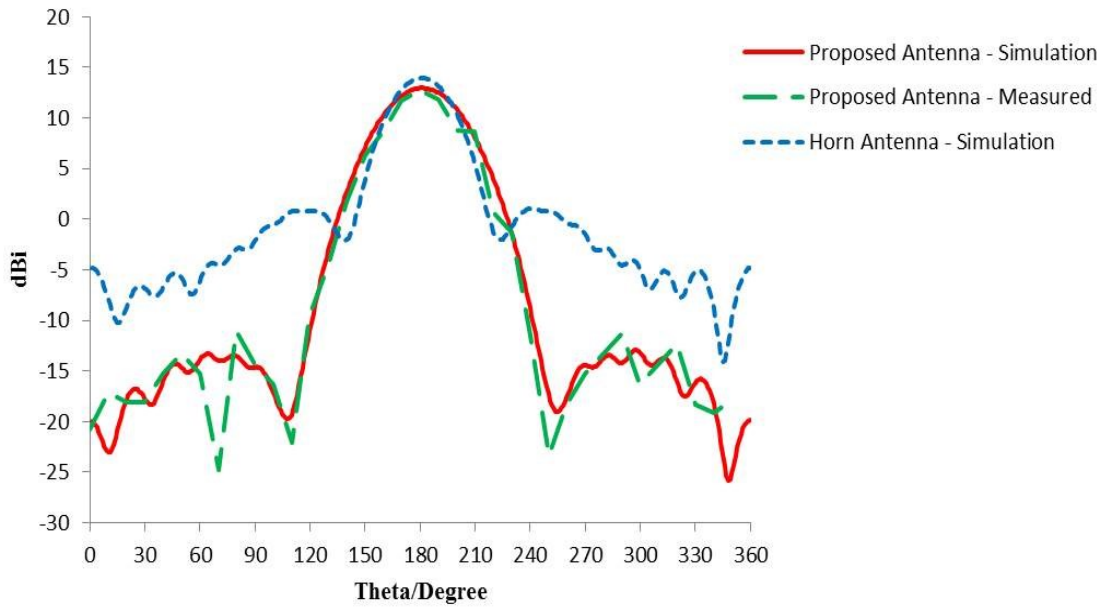
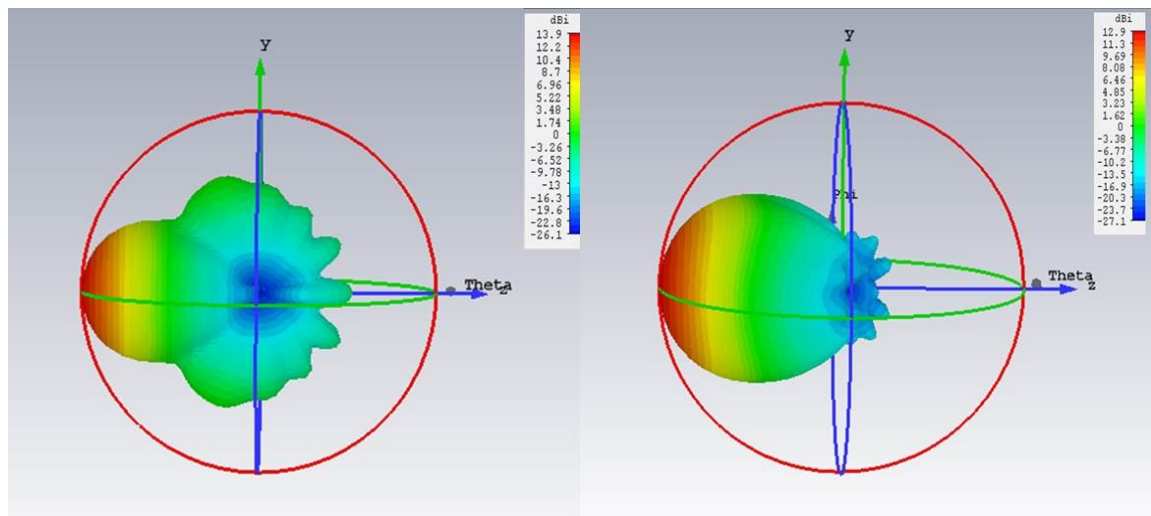


Figure 75: 2D realised gain, simulation and measurement comparison graph



(a) Horn antenna

(b) The proposed antenna

Figure 76: Simulated comparison of 3D radiation pattern

### 7.5 SUMMARY

In this research, a 3D metal printed horn antenna is investigated, with the primary goal of side-lobe reduction. The proposed antenna presented is fabricated using DMLS technology from Maraging Steel on an EOS M280 system, with a view to reducing the losses in EM radiation due to side-lobes. To achieve the proposed results a series of rows

of 3D metal printed periodic structures, which are gradually increased in height towards the aperture of horn has been considered. The results proved to be an improvement over its conventional counterpart and as the construction of the antennas with periodic structure has been done using metal only, this antenna can also find application in a high-power environment, capable of addressing breakdown issues. The research reports the first-of-its-kind antenna, where the periodic structures are selectively printed at be-spoke positions inside a horn antenna. This research can be a stepping stone for future research work on different types of metallic EBG structures that can be 3D printed, while adhering to the design restrictions imposed by AM.

Also, for existing antennas types, 3D metal printing has also opened the possibility to separately print periodic structures as an individual unit, which can be mounted onto a horn aperture to minimize the side-lobe level.

*\*\* Publication arises from this chapter has been presented in:*

*2017 IET Loughborough Antennas & Propagation Conference (LAPC), Loughborough, UK, p.p. 1-4, November/2017.*

## 7.6 REFERENCES

1. P.J.B. Clarricoats, A.D. Olver, “Corrugated horns for microwave antennas”, *Peter Peregrinus Ltd, 1984*.
2. C.A. Balanis, “Antenna Theory – analysis and design”, 2<sup>nd</sup> ed, *John Wiley and Sons, 1997*.
3. J. C. Fletcher “Horn antenna having V- shape corrugated slots”, *U.S. Patent no. 3,924,237, July/1974*.
4. K. K. Chan, S. Rao, “An accurate model for rectangular trifurcated horns”, *IEEE Transaction of. Antennas Propagations, vol. 55, no. 12, pp. 3706-3710, Dec/ 2007*.
5. J. Teniente, R. Gonzalo, C. del-Río, “Ultra- wide band corrugated gaussian profiled horn antenna design”, *IEEE Microwave and Wireless Components Letters, vol. 12, pp. 0-21, 2002*.
6. J. W. Odendaal, C. W. I. Pistorius, “Horn antenna with suppressed sidelobe level”, *Microwave and Optical Letters, vol. 4, no. 6, pp. 238-239, May/1991*.
7. T. Hongnara, K. Schraml, S. Chaimool, P. Akkaraekthalin and D. Heberling, “Side-lobe reduction of horn antenna using circular patch mushroom-like EBG structure”, *Proceedings of Global Mobile Internet Conference, Bochum, Bochum, Germany, March/2016*.
8. C. P. Scarborough, Q. Wu, D. H. Werner, E. Lier, R. K. Shaw, B. G. Martin, “Demonstration of an octave-bandwidth negligible-loss metamaterial horn antenna for satellite applications”, *IEEE Transactions on Antennas and Propagation., vol. 61, no. 3, pp. 1081-1088, 2013*.
9. H. Balegh, B. A. Arand, L. Yousefi, “Side lobe level reduction in horn antennas using graphene”, *24th Iranian Conference on Electrical Engineering (ICEE), Shiraz, Iran, May/2016*.
10. Pasternack, “(Online Gain horn antennas”, (<https://www.pasternack.com/gain-horn-antennas-category.aspx>), [Accessed: 9th July 2017].
11. A.Borgioli, R. Coccioli, G. Pelosi, J. L. Volakis, “Electromagnetic scattering from a corrugated wedge”, *IEEE Transactions of Antennas And Propagation, vol. 45, no. 8, 1997*.

# 8

## CHAPTER 8

# 3D PRINTED ARTIFICIAL DIELECTRIC LENSES

## ABSTRACT

The research presented in this chapter proposes, for the first time a 3D printed artificial dielectric lens for applications including 5G, fabricated using DMLS. The artificial dielectric lenses have been designed, simulated and proposed to be fabricated for use at E-band, using CST, a full-model simulation software. The chapter presents the focusing effect of a three-dimensional combined plano-concave and a bi-concave metallic lens. The work serves as a proof of concept for the successful fabrication of metallic lenses, through 3D metal printing. Potential applications for 5G are integrated lens antennas, for example a horn, as an alternative to parabolic reflectors.

## 8.1 INTRODUCTION

With most personal wireless devices operating within the limited carrier frequency spectrum ranging between 700 MHz and 2.6 GHz, service providers are now experiencing unprecedented congestion in this frequency range, just trying to meet existing demands [1]. The congestion in the available frequency spectrum has increased manifold, due to the demands of personal mobile bandwidth, the arrival of IoT's, smart driving cars, and smart watches.

5G can improve many aspects of current mobile communication. The core principle to establish a digital infrastructure that is capable of offering a complete roll out from 4G to 5G by 2020, connecting billions of mobile devices to each other. To achieve this goal, some of the major factors include high data rate, bandwidth, latency, energy consumption [1] [2]. To do this, many research institutes and industries are working together towards the development of 5G technology, looking at new propagation models, novel multi-

antenna transmitting architectures, and investigating the option of mm-Wave operating frequency bands [1]-[5].

On the one hand, mm-waves allows much more bandwidth for mobile communications, on other hand, achieving this will require novel components, such as the lens in this research. Working at such high frequencies the architecture required, needs to be compact and is not widely available. An important part of the 5G transceiver architecture is the antenna. With MIMO, there are concerns around intersecting waves where antennas are tightly packed. To overcome this issue, beam steering has been nominated as an alternative option, in which a highly directive system propagates a beam in a selected direction. A highly directional antenna, using the lens as a constituent part, could be used as the fundamental antenna in a very selective beam-steering array. Also, point-to-point backhaul communications can be improved if a lens focussing element is added to the communicating antennas [5]. Even though the lens designed in this research is proposed for communication application, but nonetheless, these lenses along with the energising source could also be well suited in medical applications as well, as hyperthermia applicators. Such applicators need to have focussed beams over short distances. Without focusing capabilities, applicators could potentially result in heating significant areas of healthy tissue adjacent to the target tumour [6].

Similarly, much work, as presented in this chapter has been done regarding the fabrication of microwave lenses using AM, at comparatively lower frequencies, but based on polymer printed structures, where 3D polymer printing technology has been used to vary the lenses' refractive indices, to manipulate the EM waves [5][7]-[9]. To fabricate such devices, the variation in the permittivity of the material can be introduced by varying the dimensions of the air voids in the host materials, thus, varying the effective permittivity of the lens. While 3D polymer printing lends itself to the easy fabrication of such lenses, however, lenses fabricated using polymers suffer high dielectric losses, especially at higher frequencies. Also, these lenses operate on the principle of EM waves travelling through the dielectric lens, with a phase velocity slower than the speed of light, due to the dielectric medium. The opposite is the case if the lens has been fabricated from an artificial dielectric or, as in this research, a metal alloy. Metal lenses have been built historically, but fell out of favour, due to manufacturing constraints posed by conventional manufacturing techniques. However, with the advent of 3D metal printing

technology, presented in this chapter, an attempt has been made to revive the concept of all-metal lens.

## 8.2 ARTIFICIAL DIELECTRIC LENSES

The concept of artificial dielectric lens or metallic lenses was first proposed by W.E. Koch in 1940's [10]. However, it was not exploited much afterwards, which was due to its limited bandwidth compared to the dielectric lenses, as the lens has an operating bandwidth within 10% of the carrier frequency [11] [12]. These lenses operate in the  $TE_1$  mode of propagation, and consist of an array of metallic plates, which appear as parallel plates to an incident wave's electric field. Even though these lenses have a narrow bandwidth, due to their focusing property, compact structure (at higher frequencies) and even possible beam steering deployment, they can become a suitable candidate for point-to-point 5G applications.

The artificial dielectric lens mimics the properties of naturally occurring dielectric media, along with properties that do not generally occur in nature. These lenses operate on the principle that EM waves travel through the lens with a phase velocity that is greater than the speed of light, which is the opposite of the case for a dielectric lens, where the EM waves travel slower than the speed of light, due to the dielectric medium. As the index of refraction of metallic lens is less than 1, the focusing properties of a concave metal plate lens would be equivalent to that of a convex dielectric lens having an index of refraction greater than 1. Due to this property of the lens, the EM rays propagated by the energizing horn antenna are bent towards the boresight direction, thereby further sharpening the field pattern. This property has been utilized in this work to spot focus the incoming electromagnetic waves.

In [13] [14], authors have designed and simulated artificial dielectric concave and convex lens geometry at THz waveband. The research work confirms the focussing and the defocussing effect of the lenses at higher frequencies. However, the research work was limited to simulations only. This could be due to the manufacturing constraints posed towards fabrication of metallic lenses at such high frequencies. In that regard, for the first time, in [15], the authors manufactured a THz artificial dielectric lens using a chemical etching process, with the power throughput better than if the lenses were fabricated with

conventional fabricating material such as Teflon or high-resistive silicon. However, with the development of 3D metal printing, researchers now have the freedom to manipulate the lens' parameters and properties over a wide range of frequency.

### 8.3 LENSES DESIGN AND FABRICATION

In this chapter, two artificially dielectric lenses have been designed, simulated and proposed to be fabricated using Maraging Steel (MS1), on a DMLS, EOS M280 system. The lenses proposed in this research are bi-concave and plano-concave lenses, for spot-focussing applications. These lenses are planned to be fabricated for the E-band (60-90 GHz) application due to the availability of the VNA for measurements, but nonetheless, the 3D printer used is also capable of fabricating a lens for use in the THz range, for which the construction required can be more compact.

One of the reasons the lens wasn't fabricated for a lower frequency, even though the in-house VNA is able to measure up to 20 GHz, is because of the size restriction of the structures that can be printed in the chamber of the available DMLS system. This limitation of current available printing systems means that the lens structures can only be fabricated for the higher frequencies only. However, with the recent advancement in the field of fabricating 3D metal printed structures with large dimensions, it would be possible to fabricate the lens structure for lower frequencies as well [16].

Having said that, in this research, the bi-concave lens was designed to study the behaviour of metallic lenses at 77 GHz, the plano-concave lens was designed for 60 GHz due to its thinness compared to a bi-concave geometry addressing the weight and compact structure constraints for 5G applications. The lenses in this research are frequency dependent with their cut-off frequency being dependent on the value of  $\alpha$ , the plate separation, which is critical to ensure the higher order modes of the incident electromagnetic waves, passing through the lens are cut-off. To ensure that the wave incident on this structure will propagate through it in the  $TE_1$  mode, the separation between the metallic plates should be slightly more than half a wavelength of the incident wave [10]-[12].

The effective refractive index,  $n$ , of the medium is frequency dependent and defined by  $0 \leq n \leq 1$ , where the equality holds for the modal cut-off frequency. When the effective index

reaches 0, the metallic plates are too close to each other, resulting in reflection and backscatter from the plates; whereas, if the effective index is 1, then the metallic plates are too far from each other, so no focusing action would occur for the desired frequency. For a given value of the separation distance,  $\alpha$ , the index of refraction,  $n$ , can be calculated from:

$$n = \frac{v_0}{v_{ph}} = \sqrt{1 - \left(\frac{\lambda}{2\alpha}\right)^2} \quad (5)$$

Where  $\lambda$  is the free space wavelength and  $v_0$  and  $v_{ph}$  are the free space velocity and the velocity in the waveguide between the plates, respectively. With the chosen parameters of focal,  $f$ , the index of refraction was calculated accordingly. Finally, the relationship corresponding to the radii of curvature of both the lenses ( $R_1$ ,  $R_2$ ) was calculated by the lens maker's formulae for thin lenses:

$$\frac{1}{f} = (n - 1) \left( \frac{1}{R_1} - \frac{1}{R_2} \right) \quad (6)$$

The radius of curvature ( $R_1$ ,  $R_2$ ) of the lens is measured from the center of the lens, progressively decreasing towards the periphery. The thicknesses of the parallel plate ( $t$ ) for the fabrication of the lens are crucial from the fabrication point of view as well as from the EM behaviour. From the fabrication point of view, the thickness of the individual plates is important, as there is a limit to the minimum dimension that can be 3D printed. For Maraging Steel (MS1), the minimum wall thickness that can be successfully printed is in the range of 0.3-0.4 mm [17]. The thickness further plays an important role in reflecting the EM waves back to the transmitter if made too thick, as a part of the lens, resulting in high reflection losses. In that regard, there is a proposal to push the limits of fabrication beyond the datasheet value and print the metallic plates with a thickness of 0.25 mm. That value was chosen due to prior experience in the field of AM, for successful printing metallic plates. Dimensions of both the lenses for the operational wavelength ( $\lambda$ ), having radius of curvature ( $R_1$ ,  $R_2$ ), corresponding to total height ( $h$ ) and width ( $w$ ) of the lens structure with number of plates ( $n_p$ ) is presented in **Table 9** below. It is worth mentioning here that values of focal lengths and the index of refraction are chosen without a specific purpose in mind. However, the dimensions can be tuned for different focal length, once applications are identified.

**Table 9:** Dimensions of artificial dielectric lenses

S.no	Parameters	Bi- concave (mm)	Plano- concave (mm)
1	$\lambda$	3.89	5
2	R1	32	0
3	R2	32	25
4	f	40	35
5	n	0.6	0.28
6	t	0.25	0.25
7	$\alpha$	2.15	2.6
8	h	80	50.6
9	w	80	28
10	$n_p$	29	19

One of the growing concerns in the fabrication of the metal AM parts is the surface finish of the printed component, which could potentially degrade the performance of the electromagnetic component, especially at higher frequencies, as discussed in detailed in **Chapter 3**. However, the construction of the metallic lens is such that it's not feasible to polish the surface, due to which it has been proposed to use wet blasting on the metallic component to reduce the surface roughness to a range between 2  $\mu\text{m}$ -4  $\mu\text{m}$ . The geometry of the proposed lenses is given in the **Figure 77**.

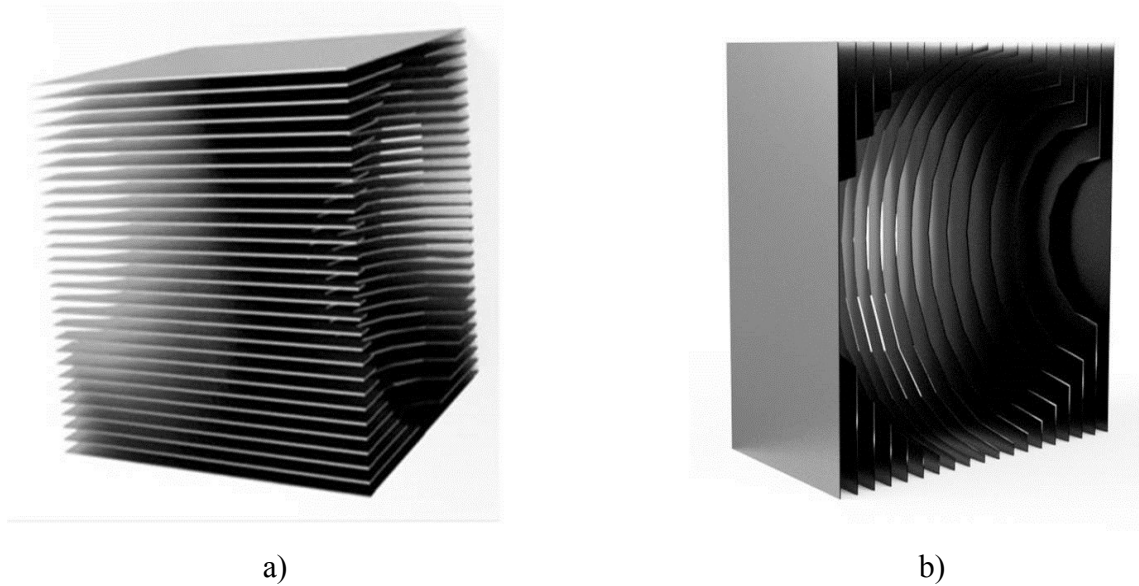


Figure 77: The geometry of the proposed artificial dielectric lenses a) bi-concave b) plano-concave

In research literature, there have been several attempts made to contemplate the behaviour of the incoming waves, in order to achieve the desired radiation characteristics, by loading a standard commercial horn antenna with thin metallic plate/wire media. In that regard, a wire plate/medium provides an interesting approach, as the spacing between the wires is critical and corresponds to the cut-off frequency. This approach has been used in research to change the polarization of the incoming waves, as well as to enhance the directivity the horn antenna [18]-[20].

This was certainly one of the reasons for fabricating not only a plano-concave, but also a bi-concave lens to push the limits of AM towards successful fabrication of a complex-shaped lens. Printing parallel metallic plates for change in polarization would have been easier, in this research, compared to a bi-concave lens, which is an angled geometry from both ends, and is extremely difficult to manufacture. Printing a lens, with such geometry was a challenge, especially in the case where the usage of support structures could have potentially increased the surface roughness, of the lens, due to which the bi-concave lens is proposed to be fabricated in an upside orientation so that the structure would be self-supportive during the printing process.

## 8.4 RF SIMULATION RESULTS

The lenses presented are simulated with an off-body arrangement, where the excitation to the lens is provided at a distance of multiple wavelengths from the lens body. The lens can be energized by any type of source, such as open-ended waveguides, horns, or patch antennas. The underlying artificial dielectric bi-concave lens has been simulated using an E-band (60-90 GHz), 15 dB horn antenna, energized using a WR-12 as a source, while a 10 dB horn antenna with WR-19 waveguide has been used for energising a plano-concave lens on CST software. One noteworthy point here is that, usually the lens in optics are energised using a point source, however, it is not possible to replicate the same in this case when the excitation is being performed at a mm-wave range. This is the reason the excitation is being performed using a horn antenna. A schematic diagram of the bi-concave artificial dielectric lens, energized with the horn antenna, illustrating the focussing action of the metallic concave lens is shown in **Figure 78**.

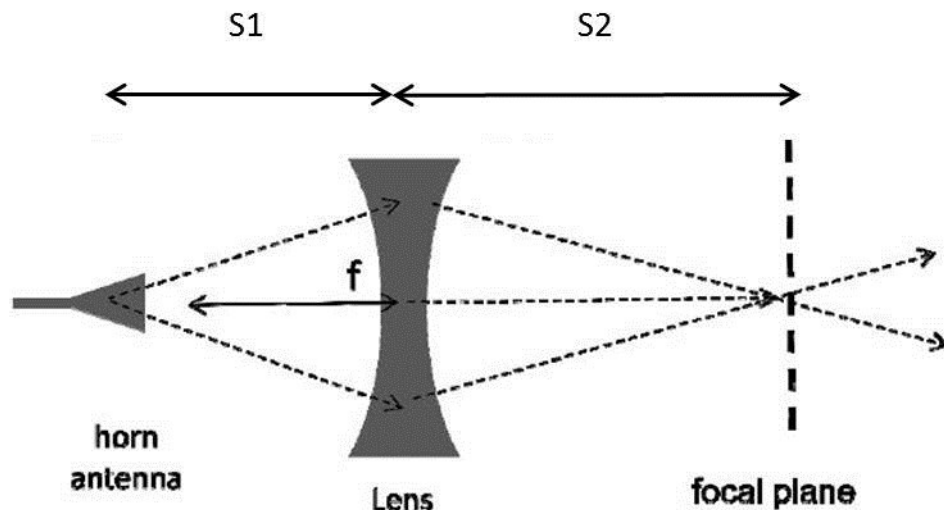


Figure 78: Schematic diagram of a bi-concave artificial dielectric lens [11]

Even though the measurements related to this experiment has not been performed yet, the set-up can be described and would require two horn antennas and a VNA with the lens structure at a distance of one focal length from the horn antenna. As the output at the other end would be a spot focus beam, it is recommended that a horn antenna with small aperture be used at the receiving side connected to Port 2 of the VNA.

In the given schematic in **Figure 78**,  $S1$  is the distance from the phase centre of the horn antenna to the centre of the lens. If the lens were designed with a focal length of  $(f)$  and

placed with its axis along boresight of the horn antenna at a distance of one focal length from the phase centre of the horn. Now, if the lens is placed more than one focal length away at a distance of  $S_1$ , it will focus the beam to an Airy disk in the focal plane located at  $S_2$ . The positioning of the Airy disk at the position  $S_2$  is governed by the equation (3).

$$\frac{1}{f} = \frac{1}{S_1} + \frac{1}{S_2} \quad (7)$$

As the dimensions of the lenses are small, the distance between the lens and the energizing horn antenna ( $S_1$ ) is of crucial importance. Having said that, if the distance between the energizing antenna and the lens is too big then the lens would be unable to capture the maximum energy from the transmitting horn antenna. In a similar fashion, if the antenna is placed too close to the lens, this results in higher backscatter and reflection from the lens.

#### **8.4.1 BI-CONCAVE LENS**

The convergence phenomenon can also be observed in **Figure 79**, where focusing action of a lens of EM waves is achieved by bi-concave artificial dielectric lens at 77 GHz using CST. The energy is spot-focused in the form of an airy disc at the output end of the lens, indicating converging EM waves, some of the energy was reflected back, due to backscattering from the metallic lens. This is also one of the reasons why the metallic lenses usually have narrow bandwidth compared to the dielectric lenses.

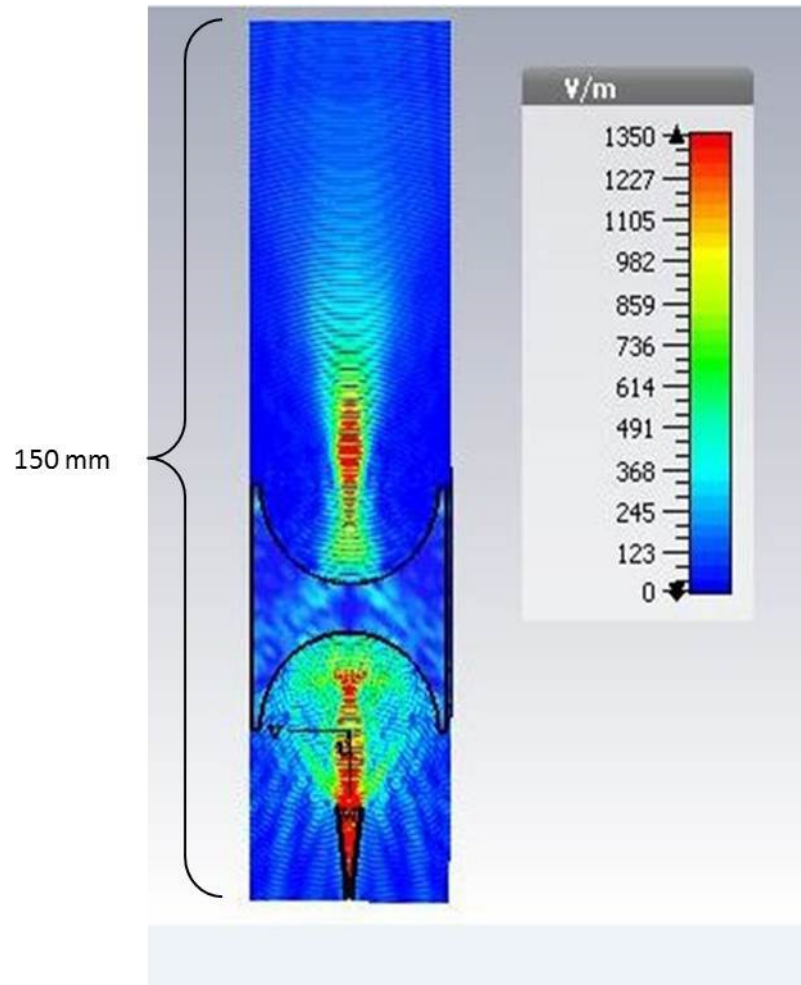


Figure 79: Focusing action of a beam energized with a horn antenna using a bi-concave artificial dielectric lens at 77 GHz, simulated using CST

**Figure 80** shows the CST carpet representation of the electric field in the focal plane, showing the focusing action of the simulated bi-concave lens at the bore-sight direction of the lens.

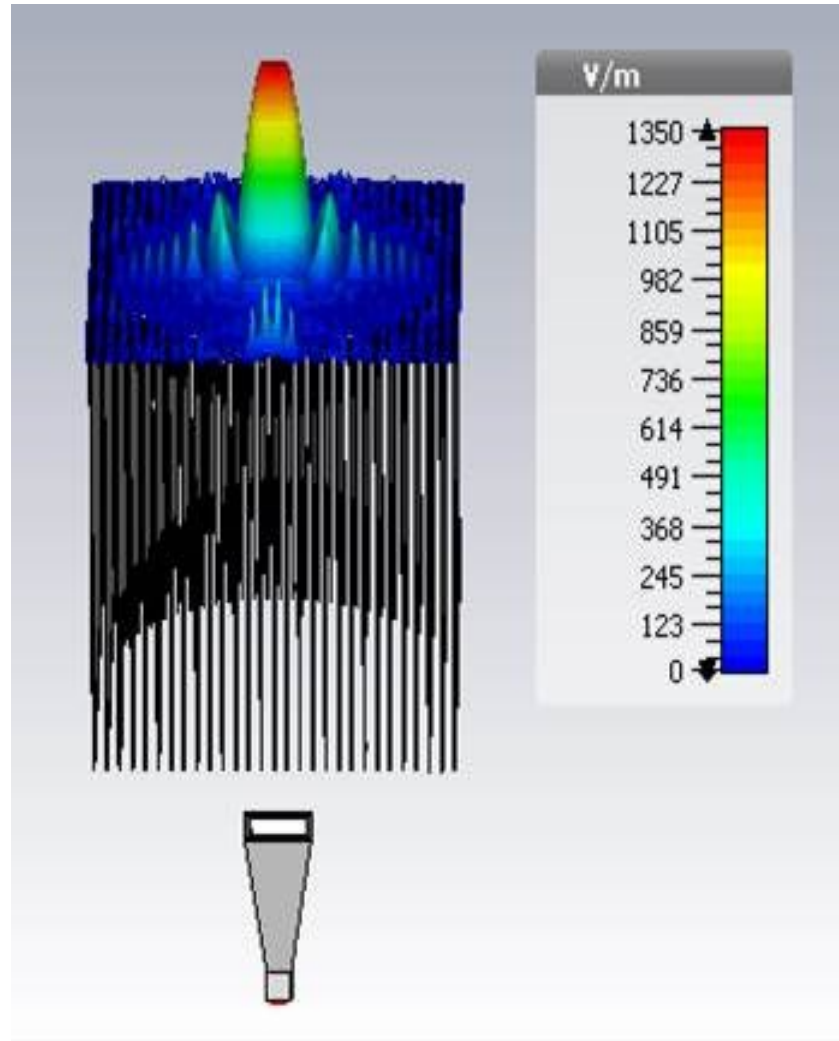


Figure 80: Carpet representation of the focusing action of the Bi-concave artificial dielectric lens at 77 GHz, simulated using CST

### 8.4.2 PLANO-CONCAVE LENS

Once the spot focusing action through a bi-concave metallic lens was confirmed, the next step was to reduce the size of the lens by modelling a plano-concave geometry, which can reduce the size of the artificial lens intact, without degrading the airy disc action at the bore sight. It should also be noted that the index of refraction chosen for this particular geometry was 0.28, which would result in an arrangement of metallic plates spaced closed to each other. The resultant arrangement of plano-concave lens geometry can easily be adapted to fit in at the aperture of the existing antenna type. This would mean an antenna, with low directivity, can be adapted to cause converging EM waves (passing through at an intended spot), while maintaining the antenna and lens combination's compact size.

As an example of this, the focusing action of a beam energized with a horn antenna using a plano-concave artificial dielectric lens at 60 GHz is presented in **Figure 81**.

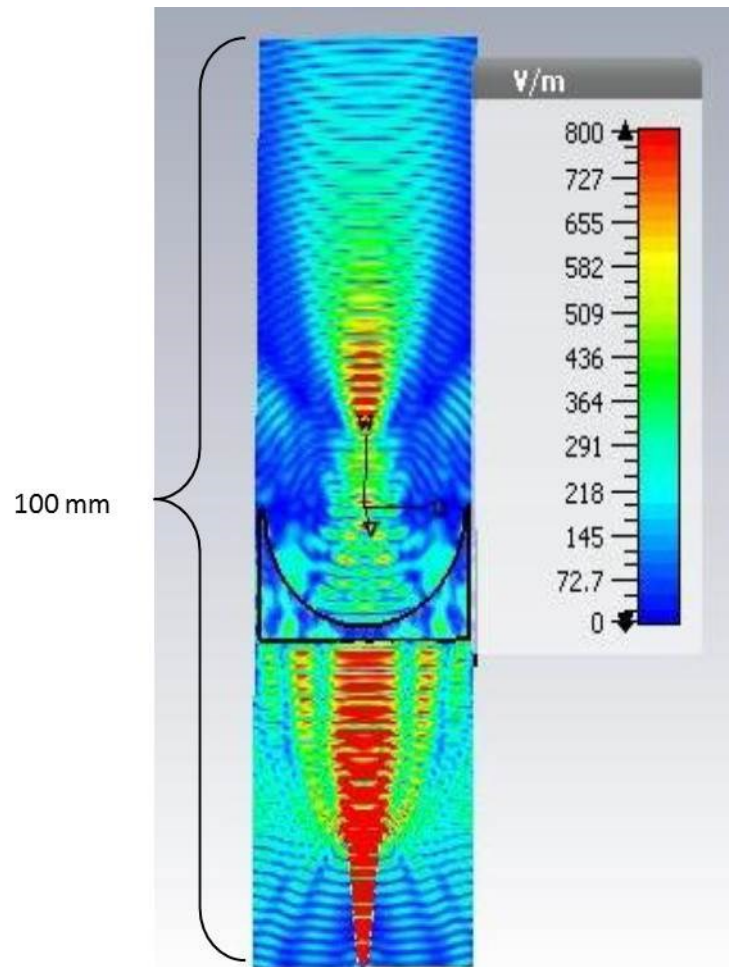


Figure 81: Focusing action of a beam energized with a horn antenna using a plano-concave artificial dielectric lens at 60 GHz, simulated using CST

As illustrated in **Figure 81**, the back scattering is much higher in this case compared to the results obtained from the bi-concave geometry. This is due to the close spacing of the metallic plates. With the simulation results obtained, the next step would be to fine tune to the lens and then compare it with the measurement results. In performing the measurements, it would be required for the lens to be accurately placed in front of and normal to the horn antenna excitation. This would require some finely tunable mechanical adjustable brackets or mounts, which could easily lead to antenna misalignment. This may only lead to a misalignment of only a few degrees, but could lead to a significant reduction of the link quality, especially at higher frequencies, where the radiation beams are much narrower. In order to improve on this, it is planned to build a new approach,

where the lens and horn antenna would be 3D printed to the aperture of the horn antenna and act as a single unit, thereby eliminating any losses due to misalignment.

## **8.5 SUMMARY**

In this chapter, the design and proposed fabrication method of mm-wave metallic lenses have been discussed for a short-range application in the E-band. The simulation results obtained through CST confirm the focusing action of the artificial dielectric lens. It is further proposed to fine tune the lens to perform the measurements and then to correlate the simulated results obtained, with the measured data. This research opens the door towards the development of future 5G /millimeter-wave antenna and system design, using 3D metal printing.

## 8.6 REFERENCES

1. T. S. Rappaport, S. Sun, R. Mayzus, H. Zhao, Y. Azar, K. Wang, G. N. Wong, J. K. Schulz, M. Samimi, and F. Gutierrez, "Millimeter Wave Mobile Communications for 5G Cellular: It Will Work," *IEEE Access*, vol. 1, pp. 335-349, 2013.
2. W. Roh, J.-Y. Seol, J. Park, B. Lee, J. Lee, Y. Kim, J. Cho, F. Aryanfar, K. Cheun, "Millimeter-wave beamforming as an enabling technology for 5G cellular communications: Theoretical feasibility and prototype results", *IEEE Communications Magazine*, pp. 106-113, Feb/ 2014.
3. J. Ala-Laurinaho, J. Aurinsalo, A. Karttunen, M. Kaunisto, A. Lamminen, J. Nurmiharju, A. V. Raisanen, J. Saily, and P. Wainio, "2-D Beam Steerable Integrated Lens Antenna System for 5G E-Band Access and Backhaul", *IEEE Transactions on Microwave Theory and Techniques*, pp. 1–12, 2016.
4. Ericsson, "(Online) Ericsson T-Mobile and Ericsson achieve over 12 Gbps on 5G connection", Available: (<https://www.ericsson.com/news/2043477>), [Accessed: 15<sup>th</sup> March 2018].
5. F. Pivit , E. Doumanis , D. Kozlov , M. Gueye , M. Gimersky- "Compact 60-GHz Lens Antenna with Self-Alignment Feature for Small Cell Backhaul", *2017 IEEE-APS Topical Conference on Antennas and Propagation in Wireless Communications (APWC), Verona, Italy, p.p. 280-283, September/2017.*
6. W. Gee, S. Lee, N. K. Bong, C. A. Cain, R. Mittra, R. L. Magin, "Focused array hyperthermia applicator: theory and experiment", *IEEE Transactions on Biomedical Engineering*, vol. 31, pp. 38-45, 1984.
7. M. Liang, W.-R. Ng, K. Chang, K. Gbele, M. E. Gehm and H. Xin, "A 3-D Luneburg Lens Antenna Fabricated by Polymer Jetting Rapid Prototyping," *IEEE Transactions on Antennas and Propagation*, vol. 62, no. 4, pp. 1799-1807, April 2014.
8. M. Liang, X. Yu, R. Sabory-García, W.-R. Ng, M. E. Gehm, H. Xin, ""Broadband electronically beam scanning structure using Luneburg lens", *IEEE International Microwave Symposium, June/2013.*
9. G. Du, M. Liang, R. Austrebert, S.-Garcia, C. Liu, H. Xin, "3-D Printing implementation of an X-band Eaton lens for beam deflection", *Antennas and Wireless Propagation Letters IEEE*, vol. 15, pp. 1487-1490, 2016.

10. W. E. Kock, "Metal-lens antennas", *Proceedings of the I.R.E. and Waves and Electrons*, vol. 34, pp. 828-836, 1946.
11. J. E. Lawrance, C.G. Christodoulou, M. R. Taha, "A high-power microwave zoom antenna with metal-plate lenses," *IEEE Transactions on Antennas and Propagation*, vol. 63, no. 8, pp. 3380-3389, 2015.
12. G. Guo, Y. Zhang, E. Li, "Design of the spot-focusing metal plate lens antenna for high-temperature measurement", *2015 IEEE International Symposium on Antennas and Propagation & USNC/URSI National Radio Science Meeting*, pp. 953-954, Vancouver, BC, Canada, July/2015.
13. T. Konno, T. Suzuki, J.C. Young, M. Saigusa, K. Takano, H. Kitahara, M. Hangyo, T. Suzuki, "Proposal and analysis of artificial dielectric lens with metallic corrugated structures for terahertz wave band", *Journals of Applied Physics. A*, vol. 109 (4), pp.1103–1108, 2012.
14. T. Suzuki, H. Yonamine, T. Konno, J. C. Young, K. Murai, F. Miyamaru, K. Takano, H. Kitahara, M. Hangyo, "Analysis and design of concave lens with metallic slit array for terahertz wave band", *Journals of Applied Physics. A*, vol. 115 (2), pp. 495–500, May/2014.
15. R. Mendis, M. Nagai, Y. Wang, N. Karl, D. M. Mittleman, "Terahertz artificial dielectric lens", *Scientific Reports.*, vol. 6, pp. 1-8, 2016.
16. New Atlas, "(Online) World's largest metal 3D-printer scales up additive manufacturing", (<https://newatlas.com/titomic-worlds-largest-metal-3d-printer/54667/>), [Accessed: 15<sup>th</sup> May 2018].
17. EOS, "(Online) EOS Maraging Steel MS1 - Material Data Sheet", ([http://ip-saas-eos-cms.s3.amazonaws.com/public/1af123af9a636e61/042696652ecc69142c8518dc772dc113/EOS\\_MaragingSteel\\_MS1\\_en.pdf](http://ip-saas-eos-cms.s3.amazonaws.com/public/1af123af9a636e61/042696652ecc69142c8518dc772dc113/EOS_MaragingSteel_MS1_en.pdf)), [Accessed 15<sup>th</sup> January 2016].
18. A. Tomaz, J. J. Barroso, P. J. Castro, U. C. Hasar, A. J. F. Orlando, "Implementation of a wire medium in a X-band horn antenna: simulation and experiment", *2014 Asia-Pacific Microwave Conference*, pp. 813-815, Sendai, Japan, Nov./ 2014.
19. M. Diblanc, E. Rodes, E. Arnaud, M. Thevenot, T. Monediere, B. Jecko, "Circularly polarized metallic EBG antenna", *IEEE Microwave and Wireless Components Letter*, vol. 15, no. 10, pp. 1-3, Oct/ 2005.

20. E. Arnaud, R. Chantalat, M. Koubeissi, T. Monediere, M. Thevenot, B. Jecko, “Improved self-polarizing metallic EBG antenna”, *Proceedings of 2019 European Conference on Antennas and Propagation (EuCAP)*, pp. 3813-3817, Berlin, Germany, March/ 2009.

# 9

## CHAPTER 9

### CONCLUSION AND FUTURE WORK

#### 9.1 CONCLUSION

3D printing presents new possibilities in the fabrication of novel, complex-shaped microwave components, which include antennas, filters, resonators and waveguides. Allowing the RF designers to fabricate any virtual geometry possible, within the design constraints. 3D printing has given an opportunity to the designers to think outside of the box, without restricting them in the same way conventional design does, due to their manufacturing constraints. With this thesis, an attempt has been made to explore the untapped possibilities for 3D printing microwave components. In that regard, the thesis presents the world's first ever 3D metal printed Sierpinski gasket antenna that has been manufactured with DMLS technique. The results obtained through the measurements of 3D printed antenna benchmarked the successful realization of complex-shaped geometry with the help of 3D printing for the fabrication of microwave components. To address the concerns about the impact of the surface quality of the 3D printed component on the RF performance, two different surface treatment techniques have been used. The techniques have been used to gradually reduce the surface roughness of the printed component, while the RF performance has been tracked as a function of reducing surface roughness, to showcase the improvement that can be achieved in a step-wise manner. Keeping in view the non-accessibility of the surface treatment techniques to the wider RF community, avoidable factors such as limiting the layer thickness of the print, as well as the importance of build orientation have been identified, that could potentially limit the surface roughness of the printed component, whose impact could be significant at higher frequencies.

As the advantage of 3D printing is not limited to creating complex-shaped geometries, but also extends to the printing of hollow interiors for the fabrication of lightweight components. In this research, for the first time ever, a metal antenna has been manufactured which weighs lighter than even a metal coated polymer antenna with comparatively much higher structural strength.

With the almost endless possibilities that 3D printing can offer over traditional manufacturing techniques, one attempt has been made in this thesis towards the improvement of the existing antenna type, by opening a whole new concept of successfully fabricating antennas, with in-built periodic structures in bespoke positions, to reduce side lobes. In addition to that, for the first time, the concept of 3D printing artificial dielectric lenses has also been proposed and discussed in detail in this work.

### **9.1.1 SIGNIFICANCE OF THIS WORK**

The most important outcome from this research is the realisation that high quality, novel microwave components can be created using a 3D printer. Furthermore, as will be outlined in more detail in the section dedicated to future work, it is now apparent that there is ample scope to research this area even deeper, to improve on the designs proposed here through, for example, improving the Sierpinski gasket antenna, reducing the weight of the lightweight antennas and designing even better antennas with in-built periodic structures for wireless applications. Some other interesting opportunities now clearly possible include the fabrication of novel-shaped, periodic structures, and also artificial dielectric lenses, for possible 5G and power applicator usage.

### **9.1.2 LIMITATIONS OF THIS WORK**

While 3D printing has been showcased with many advantages in this thesis, there were a few limitations as well to this research work. Most of the work presented in this thesis has been done in the X-band, due to the bandwidth restriction posed by the available VNA (20 GHz maximum frequency). This meant that the ability of 3D printing in fabricating complex structures and compact microwave components for higher frequencies was not completely explored and remains a very interesting opportunity for future work. Also, at such higher frequencies, where the impact of inherent surface roughness is more significant, it would be interesting to investigate how much improvement that surface

treatment techniques could bring in the performance of the electromagnetic component. Moreover, while not used in this research, with the use of highly conductive metallic powders, such as Aluminium and Copper, 3D metal printing also has the potential to eliminate concerns regarding the fabrication of lower efficiency microwave components, such as those in this research, where the fabrication has been done mostly with relatively low value conductive materials. One important aspect is that while 3D printing is capable of fabricating any virtual geometry possible (within design constraints), it requires support structures to print overhangs/cantilever sections, to support unsupported areas. This not only requires the extra processing step of its removal, but also makes some geometry un-manufacturable as well, due to the overhang angle limitations. From a monetary point of view, the technology is expensive for the mass production of components, but there is a trade-off, with benefits such as the realizing of complex shapes, light weight designs and comparatively fast production of customized components over the traditional manufacturing techniques.

## **9.2 FUTURE WORK**

### **9.2.1 FUTURE WORK ASSOCIATED AS AN EXTENSION TO THE THESIS**

In this research, an attempt has been made to explore novel areas of research into microwave component production. In that sense, as most of the components that have been 3D printed in this thesis have been antennas, there is a huge scope for the successful fabrication of other microwave components. Also, with the bountiful opportunities for research in this particular field, there is also the possibility to further look into the fabrication of lightweight microwave components, using periodic cellular lattice structures. As the weight of the microwave component can be important to some industries, one such example is the fabrication for space applications. There is an ample amount of scope for research to further minimize the weight of the component, without degrading the performance of the component, by designing different structural lattice geometries.

In one such example, which even though, not part of this thesis (as it was not core to the work), extremely lightweight, high-performing heat sinks has been fabricated for many applications, including active antennas. The lattice structures were used to serve a dual-purpose. One is to increase the surface-to-volume ratio of the component to enhance heat

dissipation and the other is to achieve a lightweight structure. This could reduce the thermal resistance, as well as improve the radiation efficiency and thus, the gain of the microwave component.

Although the main focus of this research has been towards fabricating microwave components using a 3D metal printer, it would nonetheless be interesting to explore the research area of 3D polymer printing, with different fabricating materials such as highly conductive polymers or ULTEM 100, which has a comparatively higher tensile strength than the reported ABS, for fabricating high strength-to-weight microwave components.

A further possible extension of this research would be to realize 3D metal printed electronic bandgap filters, which would allow a certain frequency band to pass through, depending on the lattice structure size and would restrict all other frequencies. This feature of lattice structures can further be utilized in the area of microwave communication to guide specified frequency, electromagnetic waves in certain directions. One of the potential projects that could arise from this concept is to design and construct a unit periodic lattice structure, with a desired density and a unit cell length, with the aim of preventing electromagnetic energy from propagating in certain directions at specified frequencies. This work could also be further extended to enhance the directivity of waveguide horn antennas. However, due to the metallic structures there would also be back scattering, although, the structure could also possibly be optimized to confine the electromagnetic energy of specific frequencies within the structure as well, thereby helping in realizing cavity resonators.

Successfully fabricating horn antenna with reduced side lobes levels with the placement of periodic structures in the bespoke positions have open a new area of research to be done. In the future, researchers can design and fabricate novel-shaped periodic structures with high impedance capability to improve the performance of the existing antennas. Also, it would be interesting to measure the co-polarisation radiation pattern of this antenna, to analyse the impact of E-plane corrugation. Also, there is an opportunity to fabricate the same periodic structures on the H-plane as well and then to further compare the results obtained with a commercially available, corrugated horn antenna. One more interesting possibility arises with this project and is, if hybrid 3D printing can be evolved, in the near future, and is used towards the production of these kind of antennas, where the antennas structure is fabricated with the help of metallic materials, while the corrugated

pattern is fabricated out of dielectric material, acting as a resistance to the incoming electromagnetic waves.

Furthermore, there can be some value added by further improving the focussing capabilities of the existing antennas. As in this research, where the concept of 3D printing artificial dielectric lenses has been discussed, there is a scope to fabricate the same for different frequencies. Also, as at higher frequencies to deal with the misalignment issues during the experimental set-up, the lens can be fabricated at the aperture of a horn antenna, increasing the focusing capabilities. One of the key the issues with 3D printing lenses is the focal length restriction, due to the size limitation of the energising source as well as the lens structure. With the development in the area of 3D printing, it is expected that sooner larger volume 3D metal printers will be available to manufacture components intended for lower wireless frequencies requirements or indeed to produce lenses that are significantly larger than the orifice of the antenna, to capture more energy.

### **9.2.2 FUTURE WORK IN THE MEDIUM TO LONG TERM**

In the medium to long term, with the growing interest of the research community to exploit the potential of AM, it can be expected to see research done towards developing electronic circuitry inside a 3D metal printed component. Also, with the advent of metal AM techniques such as DMLS, it is now possible to create porous metallic implants made from biocompatible, titanium alloy Ti-6Al-4V, such as replacement prostheses, implants etc. in animals or humans. The selection of porous metallic implants over metal implants would be done for two main reasons i) the porous implant supports bone grown growth, ii) due to the porous structure of the implants, it is possible to install or embed a small wireless sensor inside the implant. The function of the implanted sensor could be to measure the degradation of the implant or simply as a proof of concept for some future application or as an identification tag. The data from the sensor can wirelessly be downloaded from a front-end RF receiving antenna. The porous structure of the implant, which is certainly possible due to the advent of 3D printing, allows communication to happen. Otherwise, the implant would act as a Faraday Cage.

## APPENDIX

A list of peer-reviewed conference and journal published papers arising from the research work conducted are enclosed.

1. Deepak Shamvedi, Oliver McCarthy, Eoghan O'Donoghue, Paul O'Leary, Ramesh Raghavendra - "Surface Treatment of 3D Metal Printed Microwave Components", *18th Research Colloquium on Radio Science and Communications for a Smarter World, Dublin, Ireland; p.p. 8-10, March/2017.*
2. Deepak Shamvedi, Oliver McCarthy, Eoghan O'Donoghue, Paul O'Leary, Ramesh Raghavendra - "3D Metal Printed Sierpinski Gasket Antenna", *2017 International Conference on Electromagnetics in Advanced Applications (ICEAA), Verona, Italy; p.p. 633-636, September/2017.*  
*DOI: 10.1109/ICEAA.2017.8065326*
3. Deepak Shamvedi, Oliver McCarthy, Eoghan O'Donoghue, Paul O'Leary, Ramesh Raghavendra - "Improved Performance of 3D Metal Printed Antenna through Gradual Reduction in Surface Roughness", *2017 International Conference on Electromagnetics in Advanced Applications (ICEAA), Verona, Italy; p.p. 669-672, September/2017.*  
*DOI: 10.1109/ICEAA.2017.8065335*
4. Deepak Shamvedi, Oliver McCarthy, Eoghan O'Donoghue, Paul O'Leary, Ramesh Raghavendra - "3D Metal Printed Monocone Antenna with an Integrated Feed", *Proceedings of 47<sup>th</sup> European Microwave Conference (EuMW), Nuremberg, Germany, p.p. 168-171, October/2017.*  
*DOI: 10.23919/EuMC.2017.8230826*
5. Deepak Shamvedi, Cyril Danilenkoff, Sara Karam, Paul O'Leary, Ramesh Raghavendra - "3D Printed Periodic Structures in a Horn Antenna for Side-lobe Reduction using Direct Metal Laser Sintering", *2017 IET Loughborough*

*Antennas & Propagation Conference (LAPC), Loughborough, UK, p.p. 1-4, November/2017.*

*DOI: 10.1049/cp.2017.0244*

6. Deepak Shamvedi, Oliver McCarthy, Eoghan O'Donoghue, Paul O'Leary, Ramesh Raghavendra - "Progress in 3D Metal Printed Microwave Components – An Overview", *12<sup>th</sup> European Antenna & Propagation Conference (EuCAP), London, UK, p.p. 1-4, April/2018.*
7. Deepak Shamvedi, Cyril Danilenkoff, Paul O'Leary, Ramesh Raghavendra - "Investigation of the Influence of Build Orientation on the Surface Roughness of the 3D Metal Printed Horn Antenna", *12<sup>th</sup> European Antenna & Propagation Conference (EuCAP), London, UK, p.p. 1-4, April/2018.*
8. Deepak Shamvedi, Oliver McCarthy, Cyril Danilenkoff, Eoghan O'Donoghue, Paul O'Leary, Ramesh Raghavendra - "3D Metal Printed Heat Sinks with Longitudinally Varying Lattice Structure Sizes using Direct Metal Laser Sintering", *Journals of Virtual and Physical Prototyping, vol. 13, no. 4, pp. 301-310, May/2018.*  
*DOI: 10.1080/17452759.2018.1479528*
9. Deepak Shamvedi, Paul O'Leary, Ramesh Raghavendra - "Design Approach for Successful Fabrication of 3D Printed Microwave Components", *21<sup>st</sup> International Conference on Advances in Materials & Processing Technologies, (AMPT 2018) Dublin, Ireland, September/2018.*
10. Deepak Shamvedi, Oliver McCarthy, Eoghan O'Donoghue, Paul O'Leary, Ramesh Raghavendra - "Improving the Strength-to-Weight Ratio of 3D Printed Antennas: Metal versus Polymer", *IEEE Antennas and Wireless Propagation Letters.*  
*DOI: 10.1109/LAWP.2018.2870944*